AD-A087 034 COLUMBIA RADIATION LAB NEW YORK F/G 7/4
RESEARCH INVESTIGATION DIRECTED TOWARD EXTENDING THE USEFUL RAN--ETC(U)
MAR 80 G W FLYNN DAAG29-79-C-0079
UNCLASSIFIED NL

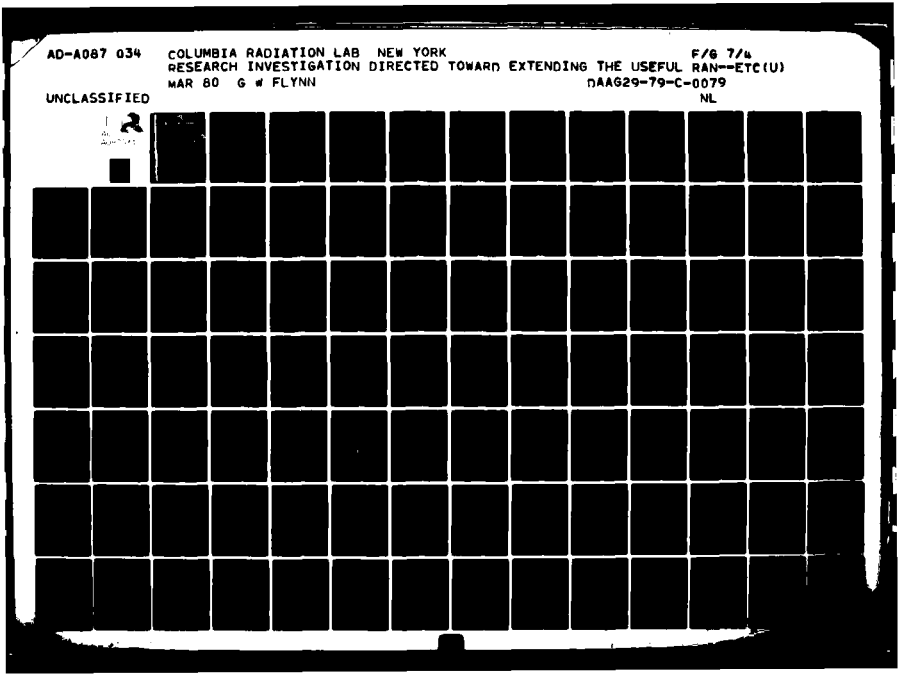

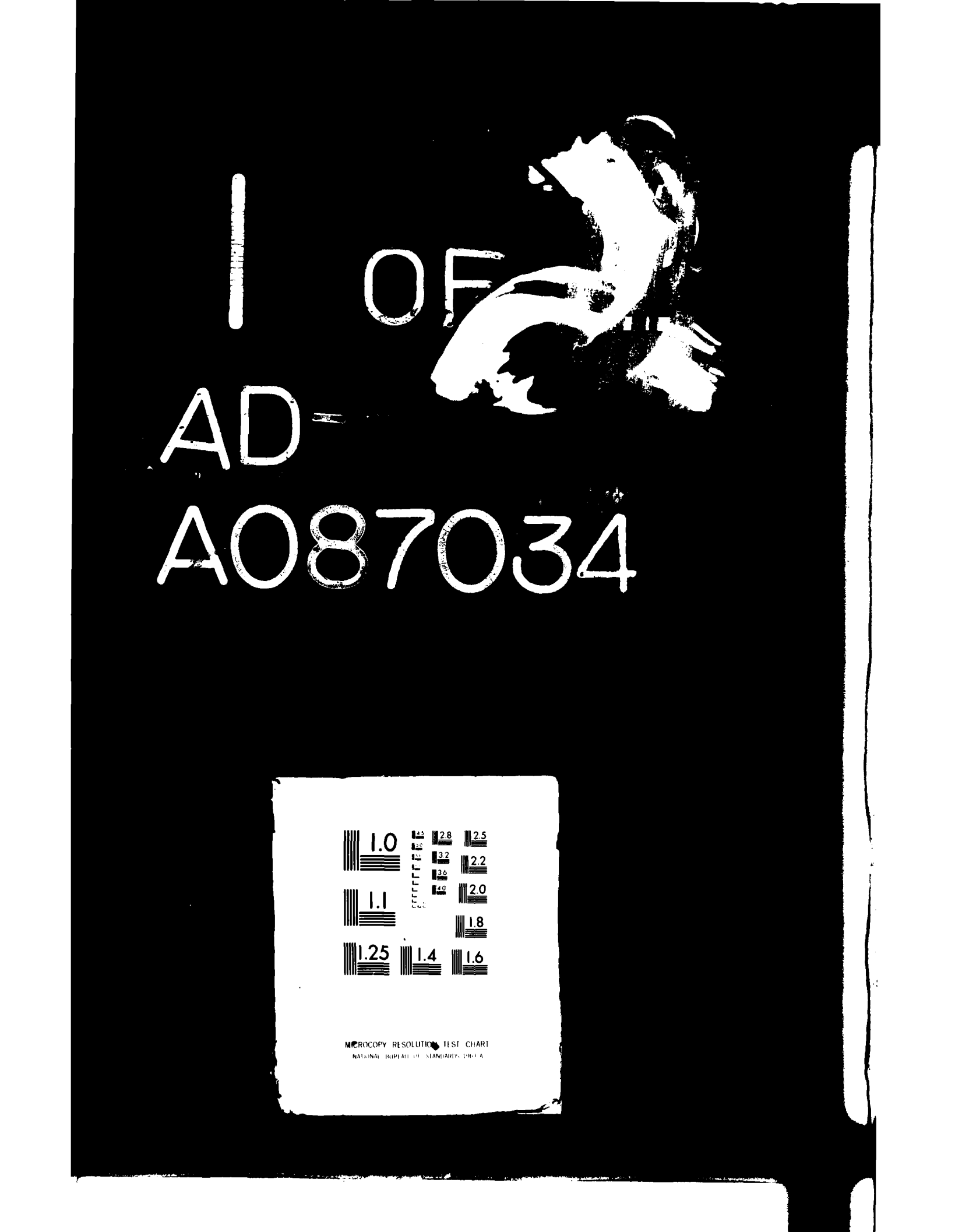
1 OF
AD-
A087034
1.0
1.1
1.25
1.4
1.6
2.8
3.2
3.6
4.0
2.5
2.2
2.0
1.8
MICROCOPY RESOLUTION TEST CHART
NATIONAL BUREAU OF STANDARDS 1963-A

COLUMBIA UNIVERSITY

DEPARTMENTS OF PHYSICS,
CHEMISTRY, ELECTRICAL ENGINEERING

PROGRESS REPORT NO. 30

April 1, 1979 through March 31, 1980

CONTRACT DAAG29-79-C-0079

APPROVED FOR PUBLIC RELEASE: DISTRIBUTION UNLIMITED

To:

THE JOINT SERVICES TECHNICAL ADVISORY COMMITTEE

REPRESENTING: THE U.S. ARMY ELECTRONICS COMMAND
THE U.S. ARMY RESEARCH OFFICE
THE OFFICE OF NAVAL RESEARCH
THE AIR FORCE OFFICE OF SCIENTIFIC RESEARCH

COLUMBIA RADIATION LABORATORY NEW YORK, NEW YORK 10027

March 31, 1980

COLUMBIA RADIATION LABORATORY

RESEARCH INVESTIGATION DIRECTED TOWARD EXTENDING THE USEFUL RANGE OF THE ELECTROMAGNETIC SPECTRUM

Progress Report No. 30

April 1, 1979 through March 31, 1980

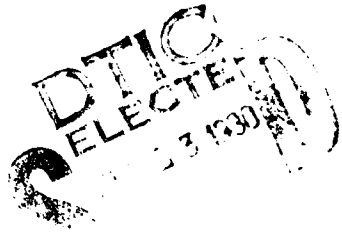

Contract DAAG29-79-C-0079

Object of the research:

Basic research in the fields of quantum electronics; electromagnetic propagation, detection and sensing; and solid state electronics.

The research reported in this document was made possible through support extended the Columbia Radiation Laboratory, Columbia University, by the Joint Services Electronics Program (U. S. Army Electronics Command and U. S. Army Research Office, Office of Naval Research, and the Air Force Office of Scientific Research) under Contract DAAG29-79-C-0079.

Submitted by: G. W. Flynn, Director

Coordinated by: P. A. Pohlman, Administrative Assistant

COLUMBIA UNIVERSITY

Division of Government-Aided Research

New York, New York 10027

March 31, 1980

The research reported in this document was made possible through support extended the Columbia Radiation Laboratory, Columbia University by the Joint Services Electronics Program (U.S. Army Electronics Command and U.S. Army Research Office, Office of Naval Research, and the Air Force Office of Scientific Research) under Contract DAAG29-79-C-0079.

Portions of this work were also supported by:

Air Force Office of Scientific Research

Grant AFOSR-79-0082

Army Research Office

Grant DAAG29-80-C-0043

National Science Foundation

Grant NSF-ENG 76-16424

Grant NSF-MPS 75-04118

Grant NSF-CHE 77-11384

Grant NSF-CHE 77-24343

Grant NSF-ENG 78-26498

Grant NSF-CHE 79-23291

Grant NSF-DMR-79-06382

Office of Naval Research

Contract N00014-78-C-0517

Naval Air Development Center

Department of Energy

Contract DOE-ET-78R-031876

Contract DE-AS02-78ER04940

National Institute of Health

Grant HL19488-04

The support of these agencies is acknowledged in footnotes in the text.

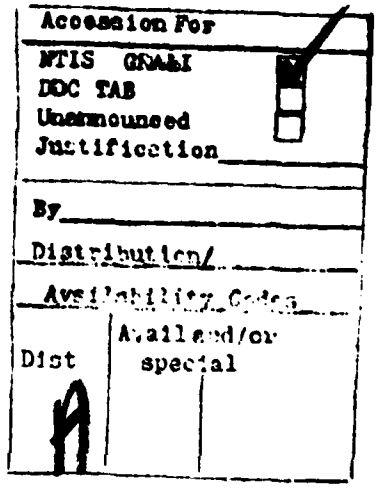

Unclassified

SECURITY CLASSIFICATION OF THIS PAGE (When Data Entered)

REPORT DOCUMENTATION PAGE	READ INSTRUCTIONS BEFORE COMPLETING FORM
1. REPORT NUMBER: Progress Report No. 30	2. GOVT ACCESSION NO.: AD-A087034
	3. RECIPIENT'S CATALOG NUMBER: (9) Progress rept. no. 30
4. TITLE (and Subtitle): (6) RESEARCH INVESTIGATION DIRECTED TOWARD EXTENDING THE USEFUL RANGE OF THE ELECTROMAGNETIC SPECTRUM	5. TYPE OF REPORT & PERIOD COVERED: 1 Apr 79 — 31 Mar 80
	6. PERFORMING ORG. REPORT NUMBER: 30
7. AUTHOR(s): (10) George W. Flynn	8. CONTRACT OR GRANT NUMBER(s): (15) DAAG29-79-C-0079 [crossed out] DAAG29-80-C-0043
9. PERFORMING ORGANIZATION NAME AND ADDRESS: Columbia Radiation Laboratory, Columbia University, New York, New York 10027	10. PROGRAM ELEMENT, PROJECT, TASK AREA & WORK UNIT NUMBERS: (16) 1L161102BH57-03 (17)
11. CONTROLLING OFFICE NAME AND ADDRESS: (11) Department of the Army, U. S. Army Research Office, Research Triangle Park, NC 27709	12. REPORT DATE: 31 Mar 80
	13. NUMBER OF PAGES: 166
14. MONITORING AGENCY NAME & ADDRESS (if different from Controlling Office): (12) 186	15. SECURITY CLASS. (of this report): Unclassified
	15a. DECLASSIFICATION/DOWNGRADING SCHEDULE

16. DISTRIBUTION STATEMENT (of this Report)

Approved for public release; distribution unlimited.

17. DISTRIBUTION STATEMENT (of the abstract entered in Block 20, if different from Report)

18. SUPPLEMENTARY NOTES

Portions of this work were also supported by the Air Force Office of Scientific Research, the Army Research Office, the National Science Foundation, the Office of Naval Research, the Naval Air Development Center, the Department of Energy, and the National Institute of Health.

19. KEY WORDS (Continue on reverse side if necessary and identify by block number)

Excimer lasers
Magnetic resonance
Two photon optical pumping
Nuclear magnetic resonance gyroscopes
Infrared excimer lasers

Continued on page v.

20. ABSTRACT (Continue on reverse side if necessary and identify by block number)

Preliminary studies of spin relaxation of optically pumped sodium in xenon gas have shown that Van der Waals NaXe cause a substantial part of the relaxation. The electron-nuclear spin exchange cross section between Na and Xe^{129} has been measured to be less than 10^{-19} cm^2. → TEN TO THE −19 TH POWER / sq CM

Calculations and preliminary experiments have shown that radiofrequency spectroscopic studies of the anomalously long lived 5D state of cesium are possible.

DD FORM 1 JAN 73 1473 EDITION OF 1 NOV 65 IS OBSOLETE

Unclassified

SECURITY CLASSIFICATION OF THIS PAGE (When Data Entered)

Block 20 continued - Abstract

Further studies of dense alkali vapors have shown that all of the alkali vapors sodium, potassium, rubidium and cesium, have absorption bands in the spectral region between 1μ and 2.5μ. The possibility that some of these bands might be useful for the construction of infrared excimer lasers is being investigated.

A model system for studies of two photon optical pumping to produce ground-state spin polarization has been selected. We intend to work with the transition $5S_{1/2}$-$5D_{3/2}$ in rubidium. A dye laser pumped by a krypton ion laser will be used to drive the transition.

Infrared emission bands of CsXe excimer states have been studied systematically as a function of temperature, and dissociation energies of the upper levels of several excimer transitions have been determined.

An apparatus to measure the Faraday rotation and circular dichroism of alkali noble gas excimers has been constructed. The results of this experiment will help to determine the quantum numbers of the upper states of the excimer transitions.

Particulate formation in mixtures of cesium vapor and deuterium or hydrogen gas has been investigated with a tunable dye laser. The stilbene dye is pumped with ultraviolet lines from an argon ion laser. Particulates, presumably CsD crystals, could be produced at very low cesium vapor density.

A new spin destruction mechanism for collisions between cesium atoms has been discovered. The new spin destruction rate is about 1% of the well known spin exchange rate. The spin destruction is probably due to the magnetic dipole-dipole interaction and it should exist for all alkali vapors.

We have determined the major energy transfer paths for COF_2 which exhibits a relaxation anomaly. The symmetric C-F stretch frequency (ν_2) transfers energy to the antisymmetric C-F stretch mode ν_4 more slowly than ν_4 empties. We have also shown that the vibrational temperature of the coupled ν_2, ν_1 modes is very high compared to ν_4. This suggests a metastable inverted population in COF_2.

Intermolecule energy transfer between SO_2 and $^{18}O_2$ has been clearly demonstrated for the first time. Intermode energy transfer has been mapped in OCS and mixtures of OCS with rare gases. Both the $SO_2/^{18}O_2$ and OCS systems are vibrationally metastable.

An extremely novel technique has been developed for producing supersonic beams of vibrationally excited molecules using relatively low power CW infrared lasers. Considerable advances have been made in the diagnostic studies of energy redistribution in supersonic expansions.

Preliminary studies of photofragmentation processes in SO_2 have been made using UV excimer laser radiation for photolysis. IR emission has been observed from vibrationally excited SO and SO_2 in the photolysis mixture.

Block 20 continued - Abstract

Picosecond laser methods have been used to generate an important chemical intermediate, diphenyl carbene $\phi\!>\!C\!:$ on photodissociation of the parent compound diphenyldiazomethane. We have discovered that excitation of the parent compound at 266 nm resulted in the generation of diphenylcarbene in an excited triplet state. This new and important channel for photodissociation was unknown prior to this work.

Picosecond laser coherent anti-Stokes Raman scattering (CARS) experiments have been carried out on gas phase benzene at room temperature. Both ground and excited state (B_{2u}) vibrational CARS signals have been observed. On photolyzing benzene with a pulse at 266 nm we have found, using CARS as a probe method, that multiphoton absorption by benzene generates fragments as small as C_2 extremely rapidly, i.e. within 25 ps. of excitation.

We report the direct measurement of electron solvation times in methanol and ethanol. A picosecond technique utilizing a laser triggered flash lamp and a streak camera is used to monitor the solvation process. The relationship of the solvation dynamics to dielectric relaxation, local heating, and pulse radiolysis results are presented.

We have discovered a new class of macroscopic reordering phenomena in gases, which is characterized by the periodic reformation of population "gratings" after standing-wave excitation. These gratings, detectable via their ability to scatter a probe laser, are useful in spectroscopic and collisional studies. We have completed the first phase of our investigation of the unusual properties of the three-pulse stimulated photon echo. We find that, in contrast to other echo effects, the stimulated echo is generated from information stored in one atomic state. Consequently, it may endure for unusually long times. We discuss our use of the stimulated echo to measure total elastic scattering cross sections. The Raman echo, excited in a vapor for the first time via a nonintermediate-state-resonant pathway, has been used to study collisional broadening of the forbidden $6P_{1/2}$-$6P_{3/2}$ transition of atomic Tℓ. The tri-level echo technique, developed by us recently, has been employed to perform the most extensive study of the noble-gas-induced broadening of forbidden 3S-nS and 3S-nD transitions in Na. The two-pulse photon echo has been employed to study fundamental features of the collisional broadening of the 3S-$3P_{1/2}$ transitions in Na. Specifically, we have performed the first demonstration that the assumption of rectilinear collision trajectories is not in general correct even in the case of broadening of electronic transitions. An extensive theoretical treatment of rephasing processes in gases has been completed and published.

We have measured photon echo intensity as a function of pulse separation on the $^3H_4$-$^1D_2$ transtion in LaF_3:Pr^{3+} (1.0% at. wt.). We have also performed preliminary photon-echo-nuclear-double-resonance (PENDOR) experiments to measure nuclear hyperfine splittings in the $^3H_4$ ground state.

A single-threshold detector is derived for a wide class of classical binary decision problems involving the likelihood-ratio detection of a signal embedded in noise. The class of problems considered encompasses the case of

Block 20 continued - Abstract

multiple independent (but not necessarily identically distributed) observations of a nonnegative (or nonpositive) signal embedded in additive and independent noise, where the range of the signal and noise is continuous. It is shown that a comparison of the sum of the observations with a unique threshold comprises an optimum detector if a weak condition on the noise is satisfied independent of the signal. Examples of noise densities that satisfy and that violate this condition are presented. A sufficient condition on the likelihood ratio which implies that the sum of the observations is also a sufficient statistic is considered. This applies, in particular, to the case of heterodyne detection in the optical, infrared, and submillimeter where the signal, local oscillator, and noise can be treated as continuous random variables.

Statistical properties such as the cumulants, and the central, factorial, and ordinary moments are obtained for photocounting distributions when the incident radiation is intensity-modulated with arbitrary statistics. The results are applied in some detail to the cases of triangular, sinusoidal, and square-wave modulation of multimode superposed coherent and chaotic radiation. The coefficient of variation, skewness, and kurtosis are obtained as a function of modulation depth. Comparison is made with experimental data in the cases of triangular and sinusoidal modulation of a laser source. A computer simulation technique useful for generating superposed coherent and chaotic radiation of arbitrary spectral shape is described. Its advantages over other techniques include flexibility and ease of implementation, as well as the capability of incorporating spectral characteristics that cannot be generated by other methods. We discuss the implementation of the technique and present results to demonstrate its validity. The technique can be used to obtain numerical solutions to photon statistics problems through computer simulation. We argue that experiments involving photon statistics can be carried out using a wideband source in place of an amplitude-stabilized source whenever the spectral characteristics of the source are not important. Experimental results that corroborate the argument are presented.

We demonstrate the equivalence of detectors with and without nonparalyzable dead time in the presence of constant-intensity radiation and additive Poisson noise. We show that the performance of a detector with dead time will be the same as that of a similar detector without dead time used under exactly the same conditions, with the same threshold number of counts and sampling time, and the same radiation intensity, but with a reduced quantum efficiency. This result is valid in general whenever a detector with dead time is used in conjunction with a Poisson point process.

Experimental and theoretical studies of electronic carrier transport and optoelectronic processes at interfaces between semiconductors, insulators and metals are presented. The particular investigations reported here are internal photoemission mechanisms at metal-germanium interfaces, the dependence of capture cross sections of $Si-SiO_2$ interface states on energy, and energy band discontinuities in semiconductor heterojunctions.

Block 19 continued - Key Words

Energy transfer
Vibrations
COF_2
OCS
SO_2
O_2
Nozzle
Vibrational temperature
Metastable
Photofragmentation
Picosecond
Laser
Raman
Photolysis
Benzene
Electron Solvation
Alcohols
Pulse radiolysis
Photodissociation
Diphenyl carbene
Fluorescence
Rydberg states
Collisional broadening
Grating echoes
Tri-level echoes
Raman echoes
Phase-matching
Photon echoes
Photon echo nuclear double resonance
Heterodyne detection
Single-threshold detection
Infrared detection
Likelihood-ratio detection
Submillimeter detection
Statistical properties
Photon counting
Wave noise
Optical detection
Dead time
Photon count antibunching
Optical communications
Optical radar
Metal-Germanium interfaces
$Si-SiO_2$ interfaces
Semiconductor heterojunctions
Interface states
Internal photoemission

TABLE OF CONTENTS

PUBLICATIONS AND REPORTS

Publications

N. D. Bhaskar, E. Zouboulis, T. McClelland, and W. Happer, "New Infrared Absorption Bands of Alkali Vapors," Phys. Rev. Lett. 42, 640 (1979). (AROD and JSEP-Work Unit 3)

N. D. Bhaskar, E. Zouboulis, R. Novak, and W. Happer, "Laser-Excited Cross Fluorescence Emission from Cesium Molecules," Chemical Phys. Lett. 63, 555 (1979). (AROD and JSEP-Work Unit 3)

N. D. Bhaskar, M. Hou, B. Suleman, and W. Happer, "Propagating, Optical-Pumping Wave Fronts," Phys. Rev. Lett. 43, 519 (1979). (AFOSR and JSEP-Work Unit 1)

R. Novak, N. D. Bhaskar, and W. Happer, "Infrared Emission Bands from Transitions Between Excited States of Cesium-Noble Gas Molecules," J. Chem. Phys. 71, 4052 (1979). (AROD)

J. Liran, J. Pietras, J. Camparo, and W. Happer, "Optical Pumping of Cesium Atoms with Second Resonance Light," Opt. Comm. 31, 169 (1979). (NSF and AFOSR)

I. Shamah and G. W. Flynn, "Laser Catalyzed Translation to Vibration Energy Conversion in CH_3F/O_2 Mixtures," J. Chem. Phys. 70, 4928 (1979). (NSF and JSEP-Work Units 4 and 5)

A. C. Tam, "Optical Pumping of a Dense Na+He+N_2 System: Application as an rf Spectrum Analyzer," J. Appl. Phys. 50, 1171 (1979). (AFOSR)

A. C. Tam, "Absorption Bands in a CsHe System Associated with Forbidden Cs Atomic Transitions," J. Chem. Phys. 69, 4753 (1979). (AFOSR)

A. Flusberg, R. Kachru, T. Mossberg, and S. R. Hartmann, "Foreign-gas-induced Relaxation of Rydberg S and D States in Atomic Sodium," Phys. Rev. A 19, 1607 (1979). (ONR and JSEP-Work Unit 10)

Y. C. Chen, K. Chiang, and S. R. Hartmann, "Photon Echo Relaxation in $LaF_3:Pr^{3+}$," Opt. Comm. 29, 1818 (1979). (NSF and JSEP-Work Unit 11)

T. Mossberg, A. Flusberg, R. Kachru, and S. R. Hartmann, "Total Scattering Cross Section for Na on He Measured by Stimulated Photon Echoes," Phys. Rev. Lett. 42, 1665 (1979). (ONR and JSEP-Work Unit 10)

R. Kachru, T. W. Mossberg, and S. R. Hartmann, "Stimulated Photon Echo Study of $Na(3^2S_{1/2})$-CO Velocity-Changing Collisions," Opt. Comm. 30, 57 (1979). (ONR and JSEP-Work Unit 10)

T. W. Mossberg, R. Kachru, E. Whittaker, and S. R. Hartmann, "Temporally Recurrent Spatial Ordering of Atomic Population in Gases: Grating Echoes," Phys. Rev. Lett. 43, 851 (1979). (ONR and JSEP-Work Unit 10)

R. Kachru, T. W. Mossberg, E. Whittaker, and S. R. Hartmann, "Optical Echoes Generated by Standing-Wave Fields: Observations in Atomic Vapors," Opt. Comm. 31, 223 (1979). (ONR and JSEP-Work Unit 10)

T. W. Mossberg, R. Kachru, and S. R. Hartmann, "Echoes in Gaseous Media: A Generalized Theory of Rephasing Phenomena," Phys. Rev. A 20, 1976 (1979). (ONR and JSEP-Work Unit 10)

P. R. Prucnal and M. C. Teich, "Single-Threshold Detection of a Random Signal in Noise with Multiple Independent Observations: 2. Continuous Case," IEEE Trans. Inform. Theory IT-25, 213 (1979). (JSEP-Work Unit 12)

M. C. Teich, Review of B. Saleh's Book entitled "Photoelectron Statistics," Am. Scientist 67, 371 (1979). (NSF and JSEP-Work Unit 13)

P. R. Prucnal and M. C. Teich, "Statistical Properties of Counting Distributions for Intensity-Modulated Sources," J. Opt. Soc. Am. 69, 539 (1979). (NSF and JSEP-Work Unit 13)

G. Vannucci and M. C. Teich, "Equivalence of Threshold Detection with and without Dead Time," Appl. Opt. 18, 3886 (1979). (JSEP-Work Unit 14)

M. C. Teich and G. Lachs, "A Neural Counting Model Incorporating Refractoriness and Spread of Excitation: I. Application to Intensity Discrimination," J. Acoust. Soc. Am. 66, 1738 (1979). (NIH)

P. R. Prucnal and M. C. Teich, "An Increment Threshold Law for Sources of Arbitrary Statistics," J. Opt. Soc. Am. 69, 1433 (1979). (NSF)

M. C. Teich, P. R. Prucnal, G. Vannucci, M. E. Breton, and W. J. McGill, "Role of Quantum Fluctuations and the Neyman Type-A Distribution in Human Vision," J. Opt. Soc. Am. 69, 1469 (1979). (NSF and NIH)

H. C. Card and R. W. Ulmer, "On the Temperature Dependence of Subthreshold Currents in MOS Electron Inversion Layers," Solid State Electron. 22, 463 (1979). (NSF and JSEP-Work Unit 15)

M. C. Teich and H. C. Card, "Photocounting Distributions for Exponentially Decaying Sources," Optics Lett. 4, 146 (1979). (JSEP-Work Unit 13)

H. C. Card and K. K. Ng, "Tunneling in Ultrathin SiO_2 Layers on Silicon: Comments on Dispersion Relations for Electrons and Holes," Solid St. Commun. 31, 877 (1979). (DOE and JSEP-Work Unit 15)

H. C. Card, "Spectroscopy of Si-SiO_2 Interface States using MOS Tunneling Structures," Solid St. Electron. 22, 809 (1979). (JSEP-Work Unit 15)

T. C. Poon and H. C. Card, "Incorporation of Bromine into Si-SiO_2 Interfaces and Effects on Interface State Distribution," Elec. Lett., 15, 756 (1979). (JSEP-Work Unit 15)

H. C. Card, "Electrostatic Effects of Interface States on Carrier Transport in Semiconductor Heterojunctions," J. Applied Physics, 50, 2822 (1979) (JSEP-Work Unit 15)

E. Y. Chan, H. C. Card, E. S. Yang, A. R. Kerr, and R. J. Mattauch, "Transport of Majority and Minority Carriers in 2-μm-Diameter Pt-GasAs Schottky Barriers," IEEE, Ed-26, 214 (1979). (JSEP-Work Unit 15)

E. Zouboulis, N. D. Bhaskar, A. Vasilakis, and W. Happer, "New Infrared Absorption Bands of Cesium Vapor," J. Chem. Phys. 72, 2356 (1980). (AROD and AFOSR)

Rekha Sapre Sheorey and George Flynn, "Collision Dynamics of Intermode Energy Flow in Laser Pumped Polyatomic Molecules: CH_3F," J. Chem. Phys. 72, 1175 (1980). (NSF and JSEP-Work Units 4 and 5)

George W. Flynn, "Collision Induced Intermode Energy Transfer in Small Molecules," Spectroscopy in Chemistry and Physics: Modern Trends, ed., F. J. Comes, A. Müller, and W. J. Orville-Thomas, Elsevier, 1980, pp. 197-205. (NSF and JSEP-Work Units 4 and 5)

T. W. Mossberg, R. Kachru, and S. R. Hartmann, "Observation Velocity Changes Associated with Atoms in a Superposition of Dissimilar Electronics States," Phys. Rev. Lett. 44, 73 (1980). (ONR and JSEP-Work Unit 10)

R. Kachru, T. W. Mossberg, and S. R. Hartmannm "Noble-gas-induced Broadening of Transitions to Rydberg S and D States in Atomic Sodium," Phys. Rev. A 21, 1124 (1980). (ONR and JSEP-Work Unit 10)

Y. C. Chen, K. Chiang, and S. R. Hartmann, "Spectroscopic and Relaxation Character of the ^3P-$^3H_4$ Transition in LaF_3:Pr^{3+} Measured by Photon Echoes," Phys. Rev. B 21, 40 (1980). (NSF and JSEP-Work Unit 11)

G. Vannucci, and M. C. Teich, "Computer Simulation of Superposed Coherent and Chaotic Radiation," Appl. Opt. 19, 548 (1980). (NSF and JSEP-Work Unit 13)

E. Y. Chan and H. C. Card, "Infrared Optoelectronic Properties of Metal-Germanium Schottky Barriers," IEEE Trans. on Electron Dev., Special issue on Infrared Materials and Devices, ED-27, 78 (1980). (JSEP-Work Unit 15)

E. Y. Chan, H. C. Card, and M. C. Teich, "Internal Photoemission Mechanisms at Interfaces Between Germanium and Thin Metal Films," IEEE J. Quantum Elec. QE-16, 373 (1980). (JSEP-Work Unit 15)

H. C. Card, "Tunneling MIS Structures," Chap. 3 of Insulating Films on Semiconductors, Inst. of Physics, London, p. 140 (1980). (DOE and JSEP-Work Unit 15)

P. Panayotatos and H. C. Card, "Recombination in the Space-Charge Region of Schottky Barrier Solar Cells," Solid St. Electron. 23, 41 (1980). (DOE)

W. Hwang, H. C. Card, and E. S. Yang, "Transition with Grain Size from Electrode-Limited to Bulk-Limited Conduction in Polycrystalline Semiconductors," Appl. Phys. Lett. 36, 315 (1980). (DOE)

N. Lifshitz, A. Jayaraman, R. A. Logan, and H. C. Card, "The Pressure and Compositional Dependence of the Hall Coefficient, in $Al_xGa_{1-x}As$ and its Significance," Phys. Rev. B 21, 670 (1980). (Bell Labs.)

E. S. Yang, C. M. Wu, and R. Y. Hung, "Variation of the Ideality Factor in the Current-Voltage Characteristics of Double Heterostructure Diodes," J. Appl. Phys. 51, 1262 (1980). (JSEP-Work Unit 15)

Eric Weitz and George Flynn, "Vibrational Energy Flow in the Ground Electronic States of Polyatomic Molecules," Advances in Chemical Physics (1980), in press. (NSF and JSEP-Work Units 4,5 and 6)

D. R. Coulter, F. R. Grabiner, L. M. Casson, G. W. Flynn, and R. B. Bernstein, "Laser Pumping of SF_6 in the Collisional Region of a Nozzle Beam: Bolometric Detection of Internal Excitation," J. Chem. Phys. 72, (1980), in press. (NSF, DOE and JSEP-Work Units 4,5 and 6)

Irwin Shamah and George Flynn, "Vibrational Relaxation Induced Population Inversions in Laser Pumped Molecules," Chem. Phys. (1980), in press. (NSF and JSEP-Work Units 4 and 5)

Marsha Isack Lester and George W. Flynn, "Intermolecule Vibrational Energy Transfer Dynamics in IR Laser Pumped $SO_2/^{18}O_2$ Mixtures," J. Chem. Phys. 72, (1980), in press. (NSF and JSEP-Work Units 4 and 5)

M. L. Mandich and G. W. Flynn, "Vibrational Energy Transfer Map for OCS," J. Chem. Phys. 73, (1980), in press. (NSF and JSEP-Work Units 4 and 5)

E. Y. Chan and H. C. Card, "Near Infrared Interband Transitions and Optical Parameters of Metal-Germanium Contacts," Applied Optics, (1980), in press.(JSEP-Work Unit 15)

K. K. Ng and H. C. Card, "A Comparison of Majority Carrier and Minority Carrier Silicon MIS Solar Cells," IEEE Trans. on Electron Devices, Special Issue on Photovoltaic Devices (1980), in press. (DOE)

K. K. Ng and H. C. Card, "Asymmetry in the SiO_2 Tunneling Barriers to Electrons and Holes," J. Appl. Phys. (1980), in press.(DOE and JSEP-Work Unit 15)

K. K. Ng and H. C. Card, "Image Force Effects on the Short Wavelength (UV) Photoresponse of Schottky Barriers," Phys. Chem. Solids, (1980), in press.(DOE and JSEP-Work Unit 15)

H. C. Card and W. Hwang, "On the Transport Theory of Schottky Barriers

to Polycrystalline Silicon Thin Films," IEEE Trans. on Electron Dev., Special Issue on Photovoltaic Devices (1980), accepted for publication. (DOE)

C. M. Wu, E. S. Yang, W. Hwang, and H. C. Card, "Grain Boundary Effects on the Electrical Behavior of Al-PolySi Schottky Barrier Solar Cells," submitted to IEEE Trans. on Electron Dev., Special Issue on Photovoltaic Devices (1980). (DOE)

H. C. Card and W. Hwang, "Minority Carrier Injection in Dark Metal-Polycrystalline Silicon Contacts," IEEE Proceedings I: Solid State and Electron Devices, (1980), in press.(DOE)

T. C. Poon and H. C. Card, "Admittance Measurements of Si-SiO_2 Interface States under Optical Illumination," J. Appl. Phys., to be published. (JSEP-Work Unit 15)

W. Hwang and H. C. Card, "Comments on Conduction Mechanisms of Metal-Nondegenerate Semiconductor Contacts" to be published.(JSEP-Work Unit 15)

C. M. Wu and E. S. Yang, "Current Suppression Induced by Conduction-Band Discontinuity in $Al_{0.35}Ga_{0.65}As$-GaAs N-p Heterojunction Diodes," J. Appl. Phys., in press.(JSEP-Work Unit 15)

N. D. Bhaskar, J. Pietras, J. Camparo, and W. Happer, "Spin Destruction in Collisions between Cesium Atoms," submitted for publication. (NSF and AFOSR)

G. Brink, A. Glassman, and R. Gupta, "Life Time Measurement of $(5d\ 6P)^3D_3$ State of Barium by Dye-Laser Spectroscopy," submitted for publication. (JSEP-Work Unit 1)

Ying Wang, M. Crawford, M. McAuliffe and K. B. Eisenthal, "Picosecond Laser Studies of Electron Solvation in Alcohols," Accepted for Publication by Chem. Phys. Lett. (NSF, NIH, and JSEP-Work Unit 8)

M. L. Mandich and G. W. Flynn, "Collisional Relaxation of Vibrationally Excited OCS in Rare Gas Mixtures," J. Chem. Phys., submitted. (NSF and JSEP-Work Units 4,5 and 6)

Rekha Sapre Sheorey and George Flynn, "$HF^{\dagger}$ Emission as a Probe of IR Multiphoton Dissociation of Carbonyl Fluoride," Chem. Phys., submitted. (NSF, DOE and JSEP-Work Unit 6)

Papers by CRL Staff Members Presented at Scientific Meetings

R. K. Bohn, K. Casleton, Y. V. Rao, and G. W. Flynn, "Energy Transfer in Laser Excited COF_2," American Physical Society Meeting, New York, New York, March 18, 1980.

H. C. Card and K. K. Ng, "Experimental Determination of Electron and Hole Tunneling Barriers of Ultrathin SiO_2 Films in MOS Structures," Semiconductor Interface Specialists Conference, New Orleans, Louisiana, November 29 - December 2, 1979

H. C. Card, "Carrier Transport Across Metal-Semiconductor and MIS Interfaces," Invited Paper, American Chemical Society Meeting, Houston, Texas, March 23-28, 1980.

H. C. Card, "Tunneling MIS Structures," Invited Paper, Institute of Physics Conference on Insulating Films on Semiconductors, Durham, England, July 2-4, 1979.

D. Coulter, "Laser Pumping of SF_6 in the Collisional Region of a Nozzle Beam: Bolometric Detection of Internal Excitation," American Physical Society Meeting, New York, New York, March 26, 1980.

K. Eisenthal, "Picosecond Laser Studies of Proton Transfer", Gordon Research Conference on Organic Photochemistry, Andover, New Hampshire, July 23-27,1979.

K. Eisenthal, "Picosecond Laser Studies in Chemistry and Biology", Picosecond Phenomena Symposium, NIH, Bethesda, Maryland, October 3-5, 1979.

K. Eisenthal, "Laser Studies and Ultrafast Phenomena in Chemistry", United States-France Meeting on Lasers in Chemistry, University of Pennsylvania, Philadelphia, Pa., November 26-28, 1979.

G. W. Flynn, "Collision Induced Intermode Energy Transfer in Small Molecules," European Congress on Molecular Spectroscopy, Frankfurt, Germany, September 5, 1979.

G. W. Flynn, "Collision Induced Intermode Energy Transfer in Small Molecules," American Chemical Society Meeting, Symposium on Large Molecule Dynamics, Washington, D.C., September 13, 1979.

S. R. Hartmann, "Grating Echoes," 10th Winter Colloquium on Quantum Electronics, Snowbird, Utah, January 14, 1980.

W. Hwang, E. S. Yang, and H. C. Card, "Current Transport Mechanisms of Metal-Polycrystalline Semiconductor Schottky Barrier Solar Cells," 14th IEEE Photovoltaic Specialists Conference, San Diego, California, January 7-10, 1980.

R. Kachru, "Carbon Monoxide-Induced Broadening of Forbidden 3S-Rydberg S (and D) Transitions in Na," Annual Meeting of the Optical Society of America, Rochester, New York, October 9, 1979.

M. Lester, "Vibrational Temperature Measurements in COF_2," American Physical Society Meeting, New York, New York, March 26, 1980.

M. Mandich, "Vibrational Energy Transfer Map for OCS," American Chemical Society Meeting, Washington, D.C., September 14, 1979.

T. W. Mossberg, "Relaxation of Rydberg S and D States in Atomic Sodium Perturbed by He, Ne, Ar, Kr or Xe," International Conference on the Physics of Electronic and Atomic Collisions (ICPEAC), Kyoto, Japan, August 29 - September 4, 1979.

T. W. Mossberg, "Stimulated Photon Echo Measurements of Atom-Atom Elastic Scattering in Buffered Atomic Vapors," International Conference on Physics of Electronic and Atomic Collisions (ICPEAC), Kyoto, Japan, August 29 - September 4, 1979.

T. W. Mossberg, "Noble-gas-induced Broadening of Transitions to Rydberg S and D States in Na," Symposium on Atomic Spectroscopy (SAS-79), University of Arizona, Tucson, Arizona, September 10, 1979.

T. W. Mossberg, "Study of Velocity-Changing Collisions (VCC) in Atomic Vapors by Stimulated Photon Echoes," American Physical Society Meeting, Washington, D.C., April 23-26, 1979.

K. K. Ng and H. C. Card, "Photocurrent and Photovoltage Mechanisms in Silicon Schottky Barrier and MOS Solar Cells," IEEE International Electron Dev. Mtg., Washington, D.C., December 5-7, 1979.

R. Novak, N. Bhaskar, and W. Happer, "Infrared Excimer Emission Bands from Tranaitions Between Excited States of Cesium-Noble Gas Molecules," Optical Society of America Topical Meeting on Excimer Lasers, Charleston, South Carolina, September 11-13, 1979.

J. Pietras, "Spin Relaxation Measurements in High Density Cesium Vapor Optically Pumped by Second Resonance Light," American Physical Society Meeting, New York, New York, March 24, 1980.

M. C. Teich, "The Neyman Type-A Distribution in Photon Counting, Nuclear Counting, and Neural Counting," Meeting of the NSF Grantee-User Group in Optical Communication Systems, Pasadena, California, June 1979.

M. C. Teich and P. R. Prucnal, "An Increment Threshold Law for Sources of Arbitrary Statistics," Annual Meeting of the Optical Society of America, Rochester, New York, October 1979.

M. C. Teich, P. R. Prucnal, G. Vannucci, M. E. Breton, and W. J. McGill, "Role of Quantum Fluctuations and the Neyman Type-A Distribution in Human Vision," Annual Meeting of the Optical Society of America, Rochester, New York, October 1979.

C. M. Wu and E. S. Yang, "A Study of Polysilicon Grain Boundaries using Schottky Barriers, "IEEE International Electron Dev. Mtg., Washington, D.C., December 3-5, 1979.

E. S. Yang, D. Dove, I. F. Chang, and M. Shafer, "Electron Trap Distribution in $AlPO_4$-Substituted Zn_2SiO_4," Electronic Materials Conference, Boulder, Colorado, June 27, 1979.

Lectures

H. C. Card, "Solid State and Optical Electronics at Columbia University," Columbia Engineering Affiliates 1979 Conference, School of Engineering and Applied Science, Columbia University, March 23, 1979.

H. C. Card, "Optical Excitation of Metal-Semiconductor Contacts," Department of Solid State Electronics, University of Manchester, Inst. of Science & Technology, June 21, 1979.

H. C. Card, "Device Physics and an Outlook for VLSI", University of Manitoba, Winnipeg, Canada, January 14, 1980.

D. Coulter, "Infrared Laser Pumping of SF_6 in the Collisional Region of a Molecular Beam," Brookhaven National Laboratory, Upton, New York, March 3, 1980.

K. Eisenthal, "Picosecond Laser Studies of Ultrafast Processes," Solid State Physics Seminar, Cornell University, Ithaca, New York, December 5, 1978.

K. Eisenthal, "Picosecond Laser Studies of Ultrafast Chemical and Physical Processes, "Colloquium, Department of Chemistry,Pennsylvania State University, University Park, Pennyslvania, February 15, 1979; Seminar, Department of Chemistry, Dartmouth College, Hanover, New Hampshire, May 3, 1979; Seminar, Department of Chemistry, Brooklyn College, Brooklyn, New York, May 9, 1979.

K. Eisenthal, "Picosecond Laser Studies of Excited State Proton Transfer," Physical Chemistry Seminar, University of California, Berkeley, California, March 13, 1979; Seminar, Department of Chemistry, University of California at Los Angeles, Los Angeles, California, March 16, 1979.

G. W. Flynn, "Vibrational Excitation in Small Molecules: The Weak and Strong Pumping Limits," Brown University, Providence, Rhode Island, May 11, 1979; Centre National de la Recherche Scientifique, Paris, France, July 24, 1979; University of Pittsburgh, Pittsburgh, Pennsylvania, January 31, 1980; Yale University, New Haven, Connecticut, February 25, 1980.

W. Happer, "Alkali Xenide Molecules, "Colloquium, Department of Physics, Stevens Institute of Technology, Hoboken, New Jersey, December 12, 1979.

W. Happer, "Laser Studies of Spin Polarized Atomic Vapors," Colloquium, Department of Physics, Columbia University, New York, New York, January 25, 1980.

S. R. Hartmann, "Echoes for Everyone," Seminar, California Institute of Technology, Pasadena, California, January 8, 1980; Colloquium,Columbia University, New York, New York, February 15, 1980; Seminar, National Research Council, Ottawa, Canada, February 20, 1980; Colloquium, Naval Research Laboratory, Washington, D.C., February 29, 1980; Seminar, Bell Telephone Laboratories, Holmdale, New Jersey, February 28, 1980; Colloquium, City University of New York, New York,March 5, 1980.

R. Novak, "Scientific Views on the Energy Crisis," Honors Colloquia, Iona College, New Rochelle, New York, March 19, 1980.

P. Prucnal, "A New Statistical Decision Theory Model for Signal Processing," Invited Research Seminar, Rice University, Houston, Texas, April 1979.

M. C. Teich, "Photon Counting in Optical Communications and Laser Radar," Seminar, United States Army Missile Research and Development Command, Redstone Arsenal, Alabama, May 1979.

M. C. Teich, "Neural Counting in Vision and Hearing," Research Seminar in Vision and Hearing, Department of Psychology, Harvard University, Cambridge, Massachusetts, November 1979.

M. C. Teich, "Neural Counting in Vision and Audition," Bioengineering Seminar, University of California, Berkeley, California, January 1980; Research Seminar, Syracuse University Institute for Sensory Research, Syracuse, New York, March 1980.

M. C. Teich, " Infrared Heterodyne Detection Theory and Application Survey," Invited Plenary Lecture, NASA International Conference on Heterodyne Systems and Technology, Williamsburg, Virginia, March 1980.

E. S. Yang, "Electron Traps and Non-Radiative Processes in Mn-Activated Zn_2SiO_4 Crystals," IBM Watson Research Center, New York, New York, May 21, 1979.

Resonance Seminars

Meetings are held periodically at Columbia University, New York, New York during the academic year and are open to all members of the New York Scientific community. Guest speakers are invited to discuss work in the general area of the research in the Columbia Radiation Laboratory.

Jonathan Heritage, Bell Laboratories, "Picosecond Raman Studies of Vibrational Relaxation in Liquids and on Surfaces", April 6, 1979.

Frederic Davidson, John Hopkins University, "Photon Absorption in Metal-Insulator-Metal Diodes", September 28, 1979.

Henry Lee, University of Stuttgart, Stuttgart, West Germany, "Probing Reaction Dynamics by Laser Induced Fluorescence", October 3, 1979.

M. El-Sayed, University of California, "Time Resolved Laser Studies on Energy Transfer and Conformational Changes", October 5, 1979.

Daniel D. Konowalow, S.U.N.Y. at Binghamton, "Better Lasers for Better Spectroscopy Through Quantum Mechanics", October 12, 1979.

Robert Pecora, Stanford University. "Dynamic Light Scattering from Macromolecules", October 17, 1979.

Carl Lineberger, University of Colorado, "Laser Photoelectron Spectrosocopy of Negative Ions and Small Free Radicals", October 18, 1979.

Frank Fang, IBM Watson Research Center, "Effects of Uniaxial Pressure on Energy Bands at Si-SiO_2 Interfaces", November 2, 1979.

Ahmed Zewail, California Institute of Technology, "Ultra Fast Relaxation of Large Molecules: Do We Really Understand Them?", December 6, 1979.

Steven E. Schwarz, University of California - Berkeley, "Infrared Electronics", December 7, 1979.

C. V. Shank, Bell Laboratories, "Surface Enhanced Raman Scattering of Molecules on a Metal Surface in High Vacuum" and "Picosecond Spectroscopy of Semiconductors", March 7, 1980.

Azi Genack, Exxon Research Laboratories, "CW and Transient Spectroscopy of Laser Induced Holes in Optical Absorption Lines", March 13, 1980.

Reinhard Neumann, Harvard University & Erstes Physikalisches Institut, Heidlberg, "High Resolution Dye Laser Spectroscopy in Ca and $Li^{+"}$, March 27, 1980.

I. ENERGY TRANSFER AND RELAXATION IN ALKALI METALS

A. NUCLEAR SPIN POLARIZATION OF Xe BY OPTICAL PUMPING*

(B. Suleman, T. McClelland, W. Happer)

It is well known[1] that an alkali atom can exchange its electronic angular momentum with the nuclear spin of a noble gas atom in an alkali-noble gas collision. The polarization of optically pumped alkali vapor can be transferred to the noble gas nuclei by these spin exchange collisions. As much as 10 % polarization of Xe^{129} has been reported[2] by using Rb vapor of about 10 % polarization. We would like to polarize Xe by using optically pumped Na vapor. By using a laser instead of a conventional lamp to pump high density Na vapor, we expect to achieve considerable Xe polarization. In addition to measuring the spin exchange cross section, we also want to study the relaxation of polarized Xe.

The origin of the spin exchange process is the contact hyperfine interaction between the alkali valence electron and the noble gas nucleus.[3] The effective Hamiltonian governing this interaction can be written as

$$V = \gamma \vec{I} \cdot \vec{S} \qquad (1)$$

where $\vec{I}$ is nuclear spin of the noble gas, $\vec{S}$ is the electronic angular momentum of the alkali atom and γ is the strength of spin exchange interaction. During a collision, the spins $\vec{I}$ and $\vec{S}$ of the colliding pair rotate rapidly around the resultant angular momentum $\vec{I} + \vec{S}$. This tendency of the spin exchange collisions to rotate the spins can be represented by an effective magnetic field which produces a shift in the Zeeman resonance frequency of the alkali atoms. The frequency

shift can be written as

$$\Delta\omega_o = 2Z\ \phi\langle I_z\rangle \tag{2}$$

where $\langle I_z\rangle$ is the polarization of the noble gas and Z is the kinetic collision rate. ϕ is the total phase angle produced during a collision and averaged over all impact parameters. A very rough estimate of frequency shift is

$$\Delta\omega_o \approx 5.61 \times 10^3\ P\ \langle I_z\rangle\ \text{sec}^{-1}\text{torr}^{-1} \tag{3}$$

where P is the pressure of Xe in the cell. The nuclear polarization of Xe^{129} can be detected by measuring the frequency shift $\Delta\omega_o$ of the Na Zeeman resonance transitions.

The apparatus we are using for producing and detecting the nuclear polarization of Xe is shown in Fig. 1. Sodium D_1 resonance light from a Spectra Physics 370 dye laser is circularly polarized and pumps the Na vapor in a cell which contains about 2 torr of Xe, 500 torr of helium and a few torr of nitrogen. The strong pump beam is kept on for about 100 seconds. We estimate that during this time the Na-Xe spin exchange collisions will produce about 0.2 % Xe^{129} polarization.

For detecting the Xe polarization, the Na ensemble is operated as a magnetometer by applying a radio frequency field from a frequency synthesizer. The incident photon flux and the RF field strength are attenuated such that they do not cause appreciable broadening of the Zeeman resonance lines and yet give us a good signal to noise ratio. The variation of light intensity with RF field is shown in Fig. 2. The driving radio frequency

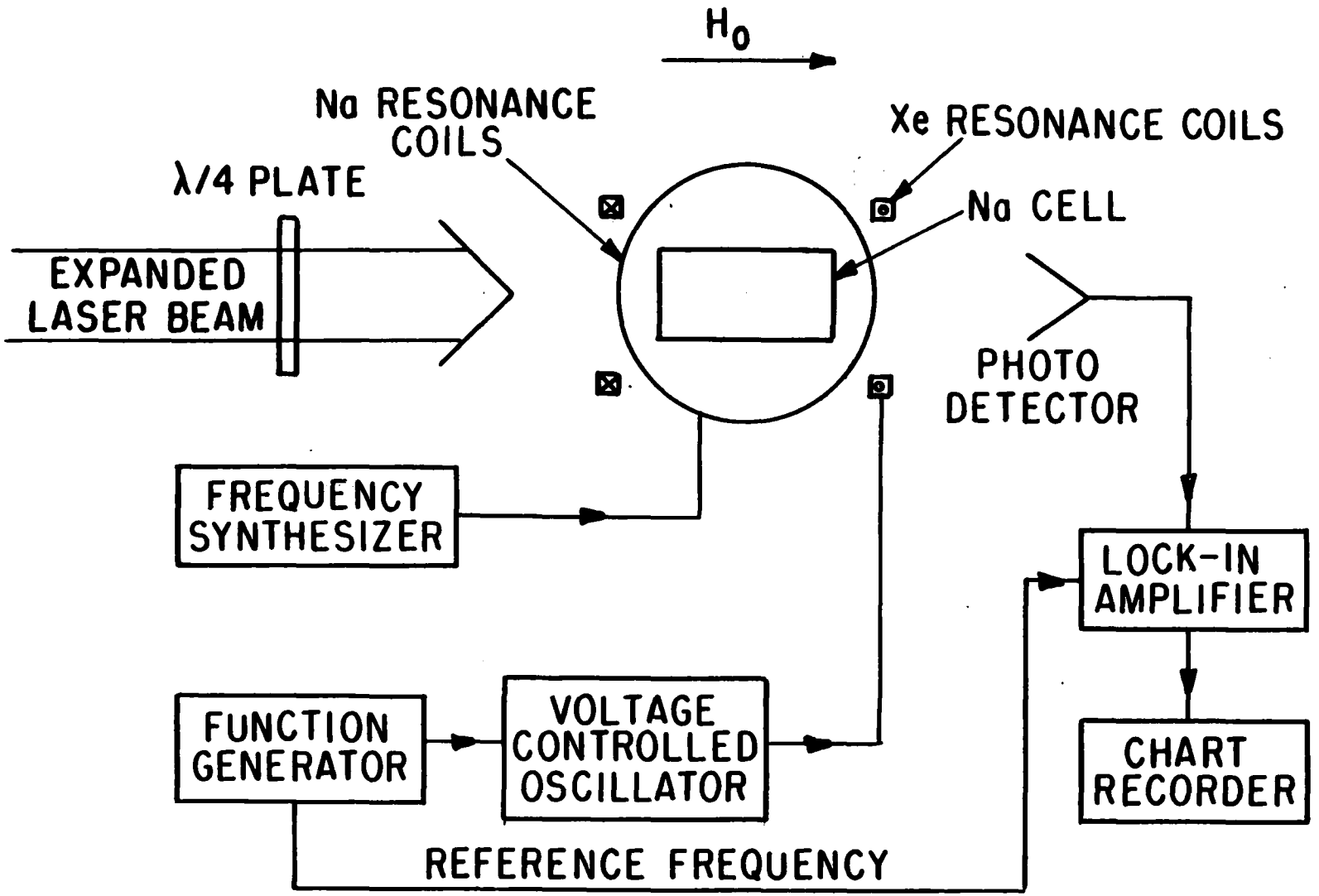

Figure 1: Frequency synthesizer produces the Na resonance frequency ω_1. The input of VCO is a triangular wave of frequency Ω produced by function generator. The frequency modulated output of VCO is fed to Xe coils.

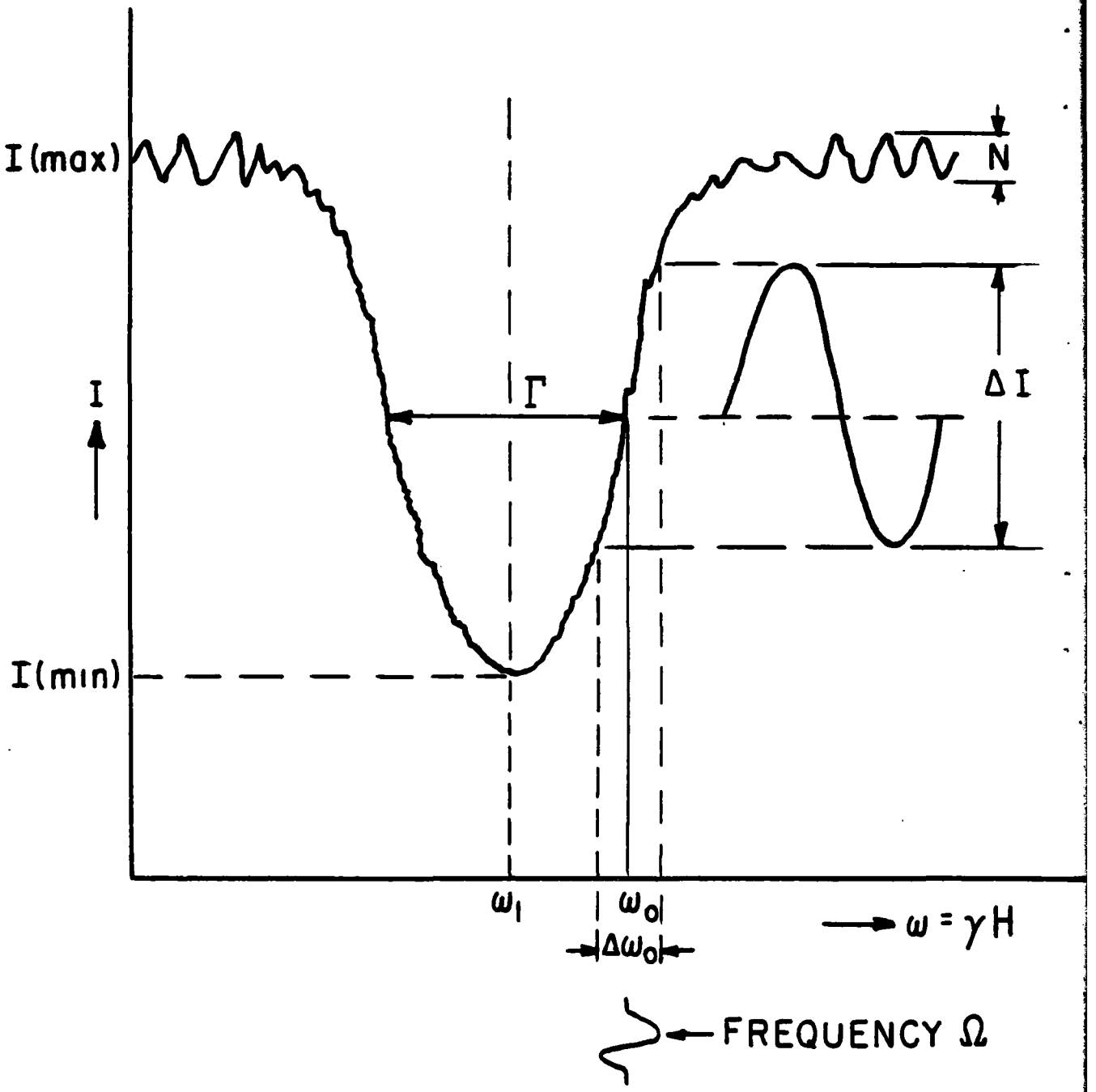

Figure 2: Signal ΔI due to frequency shift $\Delta\omega_o$ produced by adiabatic reversal of Xe spins at a rate Ω.

ω is set at the side of the line (Fig. 2) where the response of the system is maximum to variations in frequency. The Xe spins are now flipped parallel and antiparallel to the external magnetic field H_o by adiabatic fast passage. To do this an audio frequency oscillating field is applied perpendicular to H_o by a second set of Helmholtz coils. The voltage controlled oscillator produces a frequency modulation and the audio frequency field is swept through the xenon resonance frequency ($\sim$ 1.17 KHz/Gauss) at a fixed rate Ω. The adiabatic reversal of Xe spins modulates the transmitted light intensity at the same frequency Ω. The transmitted light is collected in a photodetector and is fed to a phase sensitive detector locked at frequency Ω. If we tune the frequency of the RF field to ω_o (Fig. 2), the half maximum point, then the signal ΔI is given by

$$\Delta I = \frac{\Delta\omega_o}{\Gamma} [I(max) - I(min)] \qquad (4)$$

where Γ is the full width at half maximum. For minimum detectable frequency shift $\Delta\omega(min)$, the signal ΔI has to be at least equal to noise N, so that

$$\Delta\omega(min) \geq N\Gamma / [I(max) - I(min)] \qquad (5)$$

Apart from laser noise N, the major source of noise is the fluctuation in the ambient magnetic field H_o. We are now planning to use mu-metal shields to get rid of magnetic noise. A preliminary Zeeman resonance curve is shown in Fig. 3. The noise N is mainly due to laser intensity fluctuations.

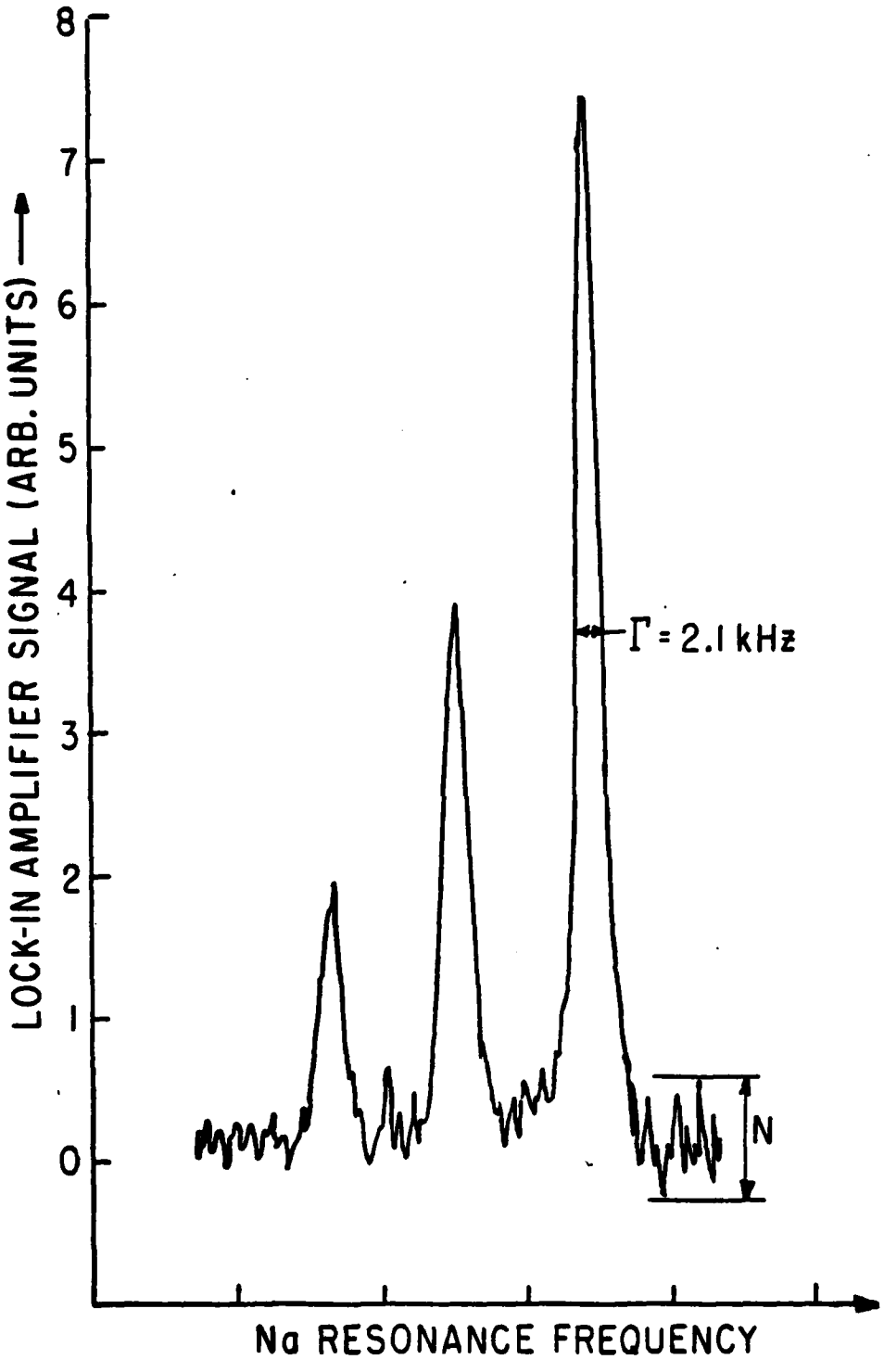

Figure 3: A chart recorder trace of resolved Zeeman lines obtained by sweeping H_o. Frequency synthesizer was kept at 3.0 MHz. The sweeping rate is about 10.6 KHz/division.

*This research was also supported by the Air Force Office of Scientific Research under Grant AFOSR-79-0082.

(1) M. A. Bouchiat, T. R. Carver, and C. M. Varnum, Phys. Rev. Lett. 5, 373 (1960).

(2) B. C. Grover, Phys. Rev. Lett. 40, 391 (1978).

(3) R. M. Herman, Phys. Rev. 137, A1576 (1964).

B. SPECTROSCOPY OF THE 5D STATE OF CESIUM*

(A. Sharma, W. Happer)

Most of the low lying states in cesium atoms have been studied with respect to their hyperfine structure. The 5D state is a conspicuous exception. Many of these states have, apart from the usual magnetic dipole and electric quadrupole interactions, additional splittings due to the polarization of the core of electrons by the single valence electron. It arises from the fact that two electrons with parallel spins have a different interaction than when they have antiparallel spins. This interaction is especially known to be very pronounced in the $nD_{5/2}$ states; so much that the magnetic dipole constant which by simplistic arguments ought to be greater than zero, actually turns out to be negative. Of the $D_{3/2}$ states we expect this effect to be most pronounced in the $5D_{3/2}$ state as it lies closest to the nucleus in the series of $D_{3/2}$ states and therefore most effective in polarizing the inner core of electrons.

We have discussed earlier[1] the problems in studying this state and the reasons why it could not be studied earlier. Since then we have made a number of computer calculations that make the experiment apparently feasible. For example, using a dye laser (Coherent Model #CR-599) we can selectively excite a few Zeeman states in the $5D_{3/2}$ level by tuning the frequency to an appropriate position in the absorption profile of cesium atoms. Figure 1 shows the absorption cross section of cesium atoms from ground state to the $7P_{1/2}$ state as a function of the single mode detuning, at 400°K with σ^+ light and with a magnetic field of 800 Gauss.

As mentioned in reference (1) we intend appl,ing a radiofrequency signal to cause transitions between the various Zeeman levels of the $5D_{3/2}$

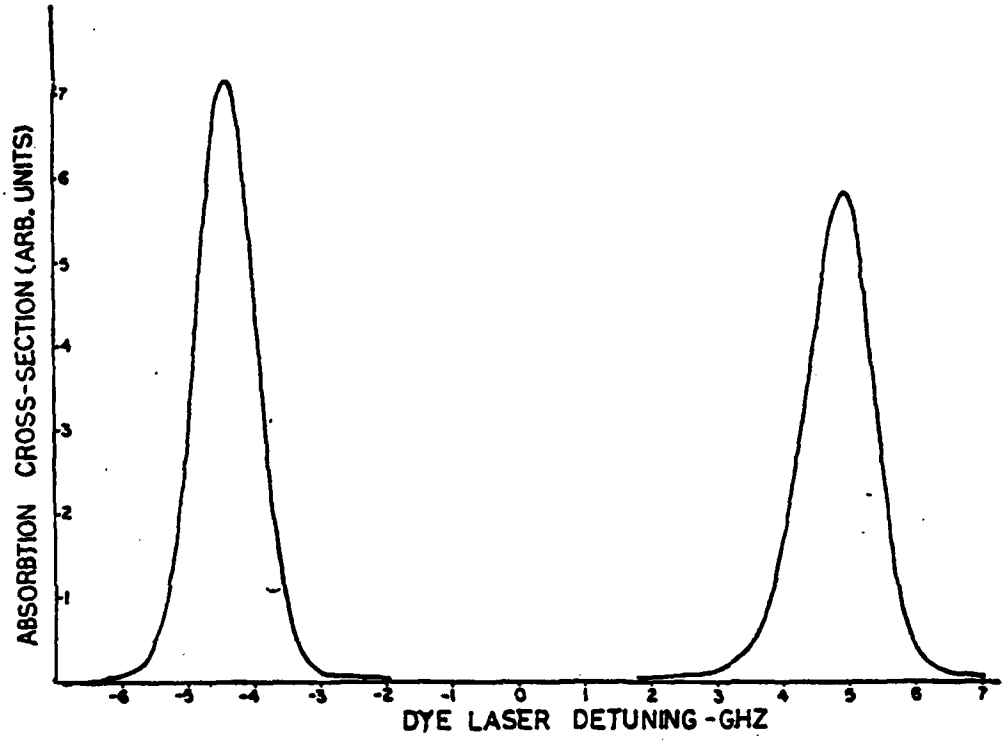
ABSORBTION CROSS-SECTION (ARB. UNITS)
1
2
3
4
5
6
7
-6
-5
-4
-3
-2
-1
0
1
2
3
4
5
6
7
DYE LASER DETUNING - GHZ

Figure 1

state and observe the change in the intensity of the fluorescent light. As an example, our calculations show that by tuning the dye laser to detuning position -5 Ghz in Figure 1, we can obtain a signal to background ratio of 3%. We are in the process of making preliminary measurements, like the amount of noise tolerable in the detection system (lead sulphide crystal cooled to 193°K) and also the temperature we can raise the cell to without destroying the polarization in the excited state by collisions.

*This research was also supported by the Army Research Office (Durham) under Contract DAAG29-80-C-0043.

(1) CRL Progress Report #29, March 31, 1979, p. 49.

C. INFRARED ABSORPTION OF ALKALI MOLECULES*

(A. Vasilakis, N. D. Bhaskar, W. Happer)

Previous progress reports discussed the new infrared absorption we discovered in potassium[1] and cesium[2] saturated vapors out to at least 2.5μ. Here we report on a recently completed study of infrared absorption in saturated sodium vapor. This study shows many similarities with potassium and cesium. The absorption from .83 to 1.18μ in saturated sodium vapor may be the analog of the ultraviolet emission continuum of H_2, possibly arising from the sodium dimer ($^3\Sigma_u^+ \rightarrow {}^3\Sigma_g^+$) transition, along with contributions from higher sodium polymers. At longer wavelengths out to 2.5μ the absorption is probably due to higher polymers of sodium (Na_3, Na_4, . . .).

A diagram of the experimental apparatus is shown in Figure 1. The length of the heat pipe is 2 m with an outside diameter of 25 mm and 3 mm wall thickness. A capillary structure of several turns of stainless steel mesh is used to return the condensed sodium liquid to the central heating region of the pipe. Helium buffer gas is used to protect the windows of the heat pipe from the hot alkali vapor. Water cooling is also applied to the ends of the heat pipe to condense the vapor before it reaches the windows. To measure the effective length of the vapor column (40–65 cm) in the heat pipe,[3] 45 thermocouples were used to measure the temperature profile along its length. Heating was provided by electrical heaters capable of supplying over 3 KW. Operating temperatures ranged from 630 to 870°C, pressure and temperature were found to agree within 10% with the empirical formula[4]

$$\mathrm{Log}_{10}\ P_{mm} = 7.4103 - \frac{5232.1}{T} \quad . \qquad (1)$$

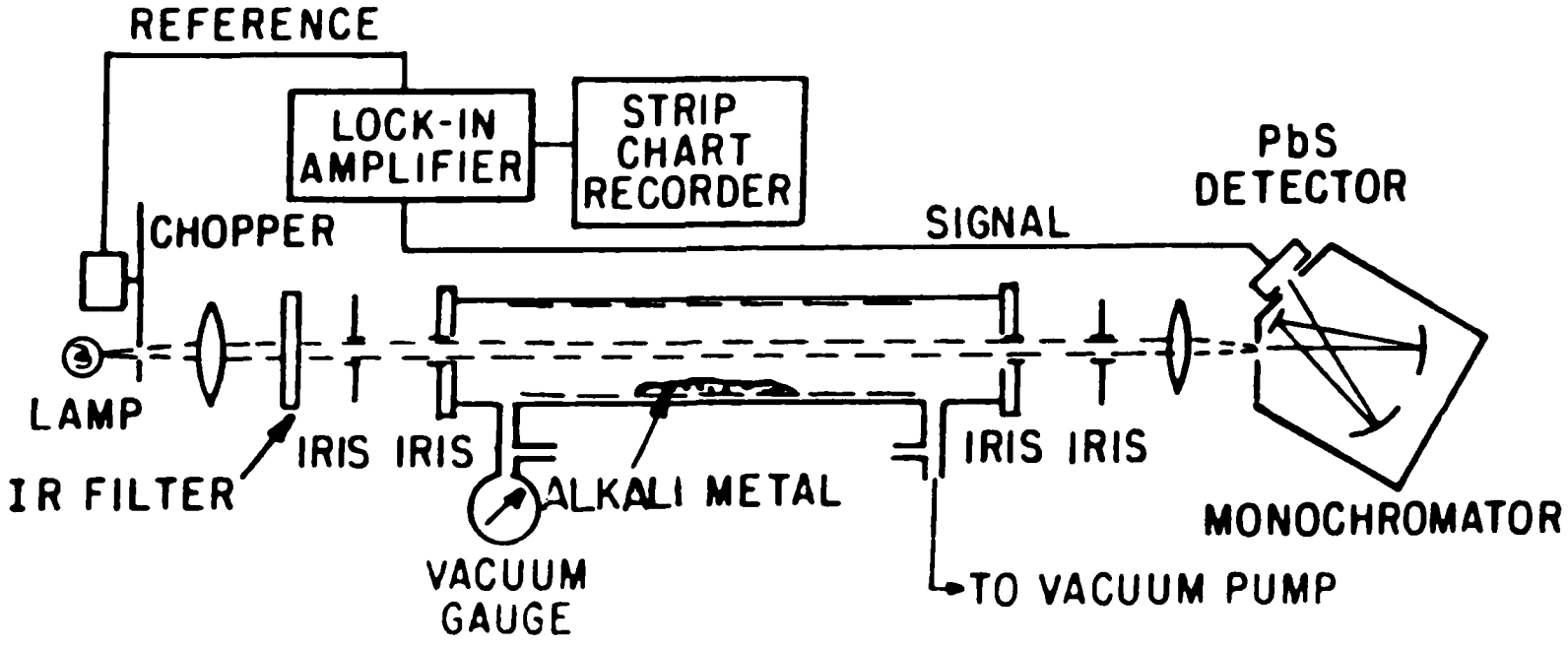

Figure 1: Apparatus used to measure the absorption coefficient of saturated sodium vapor.

The experimental procedure was as follows: the intensity $I(\lambda,T_o)$ of the light at wavelength λ at a temperature T_o transmitted through the heat pipe was measured where T_o is a temperature slightly above the melting point of sodium (no appreciable sodium vapor pressure). Then the intensity $I(\lambda,T)$ transmitted through the vapor is measured for different temperatures and the length Z of the vapor is determined by the temperature profile along the pipe. $I(\lambda,T_o)$ is then measured again; if it agrees with the first within a few percent, the data is used. We can then determine the attenuation coefficient $\alpha(\lambda,T)$ from

$$\alpha(\lambda,T) = Z^{-1} \ln [I(\lambda,T_o)/I(\lambda,T)] \qquad (2)$$

In addition, it is empirically found that the data fits the formula

$$\alpha(\lambda,T) = \exp[A(\lambda) - E(\lambda)/RT] \quad . \qquad (3)$$

The data can be graphed for $\ln \alpha(\lambda,T)$ versus $1/T$ and straight lines fitted to the data very well. The various contributions to the total absorption coefficient for various clusters of n sodium atoms are given by terms of the form

$$\alpha_n(\lambda,T) = b(\lambda) \quad N_{Na}^n \exp\left[\frac{-V(\lambda)}{RT} \right] \quad , \qquad (4)$$

where $V(\lambda)$ is the potential energy of association of n sodium atoms into a configuration for which an electronic transition of wavelength λ is possible. The number density of sodium atoms is N_{Na} and the factor $b(\lambda)$ contains oscillator strengths and phase-space factors.

Using the ideal-gas law and (1) we can rewrite Eq. (4) as

$$\alpha_n(\lambda,T) = C(\lambda) \quad \exp[-(n\varepsilon + V)] \ , \tag{5}$$

where ε is the latent internal energy of vaporization and is related to the latent heat ℓ by $\varepsilon = \ell - RT_r = 21.8$ kcal/mole. The value of ℓ is obtained from the Clausius-Clapeyron equation (1) yielding $\ell = 23.9$ kcal/mole, and $T_r = 1060.6°K$ is a typical value for the temperature. Comparing (3) and (5) we conclude that the activation energy $E(\lambda)$ is equal to the sum of the association energy V plus n factors of the vaporization energy ε,

$$E(\lambda) = n\varepsilon + V \ .$$

In Figure 2 a summary of our experimental data is shown, the attenuation coefficient $\alpha(\lambda,T)$ and the activation energy $E(\lambda)$ are plotted as a function of wavelength λ for $T = 1060.6°K$. The energies $2\varepsilon = 43.6$ and $3\varepsilon = 65.4$ kcal/mole are shown for reference in Figure 2.

For the region .84 to 1.02μ the activation energy is a little larger than we expected for absorption from the repulsive ground state, while that from 1.02 to 1.18μ has activation energies of the size one might expect for the repulsive ground state. A possible explanation for this is that trimers or higher polymers along with the $(^3\Sigma_u^+ \rightarrow {}^3\Sigma_g^+)$ transition of the dimer are responsible for absorption from .83 to 1.18μ. The activation energy after 1.18μ in saturated sodium vapor undergoes a rapid increase, similar to the behavior of potassium after 1.6μ. The jump in activation energy does not reach the 3ε level however as in the case of potassium vapor (Figure 2). We believe that bound trimers, or higher

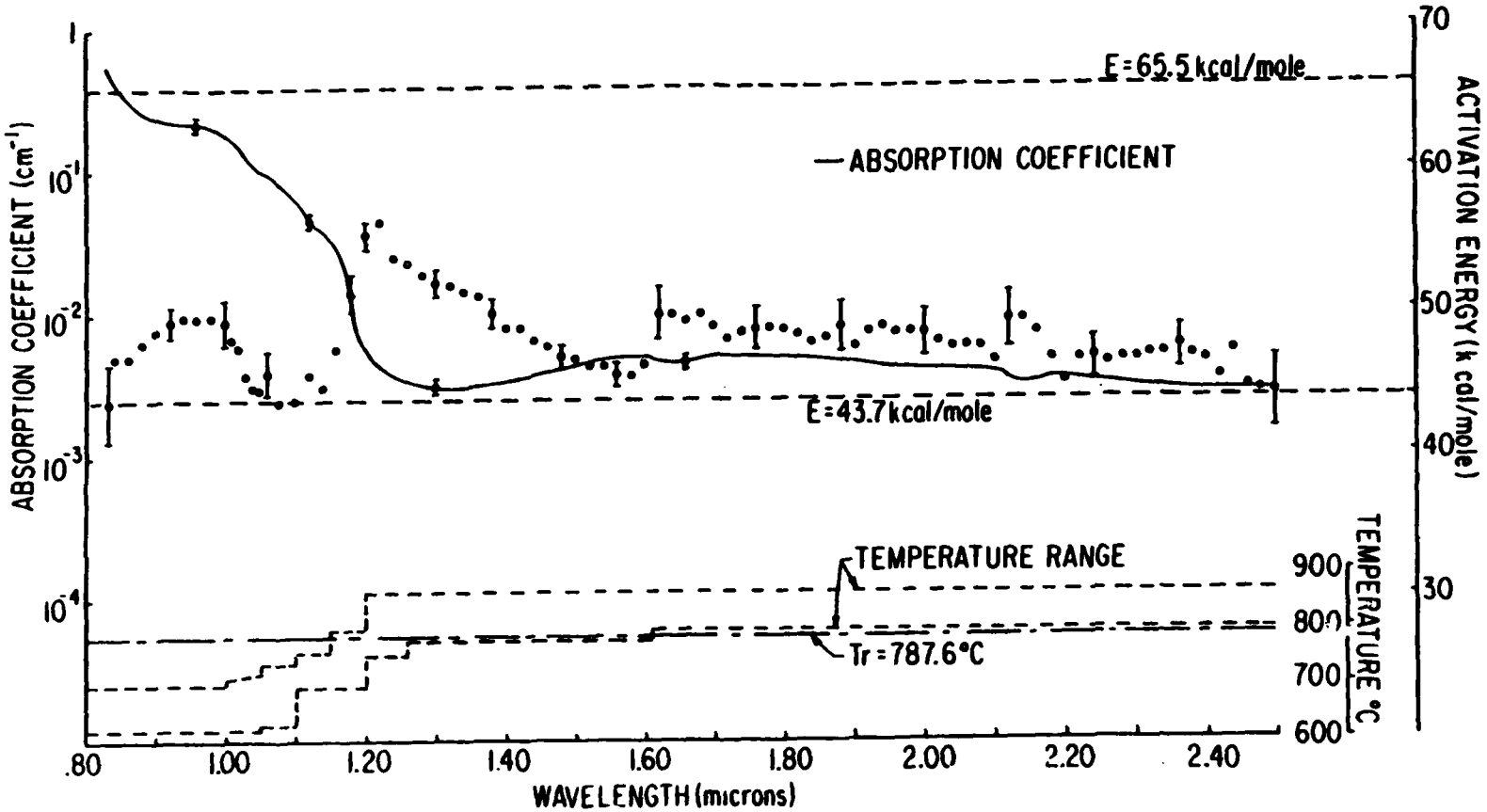

Figure 2: Activation energies (points) and attenuation coefficient (solid line) for saturated sodium vapor as a function of wavelength. The standard deviation of the activation energies were obtained by weighted least squares error analysis and are shown at representative wavelengths. The error estimates for the absorption coefficient are also shown. The absorption coefficient is shown for T = 1060.6°K (P = 300 Torr).

polymers are responsible for the jump in activation energy after the 1.18μ knee in the absorption coefficient of the sodium data.

At present we are examining absorption in saturated rubidium vapor for comparison to the other already studied alkalies. In addition, we are planning fluorescence experiments for these alkalies in the spectral regions we have studied in absorption.

*This research was also supported by the Army Research Office (Durham) under Contract DAAG29-80-C-0043, and by the Air Force Office of Scientific Research under Grant AFOSR-79-0082.

(1) N. D. Bhaskar, E. Zouboulis, T. McClelland, and W. Happer, Phys. Rev. Letters 42, 640 (1979).

(2) E. Zouboulis, N. D. Bhaskar, A. Vasilakis, and W. Happer, J. Chem. Phys. 72, 2356 (1980).

(3) C. R. Vidal and J. Cooper, J. Appl. Phys. 40, 3370 (1969).

(4) H. E. J. Schins, R. W. M. Van Wijk, and B. Dorpema, Z. Metallkde 62, 330 (1971).

D. GROUND-STATE POLARIZATION BY TWO-PHOTON OPTICAL PUMPING OF ATOMIC VAPORS*

(N. Tran, W. Happer)

The idea of remotely sensing magnetic fields by optically pumping atmospheric Xe^{129} was first proposed two years ago.[1] Due to atmospheric absorption, direct one-photon optical pumping is ruled out, and alternative two-photon pumping schemes have been proposed.

Preliminary experiments at NADC[2] failed to detect any nuclear polarization in Xe^{129}, but excellent two photon pumping rates were observed. Further feasibility studies in our laboratory,[3][4] and recent advances in excimer laser technology,[5] have maintained the interest in the original idea.

As a first step towards an ultimate practical system, we have undertaken to observe and measure the ground-state polarization of Rubidium atomic vapors with a two-photon pumping scheme. Our goal is to demonstrate the feasibility of such a scheme, and also to learn more about possible pitfalls in such systems. Although excited-state polarization has been observed in numerous multi-photon experiments, both in atomic vapors[6] and in solids,[7] to our knowledge polarization in the ground-state has yet to be detected.

The proposed pumping scheme is depicted in Figure 1, and the experimental set-up is shown in Figure 2. A Krypton ion laser is used to pump Oxazine 750 dye. The circularly polarized light beam at 7781 Å is focussed into a cell containing Rb vapor, N_2 quenching gas and helium buffer gas. Two-photon excitation takes place between the ground-state and the $5D_{5/2}$ excited state via a virtual state close to the $5P_{3/2}$ state. The

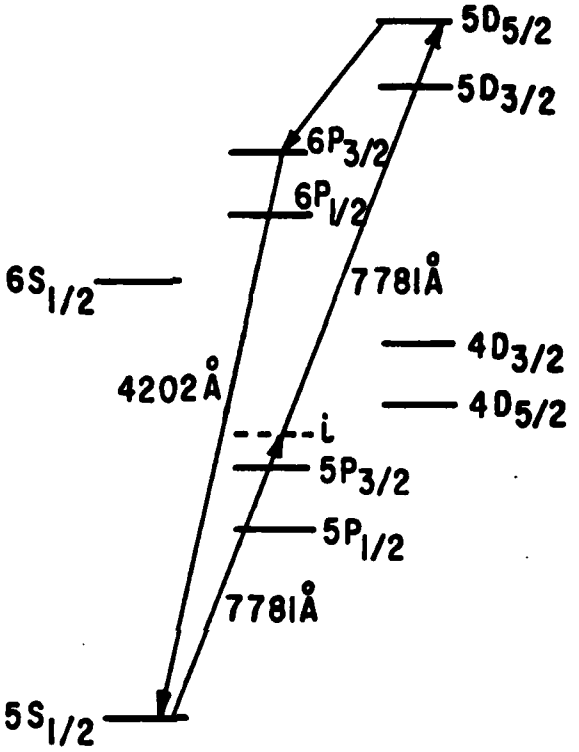
5D5/2
5D3/2
6P3/2
6P1/2
6S1/2
7781Å
4D3/2
4202Å
4D5/2
i
5P3/2
5P1/2
7781Å
5S1/2

Figure 1

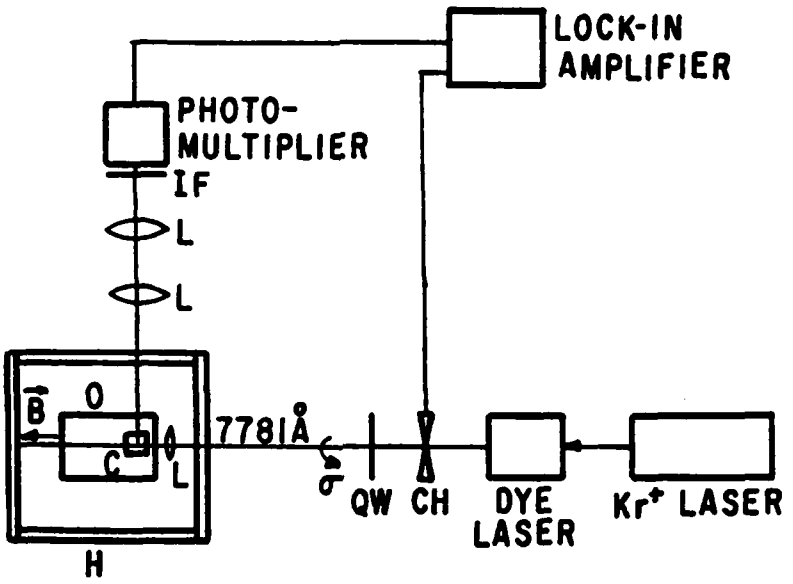

CH: Chopper

QW: Quarter-Wave Plate (7781 Å)

C: Cell

L: Lenses

O: Oven

H: Helmholtz Coils

IF: Interference Filter (4202 Å)

Figure 2

fluorescence ($6P_{3/2} \rightarrow 5S_{1/2}$) at 4202 Å is detected at 90° with a photomultiplier tube.

There are many reasons for picking these states in Rubidium for a preliminary study. By solving the steady-state pumping-diffusion problem in cylindrical symmetry (neglecting variation along the light beam), we find:[8]

$$\langle S_z \rangle(r) = \begin{cases} A\, I_o\left(\sqrt{\frac{R+\gamma}{D}}\, r\right) + \frac{R/3}{R+\gamma} & (r \leq r_o) \\ B\, K_o\left(\sqrt{\frac{\gamma}{D}}\, r\right) & (r > r_o) \end{cases}$$

Here $\langle S_z \rangle$ is the Rubidium ground-state polarization,

A and B are constants determined from boundary conditions,

I_o and K_o are modified Bessel's functions,

γ is the spin relaxation rate,

D is the diffusion constant,

r_o is the geometrical laser beam waist, and

R is the two-photon pumping rate per atom, derived earlier in reference (3).

It happens that with these particular states in Rb, pumping rates R of the order of $\sim 10^3$ sec^{-1} are possible with presently available laser power. Using values for γ inferred from recent experiments by Bhaskar et al.,[9] one can show from the above equation that percent polarizations $2\langle S_z \rangle \sim$ 10% should be obtainable. The apparatus of Figure 2 is now under construction and we hope to perform the first experimental studies of two-photon optical pumping by the fall of 1980.

*This research was also supported by the Naval Air Development Center, Warminster, Pennsylvania.

(1) W. Happer, "Laser Remote Sensing of Magnetic Fields in the Atmosphere by Two-Photon Optical Pumping of Xe^{129}," NADC Report 1978.

(2) E. Greeley and L. Bobb, private communication.

(3) W. Happer and N. Tran, "Absolute Excitation Rates and Selection Rules for Two-Photon Optical Pumping of Xenon," NADC Report 1979.

(4) W. Happer and N. Tran, "Influence of Pressure Broadening on the Two-Photon Optical Pumping Efficiency of Xe^{129} in Air," NADC Report 1979.

(5) R. T. Hawkins, H. Egger, J. Bokor, and C. K. Rhodes, to be published in Optics Letters.

(6) See, for example, F. Biraben, K. Beroff, E. Giacobino, and G. Grynberg, J. Physique Lettres (Paris) 39, L108 (1978).

(7) See, for example, P. Motisuke, S. Durbin, V. I. Safarov, and Y. R. Shen, American Physical Society Meeting, New York, March 1980.

(8) W. Happer and N. Tran, to be published.

(9) N. D. Bhaskar, J. Pietras, J. Camparo, W. Happer, and J. Liran, Phys. Rev. Letters 44, 930 (1980).

E. TEMPERATURE AND DENSITY VARIATION OF THE INFRARED BANDS OF CsXe; CESIUM POLYXENIDE BANDS*

(R. Novak, W. Happer, N. Bhaskar)

The previous Progress Report[1] described the first investigations of alkali-noble gas excimer molecules in the spectral range between 1.0 and 2.0 microns. These investigations found bands and satellites for the CsNe, CsAr, CsKr, CsXe, RbKr, RbXe, and KXe molecules. During the past year, the infrared bands of CsXe have been studied in detail. From this study, the dissociation energy of the $7S\Sigma_{1/2}$ state of CsXe has been experimentally determined and experimental evidence for the presence of $CsXe_2$ has been found.

Electronic states of an alkali-noble gas molecule are associated with the states of the free cesium atom. The nature of these states and methods of populating them have been discussed previously.[1][2] Typical data for the molecular transitions of CsXe associated with the 7S → 6P transitions of atomic cesium appear in Figure 1. The band and satellite of the molecular $7S\Sigma_{1/2} \rightarrow 6P\Pi_{1/2}$ transition are on the long wavelength side of the $7S_{1/2} \rightarrow 6P_{1/2}$ atomic transition; the bands and satellites of the $7S\Sigma_{1/2} \rightarrow 6P\Pi_{3/2}$ and $7S\Sigma_{1/2} \rightarrow 6P\Sigma_{1/2}$ transitions fall on the red side of the $7S_{1/2} \rightarrow 6P_{3/2}$ transition. The intensity of the satellite peak normalized to the $7S_{1/2} \rightarrow 6P_{3/2}$ atomic peak [$S(\lambda,[Xe],T)$] was studied for cells with densities of 0.9, 2.4, 4.5, and 6.9 Amagats (1 Amagat = $2.69 \times 10^{19}/cm^3$) in the temperature range between 150 and 400°C. This normalized satellite intensity varies as[3]

$$S(\lambda,[Xe],T) = G(\lambda,[Xe])\ T^{-1/6} \exp[(V_u(\infty) - V_u(R))/kT]$$

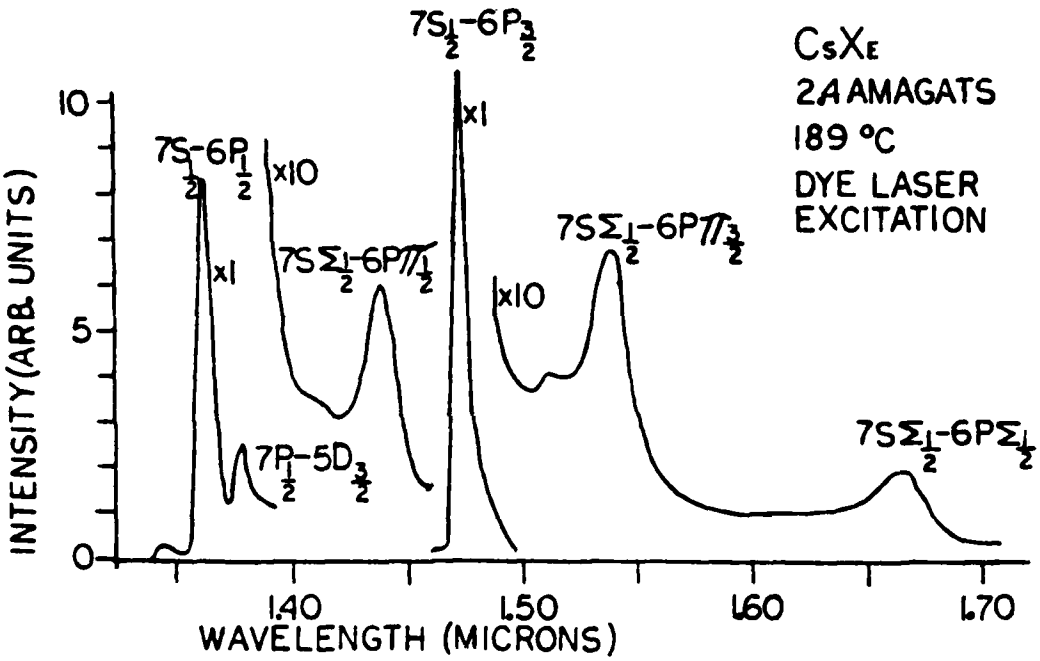

Figure 1: Infrared spectra of CsXe between 1.35 and 1.70μ.

where G is a constant and $V_u(R)$ is the potential energy curve of the upper ($7S\Sigma_{1/2}$) state. According to the Franck-Condon principle during a transition, the interatomic distance, R, remains a constant; thus, R is the interatomic distance associated with the satellite peak. A temperature profile of CsXe should yield a value for $V_u(\infty) - V_u(R)$.

The normalized intensities for the $7S\Sigma_{1/2} \rightarrow 6P\Pi_{1/2}$ satellite at 1.44μ and the $7S\Sigma_{1/2} \rightarrow 6P\Sigma_{1/2}$ satellite at 1.668μ are presented on the semilog plot of Figure 2. The linearity of the data indicates that the $7S\Sigma_{1/2}$ molecular state of CsXe is in thermal equilibrium with the $7S_{1/2}$ atomic state of cesium; the slope gives a value for $V(\infty) - V(R)$. The equality of the slopes for the two satellites indicates that each satellite originates in the same region of the upper state potential. A similar plot for wavelengths in the bands between the satellites and the atomic lines yields smaller values for the slope. This indicates that the satellites originate from the bottom of the $7S\Sigma_{1/2}$ potential well. The slope of the normalized intensities provides an experimental value of the dissociation energy of the $7S\Sigma_{1/2}$ state of CsXe; this value is taken to be 1015 ± 30 cm^{-1}.

Figure 3 compares the measured values of this experiment to the previous experiments of Sayer[4] and Hedges.[5] Sayer's value for the $7S\Sigma_{1/2}$ state is consistent with the present investigation; Hedge's values for the $6P\Pi$ states are about 100 cm^{-1} too high; the shape of the $6P\Sigma_{1/2}$ state of Hedges is not consistent with the present data.

Deviations from a straight line for high density and low temperature data (Figure 2) suggested the presence of cesium polyxenide molecules; polyxenide molecules have been previously reported for KXe.[6] Spectra

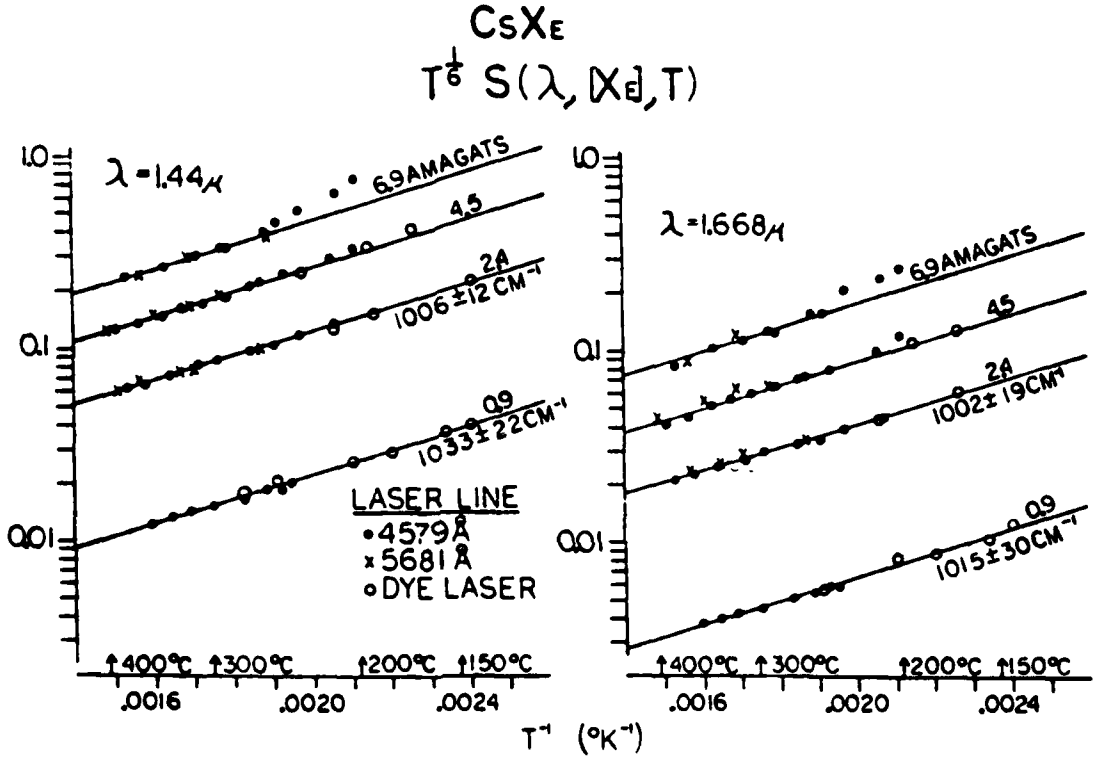

Figure 2: Semilog plot of normalized satellite intensity versus 1/T. The $T^{1/6}$ factor is needed to analyze satellite intensities.

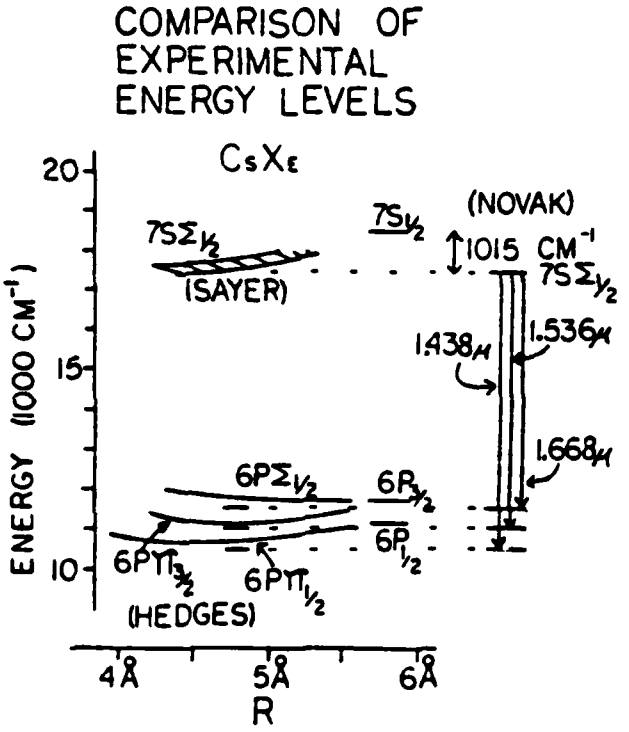

Figure 3: Comparison of energy levels found in the present experiment to previously found experimental energy levels.

were taken in both the visible (Figure 4) and infrared (Figure 5). Both spectra sets of spectra have properties similar to those of KXe_n.[7] Data for the red wing normalized to the monoxenide peak appear in Figure 6. This data suggest the following variation for the wing intensity

$$\frac{I(\lambda,[Xe],T)}{I(5723\text{Å},[Xe],T)} \propto [Xe] \exp\ [E(\lambda)/kT] \quad .$$

The consistency of the experimental points among the data for the three different densities indicates that the wing intensity is primarily due to $CsXe_2$ molecules. The potential energy of this $CsXe_2$ state is lower than the potential energy of the $7S\Sigma_{1/2}$ state of CsXe by approximately 1100 cm^{-1}; this indicates that the first xenon atom attached to the cesium atom has little effect on the electric field around the alkali core.

In summary, an experimental value for the dissociation energy of the $7S\Sigma_{1/2}$ state of CsXe has been determined to be 1015 $\pm$ 30 cm^{-1} and the first experimental evidence for the existence of $CsXe_2$ has been found.

*This research was also supported by the Army Research Office (Durham) under Contract DAAG29-80-C-0043.

(1) CRL Progress Report #29, March 31, 1979, p. 4.

(2) R. Novak, N. D. Bhaskar, W. Happer, J. Chem. Phys. 71, 4052 (1979).

(3) J. Szudy, W. E. Baylis, JQSRT, 15, 641 (1975).

(4) B. Sayer, M. Ferray, and J. Lozengot, J. Phys. B. 12, 227 (1979).

(5) R. E. M. Hedges, D. L. Drummond, and A. Gallagher, Phys. Rev. A 6, 1519 (1972).

(6) CRL Progress Report #28, March 31, 1978, p. 155.

(7) T. Yabuzaki, A. Tam, S. Curry, and W. Happer, Phys. Rev. Lett. 41, 543 (1978).

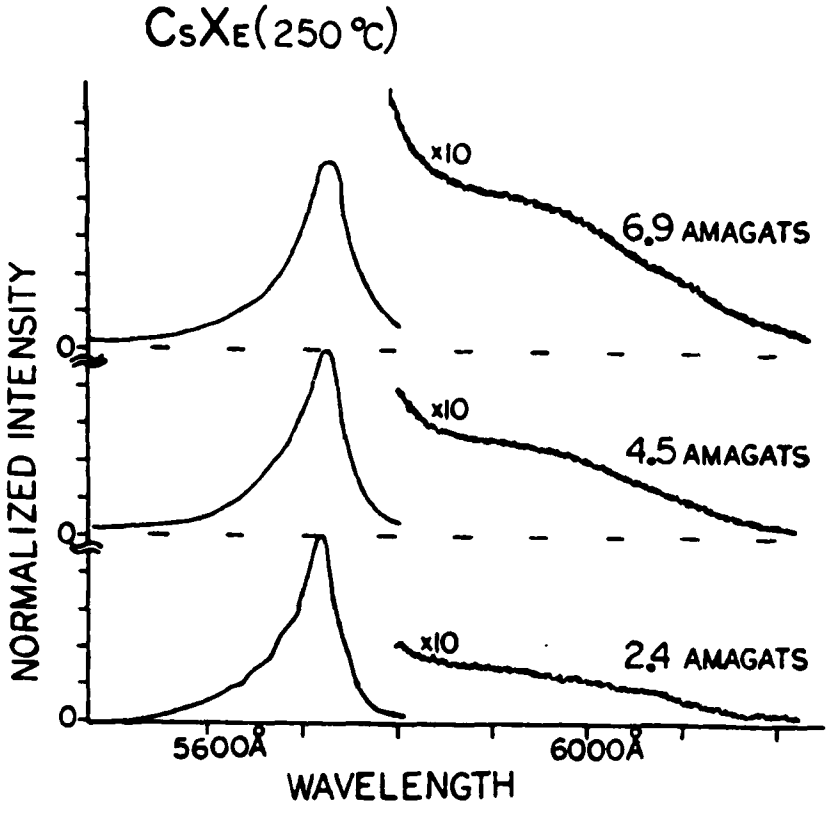

Figure 4: Visible spectra of the $7S\Sigma_{1/2} \rightarrow 6S\Sigma_{1/2}$ transition in CsXe illustrating the red wing dependence on xenon density.

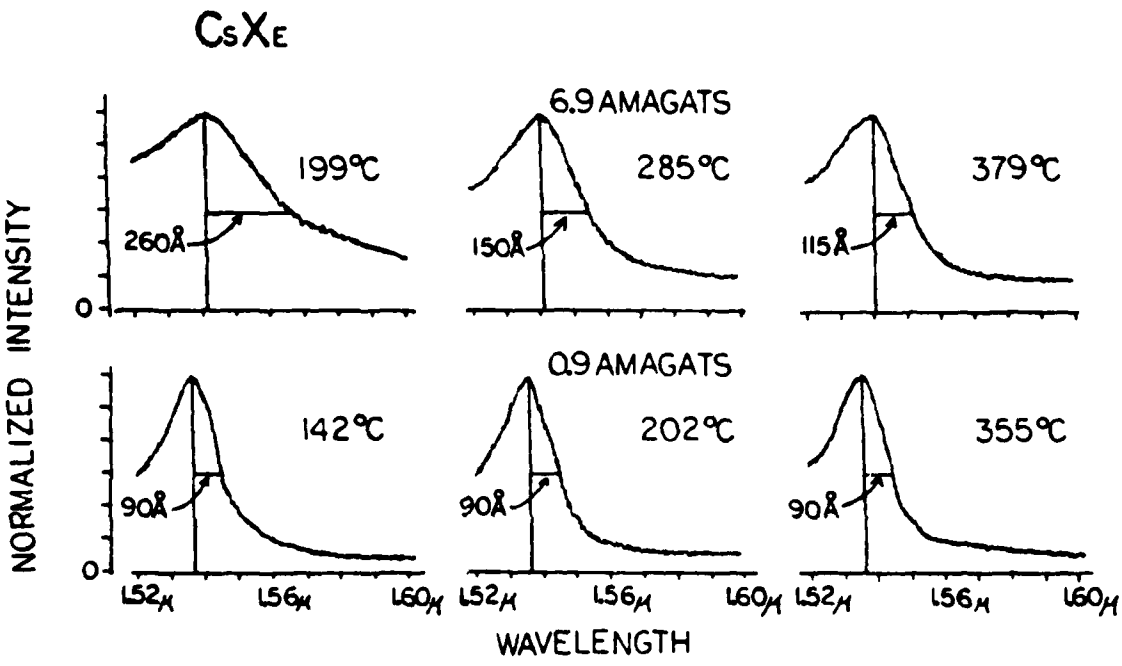

Figure 5: Infrared spectra of the $7S\Sigma_{1/2} \rightarrow 6P\Pi_{3/2}$ satellite illustrating temperature and density dependence of the band shape.

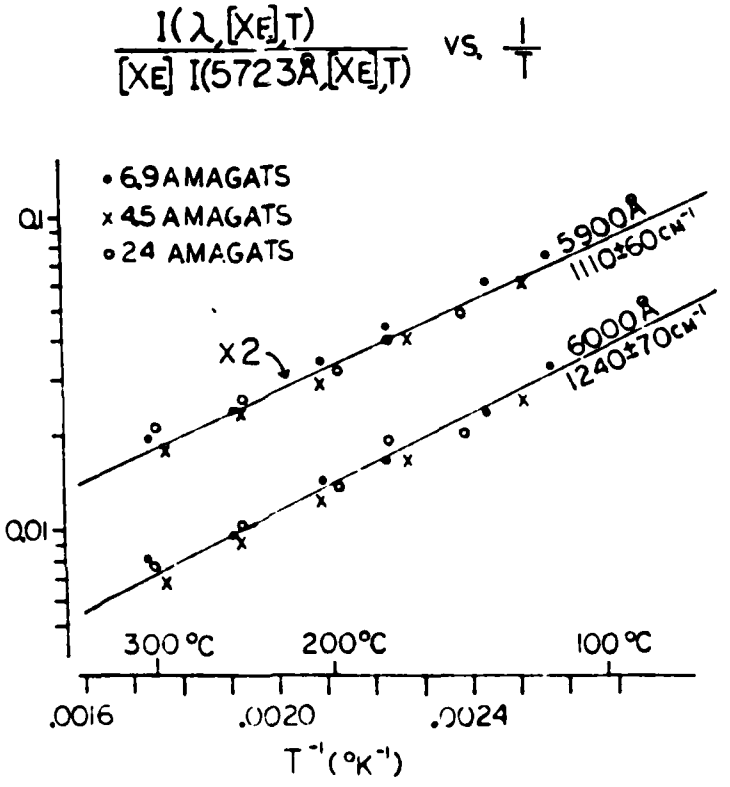

Figure 6: Normalized red wing data of the $7S\Sigma_{1/2} \rightarrow 6S\Sigma_{1/2}$ transition. Linearity indicates the presence of $CsXe_2$.

F. FARADAY ROTATION AND MAGNETIC CIRCULAR DICHROISM OF ALKALI-NOBLE GAS SYSTEMS*

(M. Islam, A. Kponou, W. Happer)

The primary objective of this experiment is to determine unambiguously the quantum numbers associated with the absorption bands of alkali-noble gas systems.[1] Initially, attention will be focussed on the cesium-xenon gas excimer. The plan is to search for both Faraday Rotation (FR) and Magnetic Circular Dichroism (MCD) of the alkali noble gas system.

In this reporting period, the apparatus described in the last year's report has been modified considerably, mainly as a result of our attempts, so far with some success, to observe FR in a solution of cobaltous nitrate[2] $Co(NO_3)_2$, which is of the same order of magnitude as estimated for Cs-Xe.

The present experimental arrangement for FR is shown in Figure 1. For MCD, a $\lambda/4$ plate is inserted between modulator and cell and the analyzer A removed. The source is a 100 W projection lamp which will be soon replaced by 150 W xenon arc lamp. This replacement has been found necessary because of the high degree of collimation and consequent loss of the light beam as it passes through the cell. Reflections of light from the walls of the absorption cell can alter its polarization and introduce error in the measurement. The iris diaphragm serves to collimate the light and to minimize reflections from the cell walls. The filter F removes second order diffraction from the light emerging through the exit slit of the monochromator.

The emergent light is polarized by the plane grating of the monochromator. The polarization depends on wavelength and therefore could lead to

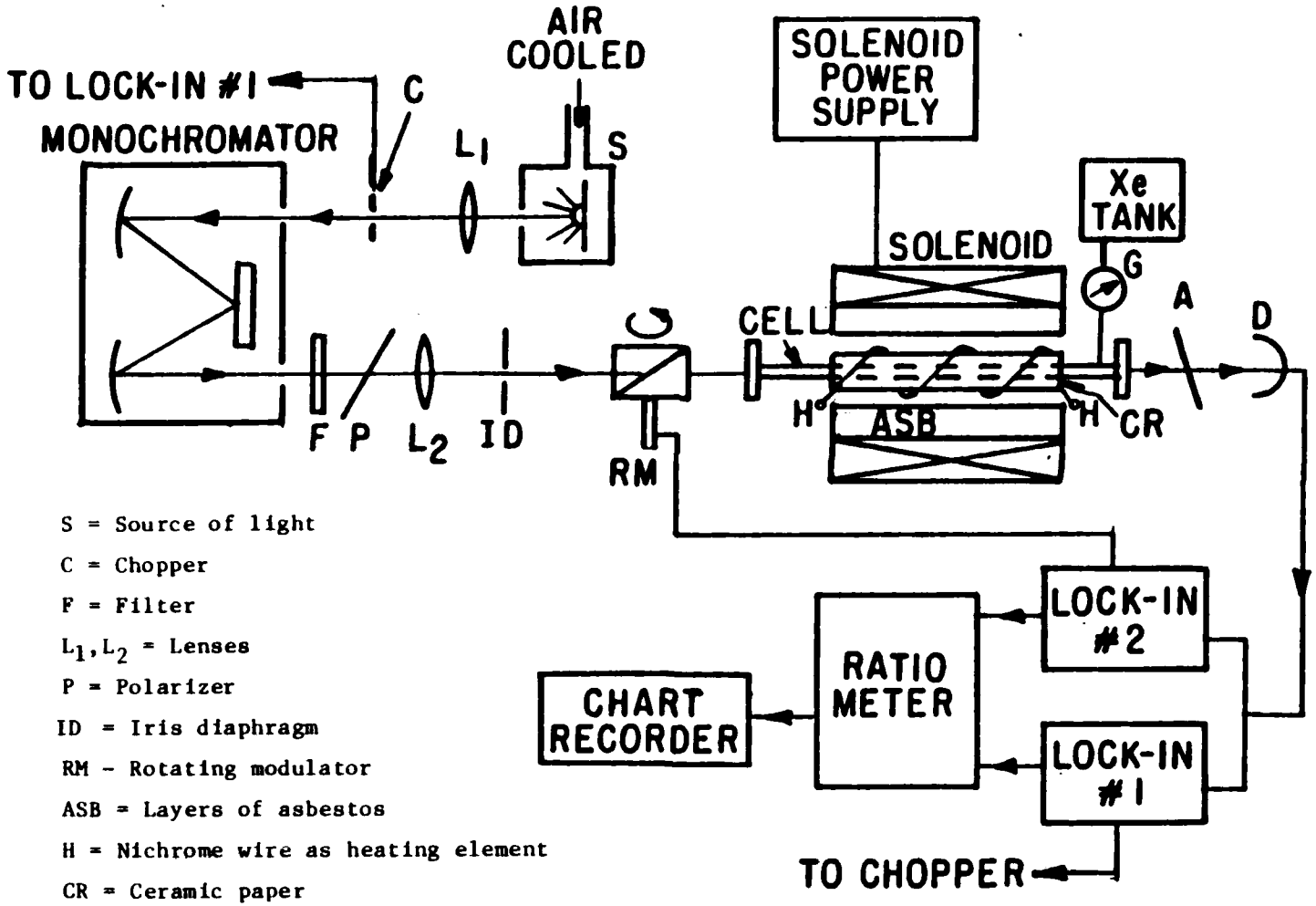

S = Source of light

C = Chopper

F = Filter

L_1, L_2 = Lenses

P = Polarizer

ID = Iris diaphragm

RM - Rotating modulator

ASB = Layers of asbestos

H = Nichrome wire as heating element

CR = Ceramic paper

G = Pressure gauge

A = Analyzer

D = Detector

Figure 1

serious errors in measuring FR. Its effect was in fact observed while studying the $Co(NO_3)_2$ solution. To avoid systematic errors due to the polarizing properties of the monochromator, a linear polarizer is used at the exit slit of the monochromator to define a wavelength independent polarization of the light before it enters the modulator. Another approach would be to place a polarization scrambler at the monochromator exit. Errors introduced by the polarizing properties of the monochromator can also be eliminated by passing white modulated light through the cell and detecting the emergent light through the analyzer by the monochromator and the subsequent detecting stages.

The principle of modulation has been retained but the modulator has been modified by using twenty-two pieces of polaroid instead of just two. Thus, there are eleven cycles of polarization modulation for each complete rotation of the modulator, resulting in a modulation frequency of 11f where f is the rotation frequency of the motor. (Examination of polarization modulation in this modulator has revealed that the number of polaroid pieces has to be 4n + 2 where n = 0, 1, 2, 3, . . .) Enhancement of modulation frequency was necessary to get rid of low frequency noise which is easily generated in the system and to achieve better signal to noise ratio.

Faraday Rotation α is given by $V_\lambda \ell B_z$ where ℓ is the length of the interaction region, B_z is the component of the magnetic field parallel to the direction of propagation of light and V_λ is the Verdet Constant of the sample at the wavelength λ involved. A long interaction region and a strong magnetic field are therefore desirable. This is especially so in this experiment because the system is in the gas phase and has a much

smaller number density than the liquid or solid phases. A solenoid magnet having a length of 34" and capable of producing an average field of about 3000 gauss over the length ($B_{average} \simeq 0.8\ B_{center}$) will be used. The magnet is water cooled.

Several unsuccessful attempts were made to prepare 33" long and 1" i.d. glass cells. Some cells cracked before Cs was distilled; in others Cs did not uniformly distribute itself over the length of the cell and it also attacked the windows of the cell. Besides, the high pressure of xenon anticipated in a loaded cell made it potentially hazardous. Among other choices of cell material, stainless steel, which is highly resistant to the attack by alkali vapors turned out to be a good alternative to glass. Such a cell has been assembled. It consists of a 304 s.s. tubing 50" long, 3/4" i.d. and 1/16" thick wall. The windows are 1/8" thick 1720 Corning glass with a useful aperture of 5/8". Inside the tube are two layers of size 100 stainless steel wire mesh 36" wide. The purpose of the mesh is to provide a uniform layer of cesium in the interaction region. By capillary action, any cesium which condenses outside the heated segment of the cell will flow toward the center. The cell at this time is ready to be loaded with Cs following the procedure described by E. Zouboulis.[3] The cell will be heated by nichrome wire wound tightly on a layer of ceramic paper wrapped around the tube. Thermal insulation between the heater and the magnet will be provided by several layers of asbestos material. The nichrome wire is wound noninductively to cancel out any magnetic field produced in the interaction region due to the alternating current passing through it.

The scheme for measuring Faraday Rotation is based on the following analysis: Let P_1 and P_2 represent the polarization of the modulated light at an angle θ and A represent the transmission axis of the analyzer at an angle ϕ about some axis OY (Figure 2). If α is the Faraday produced by the sample, the mean and difference in the transmitted intensities detected are respectively given by

$$I_m = I_o' \left[\cos^2(\phi-\alpha)\cos^2\theta + \sin^2(\phi-\alpha)\sin^2\theta\right] \quad (1)$$

$$\Delta I = I_o' \sin 2(\phi-\alpha)\sin 2\theta \quad (2)$$

where $I_o' = I_o t e^{-k\ell}$; I_o, t, k and ℓ represent the intensity of light before the cell, transmittance of the analyzer, absorption coefficient and the length of the sample respectively. It can be shown that high detection sensitivity and signal to noise ratio can be achieved by setting $\phi = 0°$ or $90°$ and $\theta = 45°$. Under this condition and for small rotation α, it follows from equations (1) and (2) that the Faraday Rotation is

$$\alpha = \frac{1}{4}\,\frac{\Delta I}{I_m} \quad . \quad (3)$$

I_m and ΔI are obtained at the lock in amplifiers #1 and #2 which are driven by reference signals generated by the chopper and the rotating modulator respectively (Figure 1). The output of the ratiometer is proportional to $\Delta I/I_m$. The constant of proportionality can be determined by producing a known rotation on the analyzer and noting the reading on the ratiometer. In the case of MCD, with magnetic field on, the difference in the transmitted intensity measures directly the difference in absorption

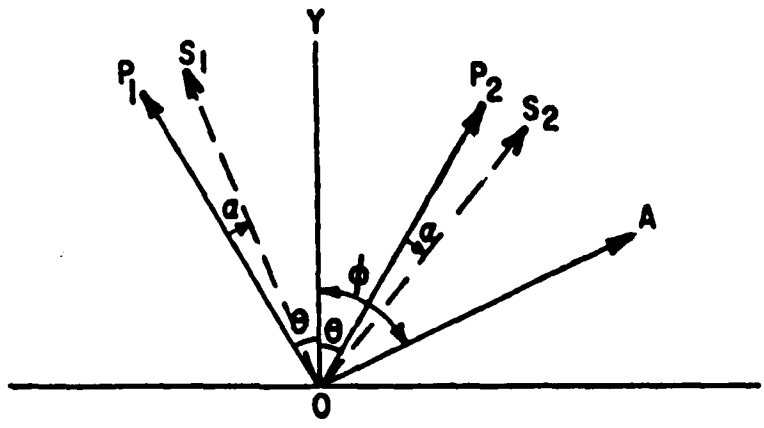

P_1, P_2 = Initial polarization of the modulated light before the cell.

S_1, S_2 = Final polarization of the modulated light after the cell.

A = Transmission axis of the analyzer.

α = Rotation of the plane of polarization produced by the sample.

θ = Angle made by each of the polarization axes in the rotating modulator.

ϕ = Angle made by the transmission axis of the analyzer.

Figure 2

between left circularly polarized and right circularly polarized light. With the magnetic field off, a zero field absorption is obtained. It is then a simple matter to obtain MCD.

From measurements that have been recently made, the system is capable of measuring a rotation of about 4×10^{-4} radians. Noise in the system is close to the shot noise limit.

*This research was also supported by the Army Research Office (Durham) under Contract DAAG29-80-C-0043.

(1) G. Moe, A. Tam, and W. Happer, J. of Mol. Spectry. 32, 181 (1976).

(2) V. Shashoua, J. of Am. Chem. Soc. 86, 2109 (1964).

(3) E. Zouboulis, Doctoral Thesis, Department of Physics, Columbia University (1979).

G. PARTICULATE FORMATION IN CESIUM-DEUTERIUM GAS CELLS*

(J. Camparo, J. Pietras, N. Bhaskar, W. Happer)

Several years ago in our laboratory Tam et al. discovered what has come to be known as "Laser Snow."[1] In mixtures of cesium vapor and helium gas they could excite the pressure broadened cesium second resonance lines with two fixed frequency blue lines of an Ar^+ laser (4545Å and 4579Å). The excited cesium atoms in the presence of hydrogen gas led to the formation of dense clouds of white particulates which fell under their own weight, hence the name laser snow. It was observed that these particulates were micron sized, and carried a positive charge ($\sim 10^4$ e). They postulated that these particulates were actually CsH crystals, and from experimental evidence they proposed a mechanism for their formation:

$$\begin{aligned} &Cs + h\nu \rightarrow Cs^*(7P) \\ &Cs^*(7P) + H_2 \rightarrow CsH + H \qquad (1) \\ &CsH + CsH \rightarrow [CsH]_2 \end{aligned}$$

the last step describing the molecular condensation into particulates.

Unfortunately, Tam's work was limited by the imperfect overlap of the Ar^+ laser lines with the cesium second resonance lines (4555Å and 4593Å). In our present work we have been able to remove this limitation by exciting the cesium vapor on resonance with a tunable dye laser. An Ar^+ laser (Spectra-Physics 171-19) operating all lines in the ultraviolet ($\gtrsim$ 2.5 W) pumps stilbene 3 dye in a Coherent 599-03E dye laser (200-300 mW). Stilbene 3 has a tuning range from 410 nm to 480 nm. This tunability has opened up a whole new range of possibilities for investigating these

particulates: we have observed them over a very wide range of cesium number densities by tuning the laser frequency to compensate for optical thickness; we have formed them in the absence of He; and we have investigated their behavior as a function of laser tuning.[2]

As shown in Figure 1, our blue laser light is split into two parts: a strong pump beam, and a weak probe beam. With this arrangement we can pump the cesium atoms into CsH molecules and crystals, and then probe their return to Cs atoms when the pump light is shut off. This method is completely analogous to that used for studying spin relaxation in the dark, and in fact we have been able to attain measurable spin polarization in sample cells containing Cs, 20 torr deuterium, and an atmosphere of He at cesium number densities $\sim 10^{14}/cm^3$. (We have obtained 50% polarization at [Cs] $\sim 10^{13}/cm^3$.) We also have a red probe beam from a He/Ne laser travelling along the same path as the blue laser beam but in the opposite direction. Since this red light is only attenuated by scattering from the particulates, we can use a red filter to unambiguously monitor the Mie scattering.

The laser light is admitted to a cell constructed from alkali-resistant aluminosilicate glass (Corning 1720). Some of our cells contain internal electrode plates (Figure 1): molybdenium rods are sealed to the glass, and non-magnetic stainless steel plates are spot welded to the rods. We found that annealing these cells in a dry hydrogen atmosphere chemically reduced MoO_3 which getters both H_2 and D_2.

The cells contain cesium metal plus varying amounts of D_2 and He. We used D_2 instead of H_2 because the literature quoted an enormously high dissociation pressure for CsD,[3] and we hoped to use this fact to study

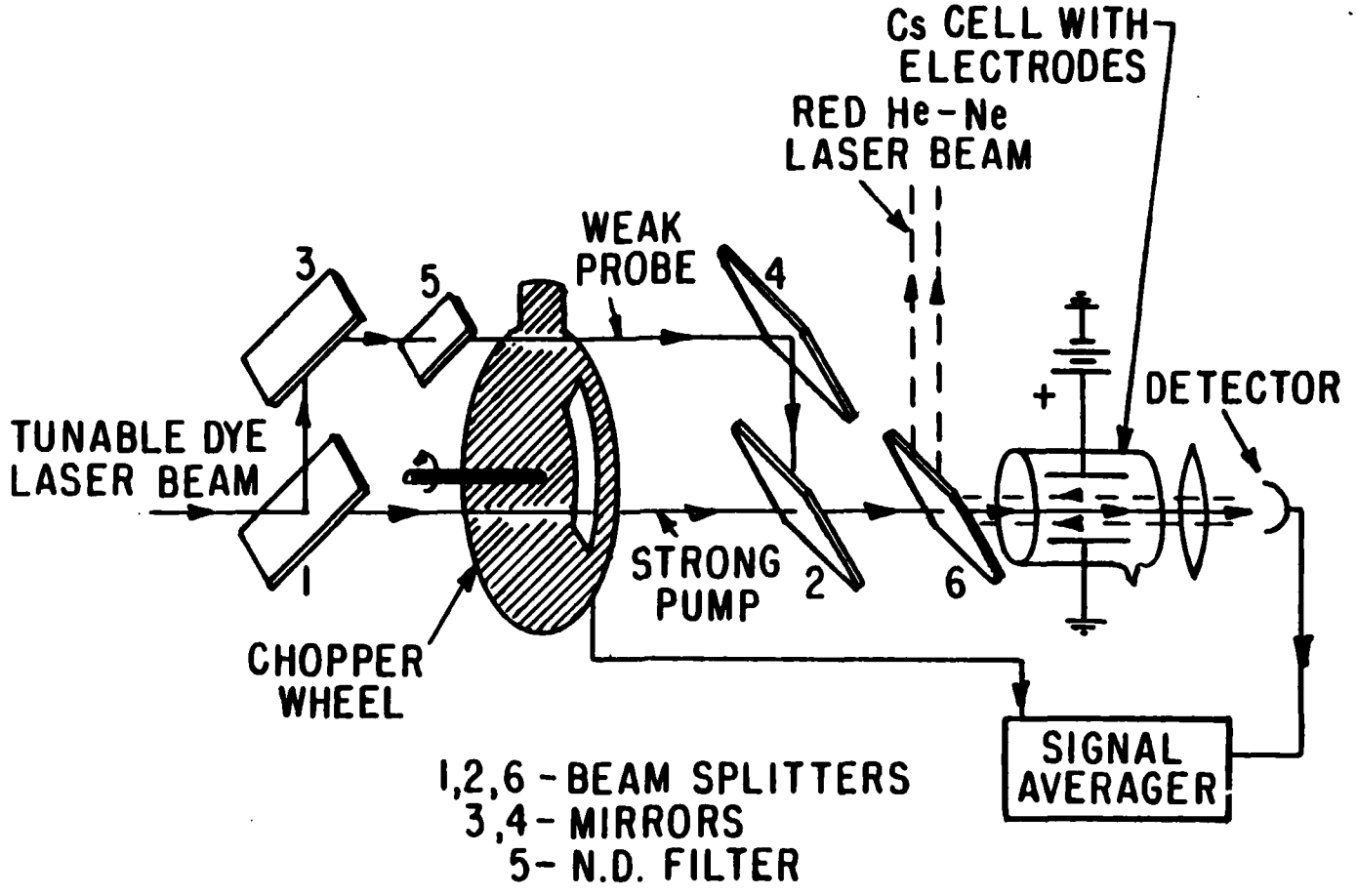

Figure 1: Experimental set up. Typical power of the tunable dye laser beam ≈ 200 mW. The intensity of the weak probe beam is only $(1/200)^{th}$ the intensity of the strong pump beam.

the atomic and molecular processes in the absence of particulate formation. However, on inspection of the original data of Hackspill and Borocco[4] we found that their empirical fit to the data is some three orders of magnitude too high. Their data is fit more reasonably by the formula,

$$\log_{10} P = 11.27 - \frac{5419}{T} \qquad (2)$$

where P is the dissociation pressure of CsD in torr, and T is the absolute temperature. This formula leads to dissociation pressures of CsD which are only about a factor of two greater than those of CsH, and so little is gained by using D_2 instead of H_2.

By measuring the terminal velocity of these particulates as they fall through the He vapor, we have been able to estimate their size by using Stokes law. To measure the velocity we displace the He/Ne beam a distance d below the strong pump beam so that its transmitted intensity is attenuated by Mie scattering from the particulates. A certain time Δt after the pump beam is blocked, the transmission of the He/Ne beam will increase (Figure 2). Thus, Δt is the time required for the particulates to fall from the pump beam through the He/Ne beam. In this manner we have determined that the CsD particulates are about one micron in diameter. As shown in Figure 2 Δt seems to decrease with decreasing laser power; this would imply that particulate size increases as the exciting photon flux decreases.

As in the original work of Tam et al.[1] we find that these CsD particulates are charged. Since individual particulates are clearly visible through a microscope as they fall through the red He/Ne light, it is a simple matter to apply an electric field between the two plates which just

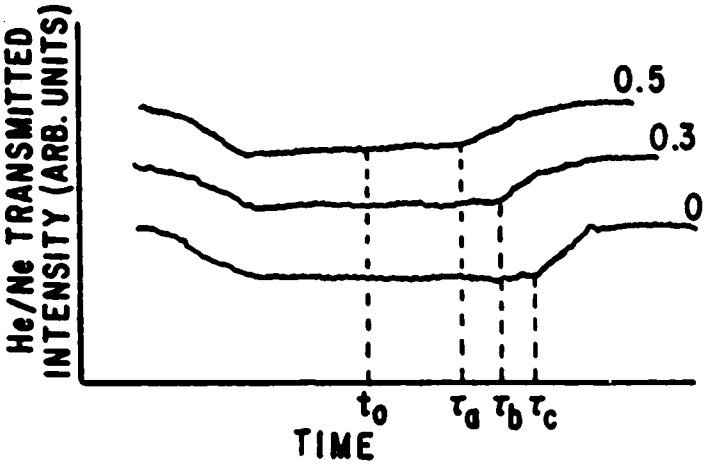

Figure 2: Transmitted intensity of He/Ne light as particulates fall through He/Ne beam which is a distance d below blue pump light. Three data sets are shown, where different neutral density filters were placed in front of pump beam (N.D. = 0, 0.3, 0.5). t_o is the time the pump light was blocked, and τ is the time when the transmitted He/Ne intensity increased. We can compute the terminal velocity of these particles: $v = d/\Delta t$, $\Delta t = \tau - t_o$.

cancels the effect of gravity. In this way we can measure the charge on the particles, and at an optical depth of > 2 cm we find that these particles carry a positive charge $\sim 10^2$ e.

At this optical depth an electric field ($\sim$ 100 V/cm) which is pulsed on will quickly sweep all the particles out of the red He/Ne beam, and there will be no visible Mie scattering. If we tune the laser closer to resonance (optical depth $\sim$ 2-3 mm) the electric field appears to have no effect on the red Mie scattering. We conclude that for the pump light tuned very near resonance these particulates are either minimally charged or completely neutral.

In addition we noticed that the particulates do not disappear uniformly throughout the entire length of the red beam as the electric field is pulsed on. We biased the electrode plates such that the particulates would be deflected upwards, and tuned the laser away from resonance (optical depth > 2 cm). When the field was pulsed on, those particulates nearest the pump laser entrance were deflected upwards first, and then those further away were deflected out of the He/Ne beam in turn. The effect can best be described as a red scattering wave retreating from the entrance face of the cell. We then tuned the laser closer to resonance, and observed that this red scattering wave changed direction: those particulates furthest away from the pump beam entrance were deflected upwards first, and then those closer to the entrance were deflected in turn.

It is easy to show that the acceleration of these charged particulates out of the red He/Ne beam is directly related to their charge to mass ratio. One possible explanation for this red scattering wave is that the charge to mass ratio of these particulates is not uniformly distributed

throughout the length of the pump beam. Since the distribution of q/M for these particulates would then appear to be dependent on laser tuning, we could conclude that the magnitude of q/M for a particulate depends on the photon flux in the neighborhood of the particulate. Also, since this red scattering wave changes direction, it would seem likely that q/M must have an extremum in its dependence on photon flux.

We have carried out some preliminary experiments to investigate the changes in transparency of the vapor cells when particulates are formed by the blue resonant light. We found that very substantial changes in the transparency did occur and that at least two mechanisms are operating. First, the incorporation of cesium atoms into the particulates depresses the atomic cesium number density and thereby increases the transparency of the vapor to the blue resonant light. Secondly, the particulate clouds which are formed by the blue laser light can become so dense that they cause significant attenuation of the laser beams. The attenuation due to particulates affects both the blue pump light and also the red, HeNe probe light. In all cases we have studied the transparency of the vapor for the blue pumping light increased with time after the pumping light was turned on.

As shown in Figure 1 the rotating chopper wheel admits the strong pump beam to the cell; the decrease in the number of absorbers in the pump beam's path depends on the incident laser intensity ($\Delta N \propto I_o^{3/4}$). The pump beam is then blocked, and the transmission of the probe beam is monitored with a photodiode and recorded with a Nicolet 1170 multichannel averager. As the vapor returns to its unperturbed state the transmitted intensity of the probe decreases.

Our results show that at least two time domains are involved in this relaxation of the vapor. When the pump beam is first turned off, absorbers quickly appear in the volume of the probe beam at a rate $\sim$ 30 sec^{-1}. This is followed by a much slower decrease in the transparency of the vapor which takes $\sim$ 10 sec to reach its steady-state value. The difference between the asymptotic transparency of the first transient and the final transparency of the vapor is $\sim$ 35%. If an electric field ($\sim$ 100 V/cm) is applied between the two electrode plates; the rate of the first transient is about four times greater ($\sim$ 120 sec^{-1}), and no slow transient is observed.

We have found that the transmitted intensity of the probe beam during the fast transient has the functional form:

$$\ell n \left(\frac{I(t)}{I_o} \right) = Ae^{-\gamma t} \qquad (3)$$

where I_o is the asymptotic value of the transmitted intensity; γ is the characteristic rate of the fast transient; and A is a constant. Some very preliminary results would indicate that the increased rate of the "field on" transient depends on the photon flux and duration of the strong pump beam.

Although our data shows that the bleaching of the vapor due to the removal of cesium atoms outweighs any increase in opacity due to Mie scattering of the particulates, the attenuation due to Mie scattering is certainly comparable to the attenuation due to the change in the atomic cesium number density. We have performed an experiment where the cell was illuminated with 300 mw of blue dye laser light and particulate buildup

was allowed to come to equilibrium in the absence of an electric field. The electric field was suddenly pulsed on and a substantial change in the transparency of the vapor was observed. When the laser was tuned so that the optical depth exceeded the cell length (optical depth $\gtrsim$ 2 cm) the application of the electric field caused a substantial ($\sim$ 20%) increase in the transmission of the vapor which was due to the removal of Mie scattering particles from the laser path by the electric field.

When the laser was tuned close to resonance so that the optical depth was about 1.5 cm or less (about 3/4 of the cell length) the application of an electric field caused the transmission of the vapor to decrease by about 30%. We do not understand this phenomenon, but it is completely reproducible. Somehow the presence of particulates makes it easier for the blue pumping light to remove free cesium atoms from the vapor. Perhaps the particulates serve as local sinks for newly created CsH diatomic molecules or small polymer clusters and without the particulates the many excited atoms and vibrationally excited D_2 molecules destroy the CsH polymers and form free cesium atoms. Further studies are underway to investigate the curious interplay of particulates with the bleaching efficiency for atomic cesium.

The particulates also cause a substantial <u>decrease</u> in the transparency of the vapor for red HeNe laser light. When an electric field is applied to the cell the particulates are swept out of the laser beam and the transmission of the HeNe laser beam increases. In contrast to the situation for the transmission of resonant light, the application of an electric field always leads to an increase in the transparency of the vapor to the HeNe light irrespective of the tuning of the blue laser.

Tam et al.[5] studied the emission spectra of CsH molecules by exciting a mixture of cesium vapor and 100 torr of He gas using the 4579 Å Ar^+ laser line. The laser excited fluorescence spectra consists of a series of P and R doublets and emission bands from Cs_2 molecules. In a similar experiment using the rotating chopper wheel we studied the intensity of the spectrally dispersed fluorescence signal from CsH as a function of time after the light is turned on. We observe an increase in the fluorescence intensity of one of the CsH doublets as a function of time. The time constant of this transient is $\approx 300\ sec^{-1}$. We observe no time dependence of the Cs_2 emission. Further study is underway to understand this transient.

In summary, we have shown that a tunable cw dye laser is a very powerful tool for investigating the properties of the photogenerated particulates in mixtures of cesium vapor and deuterium gas. We have shown that substantial changes of the vapor opacity are caused by the blue second resonance light from the cw dye laser and that the changes in opacity are due to both Mie scattering and to changes in the number density of free cesium atoms. Recovery of the opacity in the dark depends critically on whether an electric field is used to sweep the particulates out of the beam. These preliminary studies will be followed up by more detailed experiments to determine the main mechanisms involved in bleaching, particulate formation, particulate charge and recovery of the cells to normal conditions.

*This research was also supported by the National Science Foundation under Grant NSF-ENG76-16424.

(1) A. C. Tam, G. Moe, and W. Happer, Phys. Rev. Lett. 35, 1630 (1975).

(2) To be published.

(3) T. P. Whaley: Comprehensive Inorganic Chemistry, Vol. I (Pergamon Press, New York, 1973), p. 369.

(4) L. Hackspill and A. Borocco, Bull. de La Société Chimique de France, 6, 91 (1939).

(5) A. C. Tam and W. Happer, J. Chem. Phys. 64, 2456 (1976).

H. SPIN DESTRUCTION IN COLLISIONS BETWEEN CESIUM ATOMS*

(J. Camparo, J. Pietras, N. Bhaskar, W. Happer)

The evolution of spin polarization due to collisions between ground-state atoms in $^2S_{1/2}$ states is known to be dominated by spin exchange, as was first pointed out by Purcell and Field[1] and by Wittke and Dicke.[2] An atom with a $^2S_{1/2}$ ground state and a nuclear spin I will have two Zeeman multiplets of total angular momentum $F = I + 1/2$ and $F = I - 1/2$. Spin exchange collisions are extremely effective in destroying the population imbalance $\langle \vec{I} \cdot \vec{S} \rangle$ between these two multiplets. However, spin exchange collisions conserve the total spin angular momentum of the colliding pair of atoms. Thus, spin exchange collisions have no effect on the relaxation of $\langle F_z \rangle$, the projection of the total spin, nuclear plus electronic, along the direction of the ambient magnetic field.[3]

Of course rigorous conservation of spin cannot occur since various spin-spin and spin-orbit interactions come into play during a collision between $^2S_{1/2}$ atoms. These interactions can couple the spin to the translational angular momentum of the colliding pair of atoms. In the present work we have seen relaxation due to interactions of this type.

The apparatus used in this work consisted of an argon ion laser (Spectra-Physics 171-19) with $\gtrsim$ 2.5 W of power in the ultraviolet lines pumping a cw dye laser (Coherent Radiation 599-03(E)) operating with Stilbene-3 dye. Dye laser output powers of 200-300 mW could be obtained at the blue D_1 second resonance line of cesium (4593 Å). The dye laser frequency could be held constant to within 25 GHz.

The sample cells had linear dimensions of about 2 cm and were constructed from alkali-resistant aluminosilicate glass (Corning 1720). A

small amount of cesium metal was distilled into the cell and helium and nitrogen buffer gases were added before seal off. The buffer gas served three main purposes, spin confinement, pressure broadening of the optical absorption line, and fluorescence quenching. Quenching is essential in these high-density experiments to prevent multiply scattered unpolarized first resonance light from depolarizing the spins. A few hundred torr of nitrogen was sufficient to quench effectively. The pressure broadening of the optical absorption line exceeded the laser linewidth, and further frequency stabilization of the laser was not necessary.

The cell was situated in an oven with a slight upward temperature gradient which prevented condensation of the cesium vapor on the cell windows. A static magnetic field of a few gauss was produced by Helmholtz coils, and a radiofrequency magnetic field could be applied with a small orthogonal set of coils.

We measured spin relaxation in the dark by a variant of the techniques introduced by Franzen[4] and Bouchiat.[5] The linearly polarized dye laser output beam was split into two parts as described in our report on Cs photochemistry.[6] The weak probe beam was further attenuated by neutral density filters until its intensity was 200 times weaker than that of the pump beam. Both beams were circularly polarized by a $\lambda/4$ plate before entering the cell. A rotating chopper wheel allowed the strong pump beam to enter the cell for about 10 msec. Equilibrium polarizations of 10% to 60% were produced by the pump beam, which had a mean pumping rate of about 5000 sec^{-1}. The spin polarized atoms were confined to a cylindrical volume of about the same radius ($a \simeq 1$ mm) as the pump beam by the high buffer gas pressure.

After the pump beam was blocked by the chopper, the probe beam continued to pass through the cell along the same optical path as the pump beam. The probe-beam radius (b = 2 mm) was about twice as big as the pump-beam radius. The pumping rate of the probe beam was negligible. The transmitted intensity I of the probe beam was monitored with a silicon photodetector while the transmitted intensity decreased with time. The signal to noise ratio of the transient was improved by repetitively averaging the signal with a Nicolet 1170 multichannel averager for about one minute. After most of the spins had relaxed a pulse of rf was applied at the magnetic resonance frequency of the cesium atoms to destroy the remaining spin polarization and to define the transmitted intensity I_u for unpolarized atoms. The probe beam was then blocked for a few milliseconds to determine the dark current of the detection system.

The variation in the transmitted intensity I is due to the variation of the local spin polarization in the path of the probe beam. From theoretical arguments[7] we find that our data should be expressed in the form

$$\ln \ln \left(\frac{I}{I_u}\right) = \text{const.} - \gamma_o t - \ln \left(a^2 + b^2 + 4Dt\right) \qquad (1)$$

In this expression D is the diffusion constant of polarized atoms through the buffer gas, and γ_o is the bulk spin decay rate in the absence of any diffusion.

As shown in Figure 1 we plot this quantity as a function of time. Note that quite good straight lines of slope $-\gamma$ are obtained. From (1) we see that the slope can be interpreted as

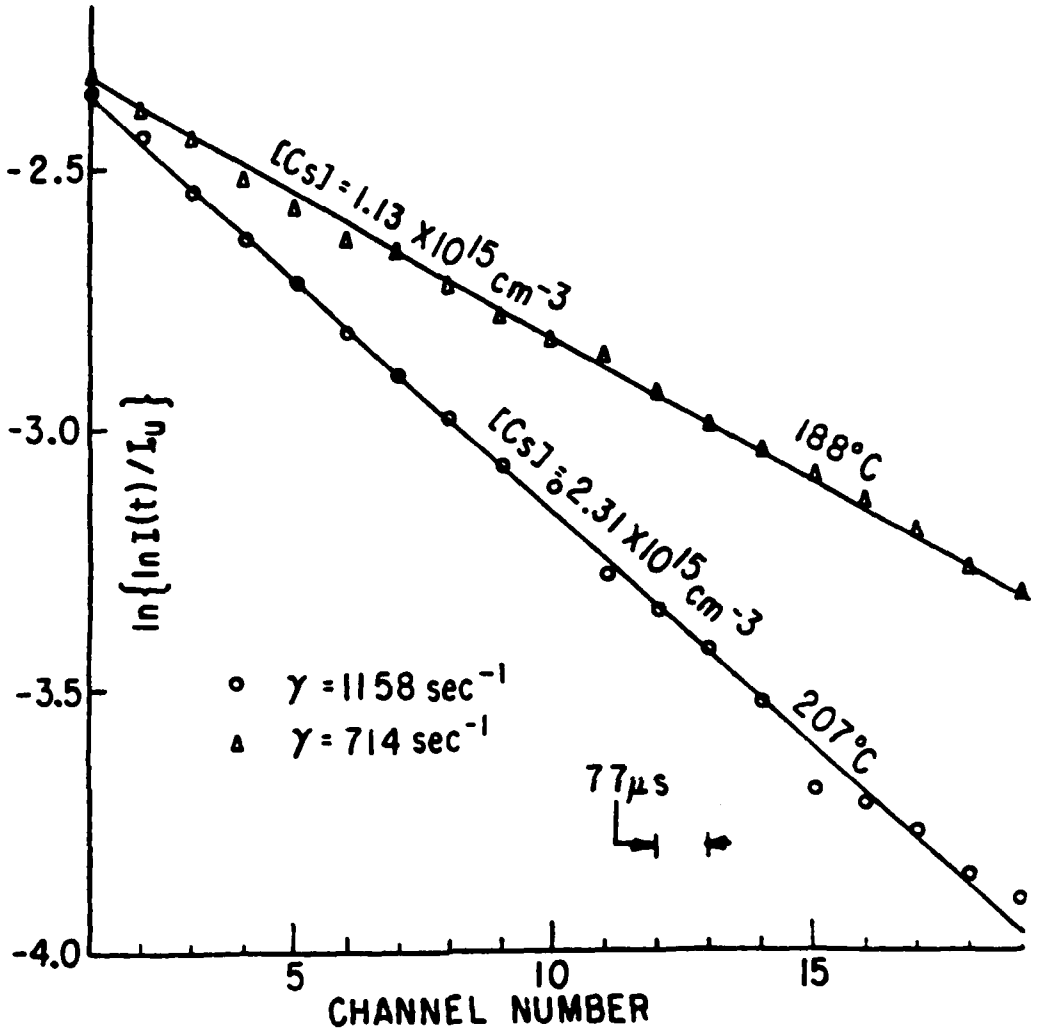

Figure 1: Temperature dependence for spin relaxation in the dark for cell C.

$$-\frac{dy}{dt} = \gamma = \gamma_o + \frac{4D}{a^2+b^2+4Dt} \qquad (2)$$

The first term γ_o is the bulk relaxation rate while the second term accounts for diffusion of spin polarized atoms out of the probe beam. In our experiments $D \lesssim 0.5\ cm^2\ sec^{-1}$ and $a^2+b^2 \simeq 5\times10^{-2}\ cm^2$ so the diffusional contribution to the decay rate is

$$\gamma_D = \frac{4D}{a^2+b^2+4Dt} \lesssim 40\ sec^{-1} \qquad (3)$$

From Figure 1 we see that the measured slopes are much greater than the estimate (3) of the diffusion rate. Note that in our work it is not very useful to discuss the diffusion in terms of normal modes of the cell, since dozens of normal modes are excited. The formula (2) can be obtained by summing over many modes.

Data like that of Figure 1 were obtained from three different cells, and the measured decay rates γ are plotted versus the cesium number density[8] in Figure 2. After accounting for the effects of the nuclear spin we find that the rate constant is

$$K = \frac{d\gamma}{d[Cs]} = 7.88 \times 10^{-12}\ cm^3\ sec^{-1} \qquad (4)$$

We may define a mean cross section

$$\sigma = K(\bar{v})^{-1} = 2.03 \times 10^{-16}\ cm^2 \qquad (5)$$

where $\bar{v} = (\frac{16kT}{\pi M})^{1/2} = 3.88 \times 10^4\ cm\ sec^{-1}$ is the mean relative velocity of

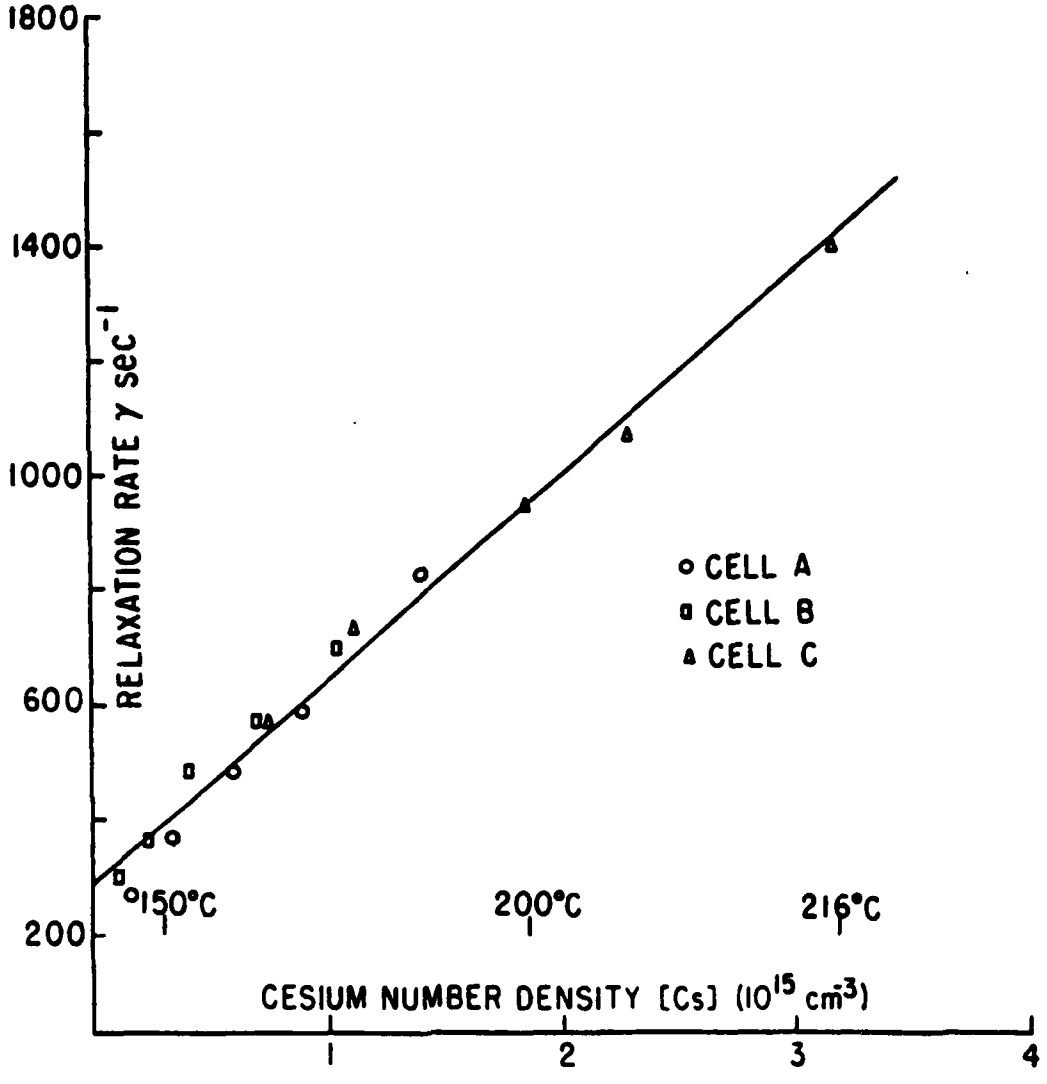

Figure 2: Dependence of relaxation rate γ on cesium number density for three sample cells. The buffer gas pressures at 20°C were: cell A: 200 Torr N_2, 550 Torr He; cell B: 200 Torr N_2, 530 Torr He; cell C: 760 Torr N_2, 2090 Torr He.

a pair of cesium atoms at 200°C. Cell C, made by cooling at constant pressure the same gas mixture contained in cell A to liquid nitrogen temperature before seal off, contained 3.8 times as much buffer gas density as cell A. Since there is no significant difference between the rate constants for cell A and C we conclude that three-body effects[9] are negligible and the temperature dependent relaxation is primarily due to cesium-cesium binary collisions.

In a cell with high buffer gas pressure we expect the diffusional relaxation rate to be less and the relaxation rate due to collisions between cesium atoms and buffer gas atoms to be greater than in a cell at low buffer gas pressure. These effects partially compensate; they are not expected to depend strongly on temperature, but they may account for the slight systematic differences between data from cells A, B and C in Figure 2.

The cross section $\sigma = 2.03\times10^{-16}$ cm^2 measured here for electron spin destruction due to cesium-cesium collisions is much smaller than the cross section for spin exchange[10] $\sigma_x = 2.2\times10^{-14}$ cm^2, but much larger than the cross section for spin destruction in alkali-noble gas collisions[11] $\sigma \lesssim 10^{-19}$ cm^2. In alkali noble gas collisions the spin depolarization is known to be due to the spin-rotation interaction[12]

$$H_{SN} = \gamma \vec{S}\cdot\vec{N} \tag{11}$$

where the coupling constant γ is of the order 10^{-4} cm^{-1}. A similar spin-rotation interaction must exist for a pair of cesium atoms on the $^3\Sigma$ ground-state potential curve, but there is no obvious reason why it should be big enough to account for the relaxation rates observed in this

experiment. However, a pair of cesium atoms on the $^3\Sigma$ ground state potential curve is also subject to the spin-spin interaction

$$H_{SS} = \frac{2}{3} \lambda \, [3 \, S_\xi \, S_\xi - S(S+1)] \qquad (12)$$

which does not exist for an alkali-noble gas pair. Furthermore, the interaction constant λ is known to be quite large, for example,[13][14] λ = 2.0 cm^{-1} for O_2, λ = 5.3 cm^{-1} for SO. It is reasonable to suppose that $\lambda \simeq 1$ cm^{-1} for a pair of cesium atoms on the $^3\Sigma$ potential curve at the distance of closest approach during a collision. The spin-spin interaction is of the right order of magnitude to account for spin destruction rates reported here.

*This research was also supported by the National Science Foundation under Grant NSF-ENG76-16424.

(1) E. M. Purcell and G. B. Field, Astrophys. J. 124, 542 (1956).

(2) J. P. Wittke and R. H. Dicke, Phys. Rev. 103, 620 (1956).

(3) A. Moretti and F. Strumia, Phys. Rev. A 3, 349 (1971).

(4) W. Franzen, Phys. Rev. 115, 850 (1959).

(5) M. Bouchiat and F. Groasetête, J. Physique 27, 353 (1966).

(6) J. Camparo, J. Pietras, N. D. Bhaskar, and W. Happer (In this Progress Report).

(7) N. D. Bhaskar, J. Pietras, J. Camparo, and W. Happer, Phys. Rev. Lett. 44, 930 (1980).

(8) A. N. Nesmeyanov, Vapor Pressure of the Elements (Academic Press, New York, 1963), p. 406.

(9) M. A. Bouchiat, J. Brossel, and L. C. Pottier, J. Chem. Phys. 56, 3703 (1972).

(10) K. Ernst and F. Strumia, Phys. Rev. 170, 48 (1968).

(11) W. Happer, Rev. Mod. Phys. 44, 169 (1972).

(12) R. A. Bernheim, J. Chem. Phys. 36, 135 (1962); R. H. Herman, Phys. Rev. 136, A1576 (1964).

(13) M. Tinkham and M. W. P. Strandberg, Phys. Rev. 97, 937 (1955).

(14) J. M. Daniels and P. B. Dorain, J. Chem. Phys. 45, 26 (1966).

I. SPIN EXCHANGE AND RELAXATION IN Na-NOBLE GAS MIXTURES*

(B. Suleman, M. Hou, N. Bhaskar, T. McClelland, W. Happer)

We have studied the relaxation of optically pumped sodium vapors in diamagnetic gases Helium and Xenon. The apparatus (Figure 1) used to measure the relaxation rates was essentially the same as described in an earlier report.[1] For better signal to noise ratio and higher time resolution a Nicolet Model SD-71B multichannel analyzer was used instead of an eductor for averaging the transmission of a weak probe beam. Circularly polarized pump and probe beams were used to monitor the relaxation of the observable $\langle S_z \rangle$. During measurements of $\langle S_z \rangle$ we tuned the laser to the center of gravity of the two hyperfine levels to avoid any hyperfine pumping and production or monitoring the observable $\langle \vec{I} \cdot \vec{S} \rangle$. For measuring the observable $\langle \vec{I} \cdot \vec{S} \rangle$ a linearly polarized pump and probe was used and the laser was tuned such that it overlapped more strongly with one of the two hyperfine levels. Reproducible results could be obtained only when the dye laser was operated in a single mode, since the relative amounts of $\langle S_z \rangle$ and $\langle \vec{I} \cdot \vec{S} \rangle$ produced depend critically on the laser frequency.

The observables $\langle S_z \rangle$ and $\langle \vec{I} \cdot \vec{S} \rangle$ relax to a Boltzmann distribution after the pump beam is turned off. A typical trace of the signal, which shows the change in transmission of probe with time, is shown in Figure 2. The probe intensity I(t) at time t after passing through an optically thick vapor can be written as

$$\frac{t}{T_1} = \ln \ln[I(t)/I(\infty)] + \ln \ln[I(o)/I(\infty)] \qquad (1)$$

where $I(\infty)$ is the intensity when the vapor has returned to Boltzmann

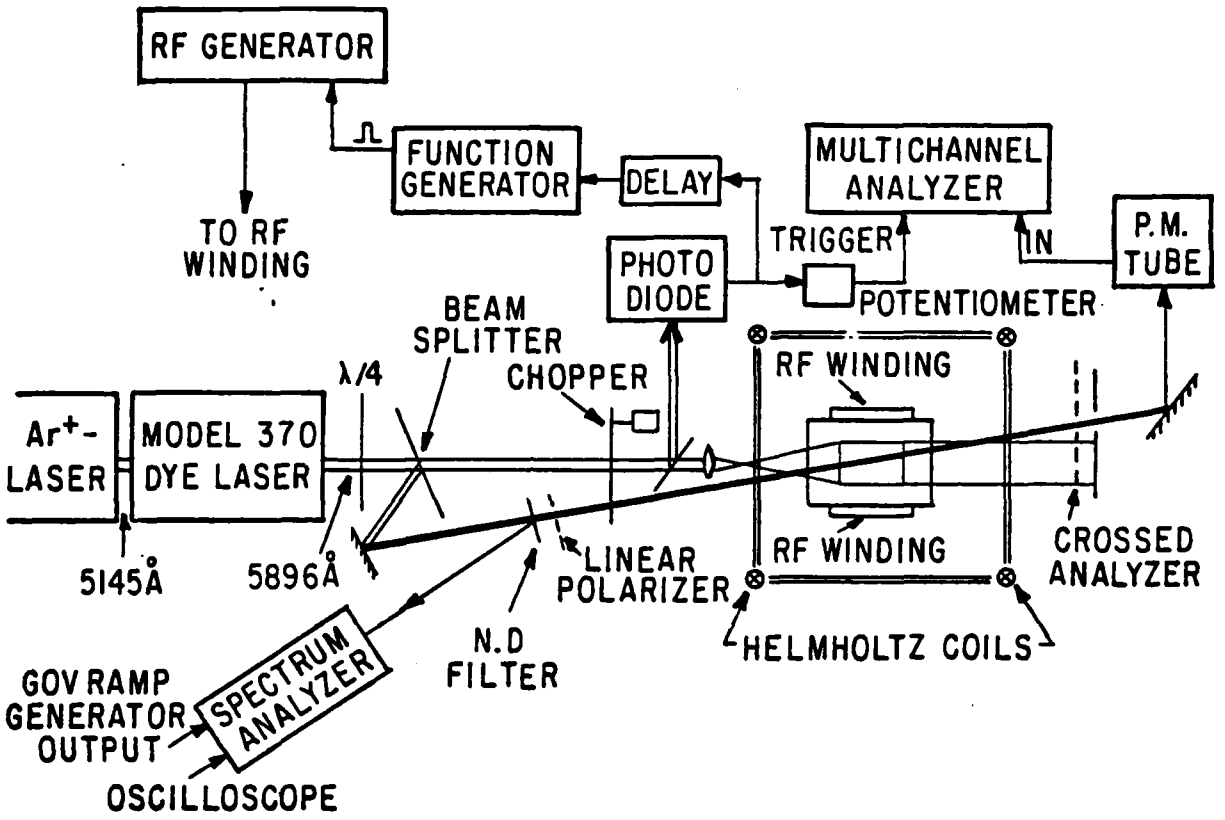
RF GENERATOR
TO RF WINDING
FUNCTION GENERATOR
DELAY
MULTICHANNEL ANALYZER
TRIGGER
IN
P.M. TUBE
PHOTO DIODE
POTENTIOMETER
BEAM SPLITTER
λ/4
CHOPPER
RF WINDING
Ar+- LASER
MODEL 370 DYE LASER
5145Å
5896Å
LINEAR POLARIZER
RF WINDING
CROSSED ANALYZER
N.D FILTER
HELMHOLTZ COILS
GOV RAMP GENERATOR OUTPUT
SPECTRUM ANALYZER
OSCILLOSCOPE

Figure 1

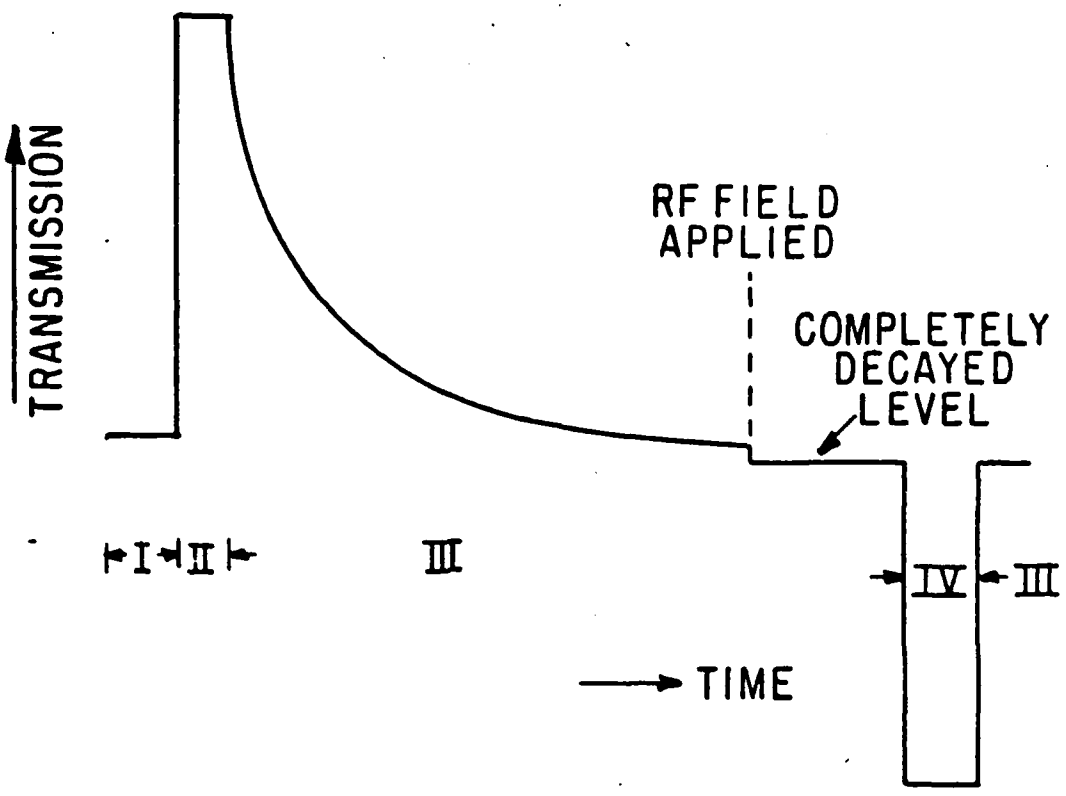
TRANSMISSION
RF FIELD
APPLIED
COMPLETELY
DECAYED
LEVEL
I
II
III
IV
III
TIME

Figure 2

equilibrium and T_1 is the decay constant of the observable being measured. If we observe either $\langle S_z \rangle$ or $\langle \vec{I} \cdot \vec{S} \rangle$ for a sufficiently long time, we always find that the observables decay with a single exponential, i.e.

$$\frac{d}{dt} \langle S_z \rangle = -\frac{1}{T_1} \langle S_z \rangle \tag{2}$$

$$\frac{d}{dt} \langle I \cdot S \rangle = -\frac{1}{T_2} \langle I \cdot S \rangle \tag{3}$$

A typical plot of $\ell n \ \ell n \ [I(t)/I(\infty)]$ vs t is shown in Figure 3. From the slope of these lines the decay rate $1/T_1$ or $1/T_2$ was measured.

Four major relaxation mechanisms contribute independently to the experimentally observed rates $1/T_1$ and $1/T_2$.

1) Diffusion: The optically pumped sodium vapor diffuses through the buffer gas (Helium) to the walls of the cell. Every collision with the cell walls completely destroys the polarization. The slowest decay rate $1/T_D$ of any observable in cylindrical cells of length L and radius r is

$$\frac{1}{T_D} = \left[\frac{\pi^2}{L^2} + \frac{(2.405)^2}{r^2} \right] \times D_o \left(\frac{760}{P}\right)$$

where D_o is the diffusion constant at 760 Torr of buffer gas which has a pressure P in the cell.

2) Binary Collisions: The spin orbit interaction in sudden binary alkali-noble gas collisions[2] causes the observable $\langle \vec{I} \cdot \vec{S} \rangle$ to relax with a single time constant[3] $1/T_H$ such that

$$\frac{1}{T_H} = [N] \bar{v} \sigma_B$$

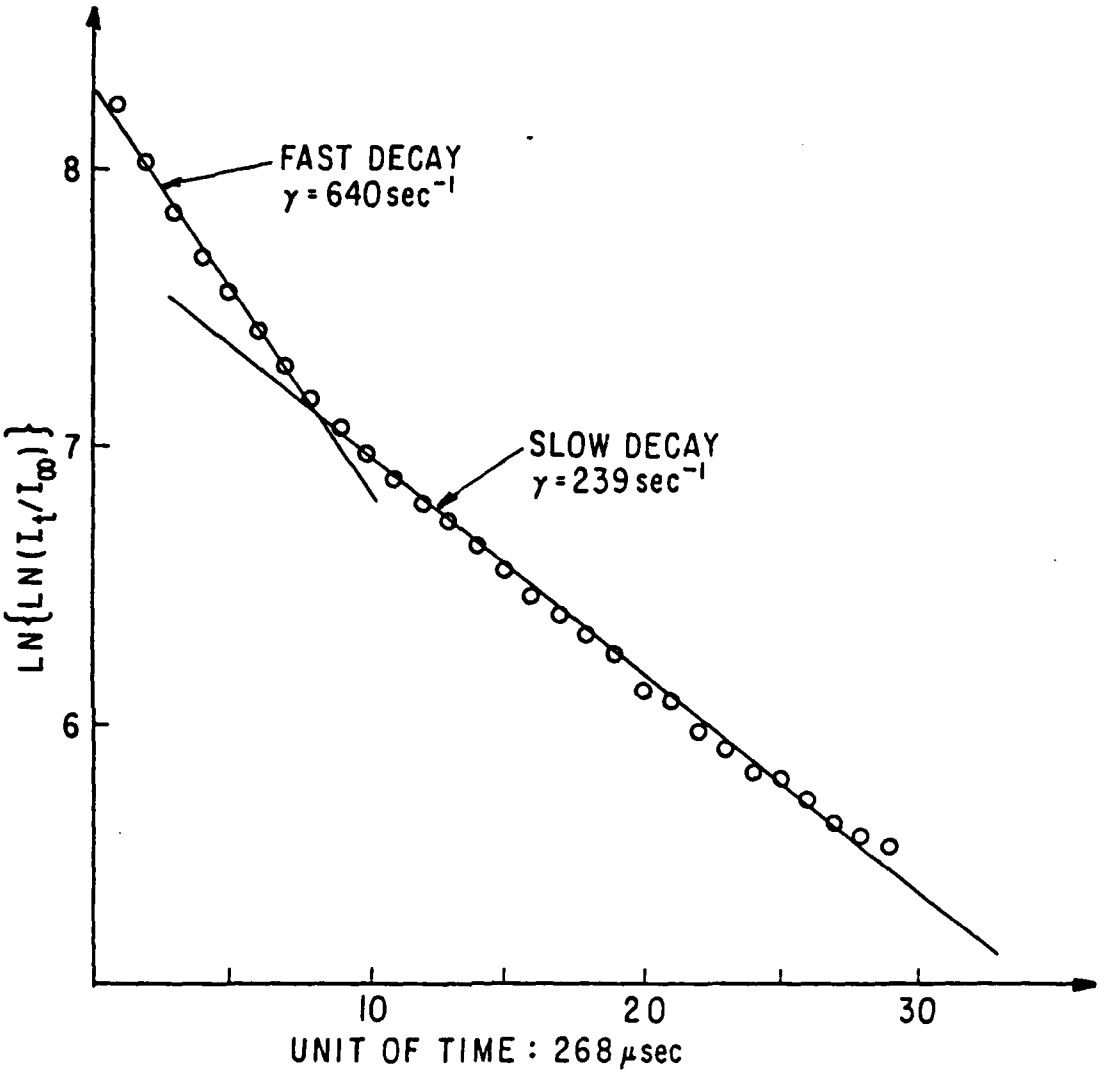
FAST DECAY
$\gamma = 640\,sec^{-1}$
SLOW DECAY
$\gamma = 239\,sec^{-1}$
8
7
6
$LN\{LN(I_t/I_\infty)\}$
10
20
30
UNIT OF TIME : 268 μsec

Figure 3

where [N] is the number density of the noble gas, $\bar{v}$ is the average relative velocity of the colliding pair and σ_B is the electron randomization cross section, for binary alkali-noble gas collisions.

The slowest relaxation rate of the observable $\langle S_z \rangle$ due to binary collisions is f/T_H where f is the slowing down factor due to the nuclear inertial effect.[4] It varies between 1/6 and 1/8 for Na(I = 3/2) depending on whether the Na vapor is in spin temperature equilibrium or not.

3) Three Body Collisions: If the sodium and noble gas atoms collide in the presence of a third particle, alkali-noble gas molecules can be formed due to weak attractive Van der Waal's forces. The observable $\langle S_z \rangle$ relaxes with a time constant $1/T_S$. During the lifetime of the Van der Waals molecule the atomic populations are redistributed among the Zeeman sublevels in a particular hyperfine multiplet. Very few transitions take place between hyperfine levels, and as a consequence $\langle \vec{I} \cdot \vec{S} \rangle$ does not relax.[5] The decay rate $1/T_S$ depends on the external magnetic field and on the pressure of the buffer gas which serves as a third body.

4) Spin Exchange Collisions: Two colliding alkali atoms can interchange their spins during collision. This spin exchange can very effectively relax $\langle \vec{I} \cdot \vec{S} \rangle$. If $\langle S_z \rangle$ is maintained at zero then the relaxation rate of $\langle \vec{I} \cdot \vec{S} \rangle$ due to spin exchange is[4]

$$\frac{1}{T_{ex}} = [Na]\, \bar{v}\, \sigma_{ex} \qquad (4)$$

where [Na] is the sodium number density and σ_{ex} is spin exchange cross section.

From the above discussion it is clear that the relaxation rate $1/T_1$ of $\langle S_z \rangle$ is

$$\frac{1}{T_1} = \frac{1}{T_D} + \frac{f}{T_H} + \frac{1}{T_S} \tag{5}$$

The relaxation rate $1/T_2$ of $\langle \vec{I} \cdot \vec{S} \rangle$ is

$$\frac{1}{T_2} = \frac{1}{T_D} + \frac{1}{T_H} + \frac{1}{T_{ex}} \tag{6}$$

Discussion of Results: The depolarization cross section for Na-He collisions is very small ($\sim 10^{-26}$ cm^2) therefore Helium merely serves as a buffer gas or as a third body. To get the diffusion constant in Helium we measured the relaxation of $\langle S_z \rangle$ in cells with no xenon. A plot of $1/T_1$ vs P^{-1} is shown in Figure 4. From the slope of the line we get

$$D_o(\text{Na-He}) = (0.35 \pm 0.19) \text{ cm}^2/\text{sec}$$

The relaxation rates of $\langle \vec{I} \cdot \vec{S} \rangle$ and $\langle S_z \rangle$ at different temperatures are shown in Figure 5. From equations 5 and 6 we have

$$\frac{1}{T_2} \text{ (no xenon)} = \frac{1}{T_D} + \frac{1}{T_{ex}} \tag{7}$$

$$\frac{1}{T_2} \text{ (2 torr xenon)} = \frac{1}{T_D} + \frac{1}{T_{ex}} + \frac{1}{T_H} \tag{8}$$

$1/T_{ex}$ is the only term which depends on sodium number density. From the slope of two parallel lines we get

$$\sigma_{ex} = 1.57 \times 10^{-14} \text{ cm}^2$$

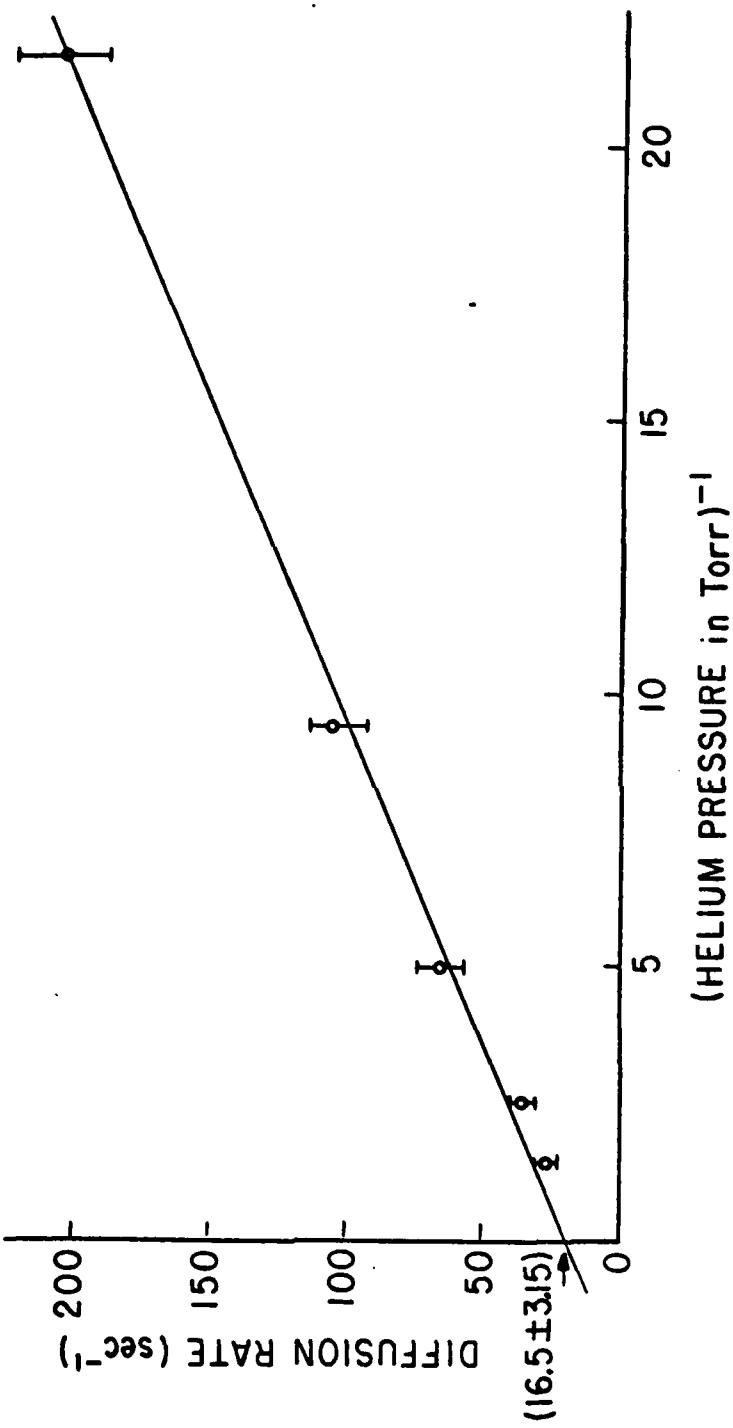
DIFFUSION RATE (sec⁻¹)
200
150
100
50
0
(16.5±3.15)
5
10
15
20
(HELIUM PRESSURE in Torr)⁻¹

Figure 4

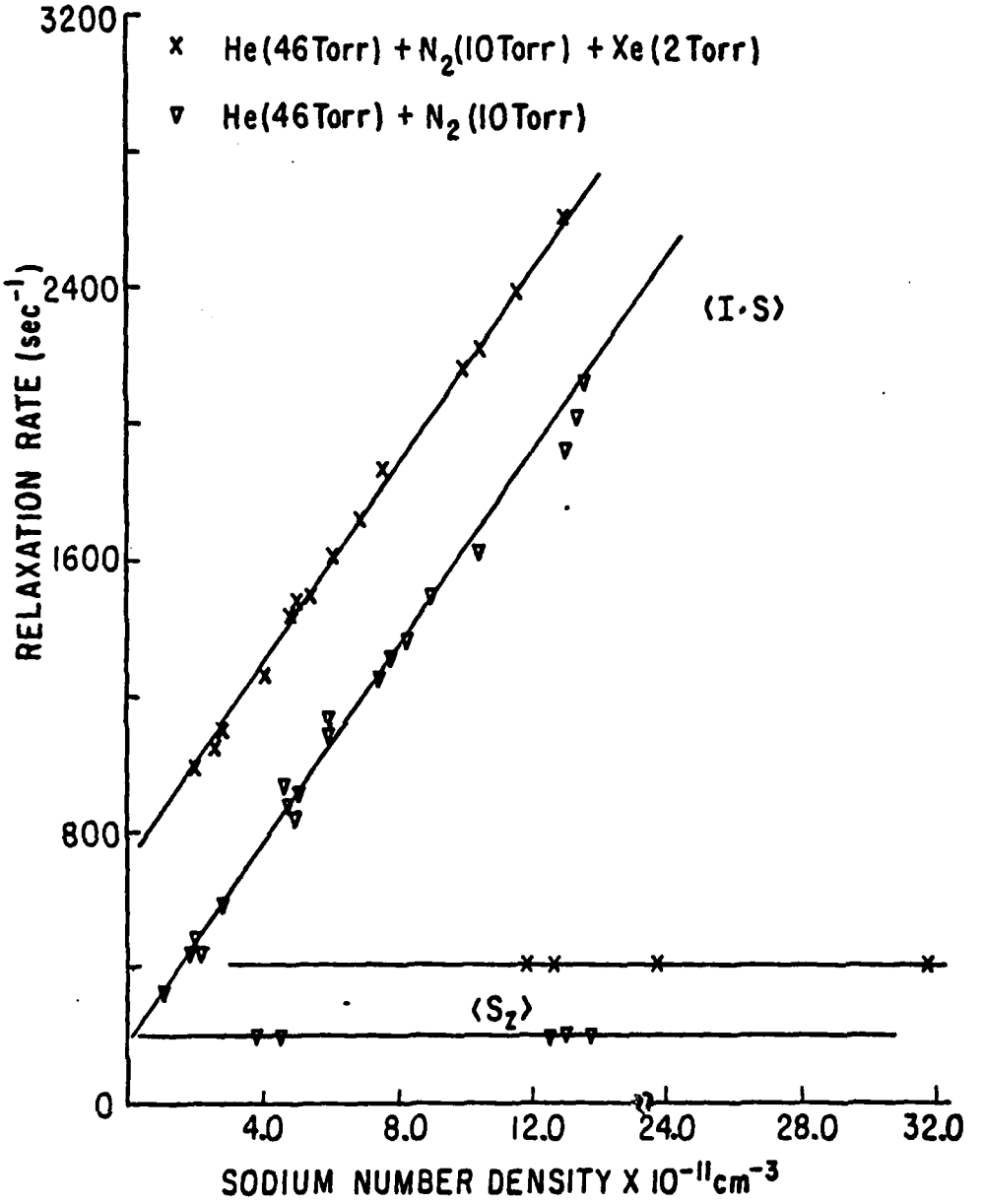
3200
2400
1600
800
0
RELAXATION RATE (sec⁻¹)
× He(46Torr) + N2(10Torr) + Xe(2Torr)
▽ He(46Torr) + N2(10Torr)
⟨I·S⟩
⟨Sz⟩
4.0
8.0
12.0
24.0
28.0
32.0
SODIUM NUMBER DENSITY X 10⁻¹¹cm⁻³

Figure 5

The difference between the relaxation rates of $\langle \vec{I} \cdot \vec{S} \rangle$ with 2 torr of xenon and with no xenon at a fixed sodium number density gives us $1/T_H$ (see equations 7 and 8), the relaxation rate due to Na-Xe binary collisions.

$$\frac{1}{T_{xe}} = 232 \text{ Sec}^{-1} \text{ per torr of Xe.}$$

So the binary sodium spin depolarization cross section is

$$\sigma_B \text{ (Na-Xe)} = 1.19 \times 10^{-19} \text{ cm}^2 .$$

Three body effects: The relaxation rate of $\langle S_z \rangle$ at different helium pressures for 2 torr of xenon is shown in Figure 6. The absence of a straight line clearly indicates that $\langle S_z \rangle$ does not relax due to binary collisions alone. At high helium pressures the Na-Xe molecules break up more rapidly due to collisions with He atoms and there is less time available for spin relaxation within the Van der Waals molecule. This decreases the relaxation rate $1/T_S$. At lower helium pressure ($\sim$ 46 torr) the relaxation due to Van der Waals molecules is more dominant.

To further investigate the three-body effect, the external magnetic field H_o was varied. The relaxation rate of $\langle S_z \rangle$ vs H_o is shown in Figure 7. At high fields the total angular momentum $\vec{F}$ ($= \vec{I}+\vec{S}$) precesses around H_o instead of coupling to the rotational angular momentum $\vec{N}$ of the tumbling Na-Xe molecule. This decoupling slows down the relaxation $1/T_S$, and hence the total relaxation rate decreases with increasing H_o. From the half width of the curve the estimated life time of the Van der Waals molecules is of the order of 10^{-8} sec. A systematic study of

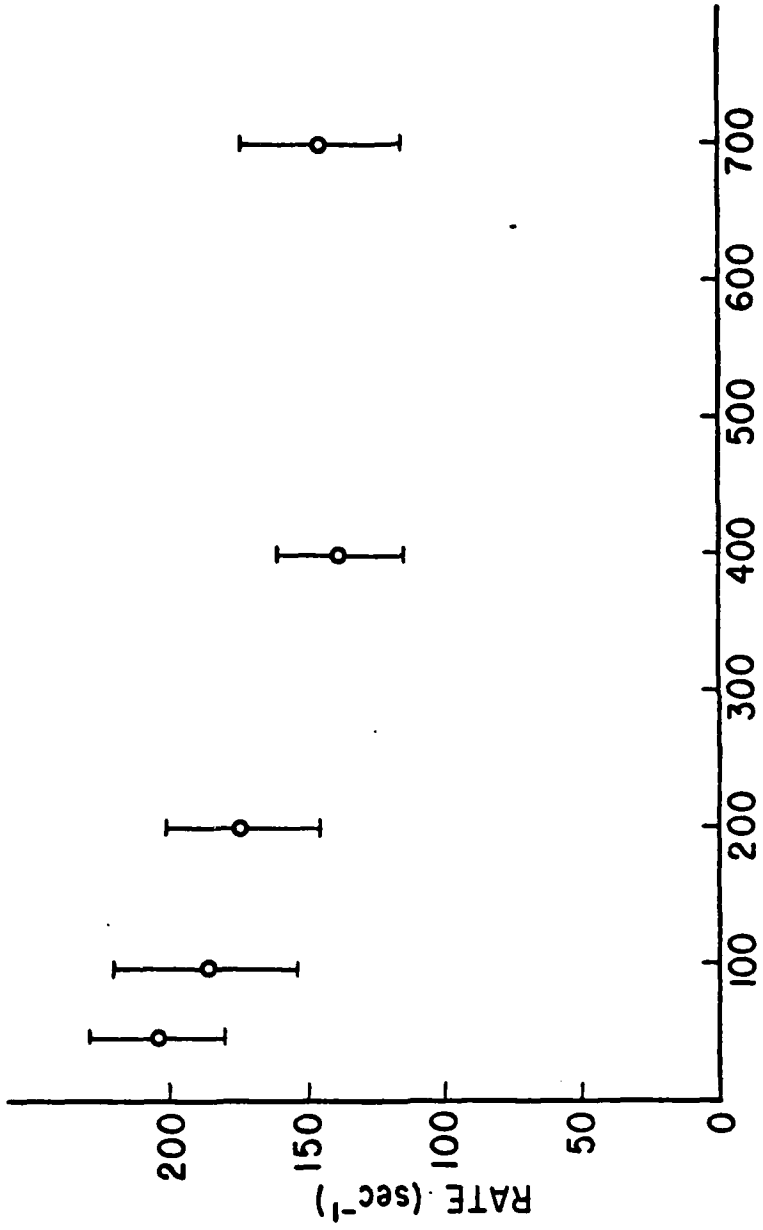
RATE (sec⁻¹)
200
150
100
50
0
100
200
300
400
500
600
700
HELIUM PRESSURE in Torr

Figure 6

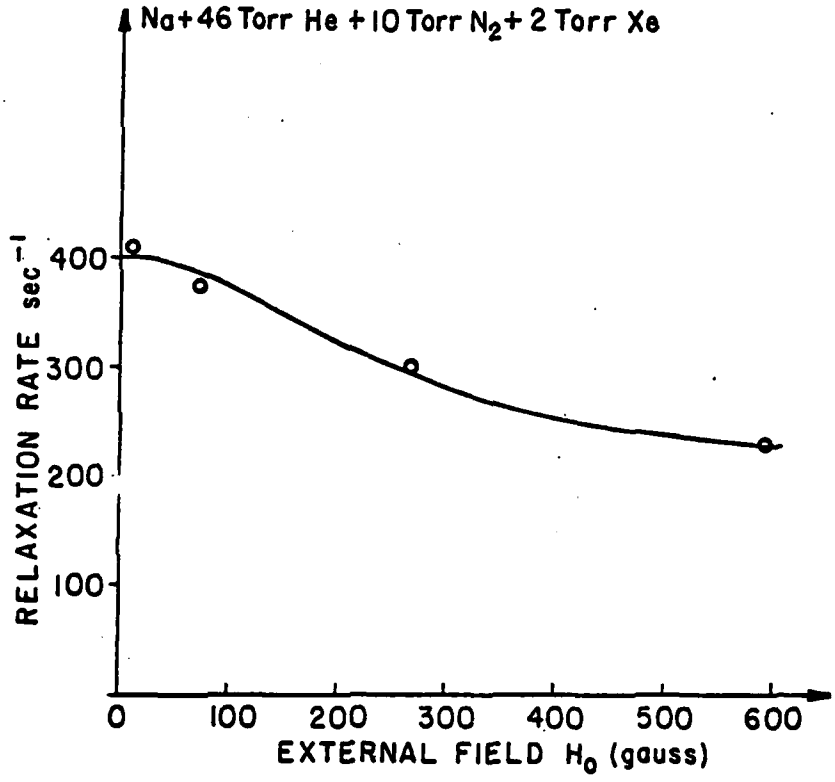
Na+46 Torr He + 10 Torr N_2 + 2 Torr Xe
RELAXATION RATE sec^{-1}
400
300
200
100
0
100
200
300
400
500
600
EXTERNAL FIELD H_0 (gauss)

Figure 7

the three-body effects is necessary for a better understanding of the relaxation mechanism of the Na-Xe system. We plan to start these experiments in the near future.

*This research is also supported by the Air Force Office of Scientific Research under Grant AFOSR-79-0082.

(1) CRL Progress Report #29, March 31, 1979, p. 13.

(2) R. A. Bernheim, J. Chem. Phys. 36, 135 (1962).

(3) M. A. Bouchiat, J. Phys. 24, 379 (1963).

(4) W. Happer, Rev. Mod. Phys. 44, 169 (1972).

(5) C. C. Bouchiat, M. A. Bouchiat and L. C. L. Pottier, Phys. Rev. 181, 144 (1969).

II. ENERGY TRANSFER AND RELAXATION IN SMALL POLYATOMIC MOLECULES

A. METASTABLE ENERGY DISTRIBUTIONS IN COF_2*

(R. Bohn, G. W. Flynn)

The molecule COF_2 provides a system which exhibits a variety of interesting phenomena. Since it absorbs many CO_2 laser lines, COF_2 can be easily excited in the infrared. There have been reports of visible emission[1] and photofragmentation[2] following intense laser excitation of this molecule.

We have studied the intermode energy transfer of COF_2 following excitation of the ν_2 symmetric C-F stretching frequency. Fluorescence emission has been observed from all fundamental levels on time scales ranging from microseconds to milliseconds after laser pumping.[3][4] A major question which we have been able to answer in the past ye- is the mechanism for filling of the ν_4 antisymmetric C-F stretch mode. This state is 282 cm^{-1} higher in energy than the initially excited ν_2 state. The fluorescence from ν_4 exhibits extremely unusual behavior since it consists of both a fast exponential growth and a slow exponential growth followed by overall slow decay. Kinetically such a pattern of dynamic energy flow is remarkably rare, and we have determined that ν_4 is a level that empties faster than it fills. The overall mechanism for energy transfer involving ν_4 is

Laser Excitation	$COF_2(0) + h\nu_L \rightarrow COF_2(\nu_2)$	(1)
Endothermic V-V Energy Transfer	$COF_2(\nu_2) + M \rightleftarrows COF_2(\nu_4) + M - 282\ cm^{-1}$	(2)

Resonant V-V Energy Transfer

$$COF_2(\nu_4) + M \rightleftarrows COF_2(\nu_3 + \nu_5) + M \quad (3)$$

Reverse Ladder Climbing V-V Energy Transfer

$$COF_2(\nu_3 + \nu_5) + COF_2(0) \rightleftarrows COF_2(\nu_3) + COF_2(\nu_5) \quad (4)$$

The levels $2\nu_3$ and $2\nu_5$ may also be involved in steps (3) and (4). The crucial feature of this scheme is that step (2) occurs with about 1/5 the probability of step (3) thus leading to the unusual fluorescence behavior observed for the ν_4 state.

We are currently developing a consistent set of coupled differential equations which will allow us to describe fully the energy transfer pathway for all the modes of COF_2. Currently we are faced with only one vexing question. Step (2) competes with the exothermic V-V event

Exothermic V-V Energy Transfer

$$COF_2(\nu_2) + M \rightleftarrows COF_2(\nu_6) + M + 199\ cm^{-1} \quad (5)$$

The overall fluorescence pattern is a sensitive function of this competition and we have not yet been able to establish the degree of importance of the event (5). We expect to determine the cross section for this process in the next few months.

In addition to the visible emission[1] and photofragmentation[2] phenomena mentioned above, we have also shown that COF_2 is an excellent candidate for a new class of laser system.[5] Gain calculations suggest the possibility of laser action on the $\nu_1 \rightarrow \nu_4$, $\nu_1 \rightarrow \nu_6$, $\nu_1 \rightarrow \nu_3$, and / or $\nu_1 \rightarrow \nu_5$ transitions.

*This research was also supported by the National Science Foundation under Grant NSF-CHE77-24343.

(1) J. W. Hudgens, J. L. Durant, Jr., D. J. Bogan, and R. A. Coveleskis, J. Chem. Phys. 70, 5906 (1979).

(2) R. Sheorey and G. Flynn, Chem. Phys.,Submitted for publication; Columbia Radiation Laboratory Progress Report #29, March 31, 1980.

(3) K. R. Casleton and G. W. Flynn, J. Chem. Phys. 67, 3133 (1977).

(4) K. Casleton, Y. V. C. Rao, and G. W. Flynn, Columbia Radiation Laboratory Progress Report #29, March 31, 1980.

(5) I. Shamah and G. Flynn, "Vibrational Relaxation Induced Population Inversions in Laser Pumped Polyatomic Molecules," Chem. Phys., accepted for publication.

B. VIBRATIONAL TEMPERATURE MEASUREMENT IN STRONGLY PUMPED COF_2*

(M. I. Lester, G. W. Flynn)

Infrared laser-induced fluorescence studies in small polyatomic molecules have shown that most vibration to vibration (V-V) energy transfer processes occur on a relatively fast time scale compared to overall vibration to translation/rotation (V-T/R) relaxation.[1] The V-V energy transfer processes fall into two basic categories: intramode processes which redistribute excess vibrational energy throughout the various levels of a particular vibrational mode and intermode processes which couple the distinct vibrational modes of the molecule. The intramode processes are controlled by near-resonant 'ladder-climbing' collisions of the form

$$M((v_j-1)\nu_j) + M(\nu_j) \rightleftharpoons M(v_j\nu_j) + M(0) \qquad (1)$$

which typically occur in 1-10 gas kinetic collisions. Intermode vibrational energy transfer usually requires several hundred gas kinetic collisions through nonresonant processes of the type

$$M(\nu_i) + M \rightleftharpoons M(\nu_j) + M + \Delta E = E_i - E_j \qquad (2)$$

where v_j is the quantum number of the mode ν_j having energy E_j. Following state selective excitation of the molecule with a CO_2 laser, these collisional processes can establish a distinctly non-thermal steady state population distribution in the vibrational modes.[2] Under the steady state condition, the population in each mode can be described in the harmonic oscillator limit by a characteristic vibrational temperature, T_i.[2]-[4] Further, the vibrational temperatures of individual modes are

related strictly by the mechanism which couples the modes. Prior to overall vibrational relaxation, these vibrational temperatures are in general different from the instantaneous translational/rotational temperature, T. Under strong excitation conditions, collisons can also serve to enhance the absorption of the molecule. If the laser pulse duration is long compared to the mean time between molecular collisions, ladder climbing collisions (1) can remove population from the pumped state and allow the molecule to exceed the conventional 2-level saturation limit of 1/2 photon absorbed per molecule. Thus, collisional processes can lead to multiphoton absorption as well as highly non-equilibrium vibrational energy distributions.

We are currently investigating these vibrational energy distribution and excitation effects in carbonyl fluoride (COF_2). This system is a particularly interesting one to study under intense IR excitation conditions since there have been recent reports of photofragmentation,[5]

$$COF_2 + nh\nu\ (10.6\mu) \rightarrow COF + F \qquad (3)$$

and reverse internal conversion[6] with the resultant emission of vis-UV luminescence under similar conditions. In addition, the kinetic pathway information derived from these studies can compliment the results obtained from IR laser-induced fluorescence studies. We have begun measurements of the mode vibrational temperatures in COF_2 using the cold gas filter technique.[7][8]

The cold gas filter technique provides a relative measurement of the total fluorescence intensity at a frequency ν_j from all states in the particular mode, I_T, to the total fluorescence intensity minus the

v_j = 1→0 component, $I_T - I_1$. This is accomplished by observing the fluorescence emanating from a particular mode through a cell of length L' placed between the fluorescence window and the detector. The fluorescence intensity is measured with the cell empty and with the cell filled to some pressure P' of the gas under study which removes the v_j = 1→0 emission. From the ratio of these fluorescence intensities, the vibrational temperature can be determined from the expression

$$\frac{I_T - I_1}{I_T} \sim 1 - [1 - e^{-h\nu_i/kT_i}]^2 \qquad (4)$$

where ν_i is the frequency of mode i with vibrational temperature T_i. Note that equation (4) is strictly valid only for a diatomic molecule in the harmonic oscillator limit, yet it can be used for a polyatomic system to yield a reasonable estimate of the vibrational temperatures in the individual modes.

Although the cold gas filter is designed to eliminate all fluorescence emanating from the v=1 level, in practice it only removes 85-95% of this emission for heavy polyatomics. The remainder of the light leaks through the filter because it terminates on high J levels in the ground state (v=0) with very small population. In principle, this emission could be eliminated by significantly increasing the pressure (P') in the cold gas filter above the sample cell pressure, but this introduces additional complications due to pressure broadening. The initial work using the cold gas filter technique to measure vibrational temperatures attempted to correct for this leftover emission by an extrapolation procedure. In the present measurements, we have attempted to improve the accuracy of the

AD-A087 034 COLUMBIA RADIATION LAB NEW YORK F/G 7/4
RESEARCH INVESTIGATION DIRECTED TOWARD EXTENDING THE USEFUL RAN--ETC(U)
MAR 80 G W FLYNN DAAG29-79-C-0079
UNCLASSIFIED NL

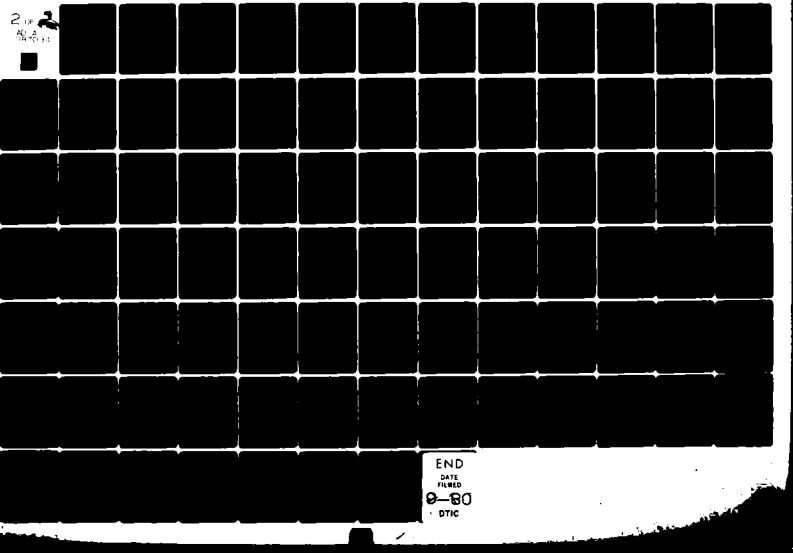

END
DATE FILMED
8-80
DTIC

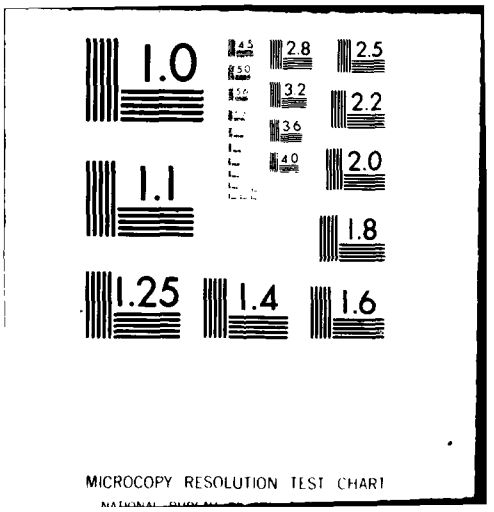
1.0
1.1
1.25
1.4
1.6
1.8
2.0
2.2
2.5
2.8
3.2
3.6
4.0
MICROCOPY RESOLUTION TEST CHART

technique by employing a calibration procedure for the cold ga
The calibration consists of using a weak laser source to excit
only into the v=1 level of a given mode. By monitoring the fl
through the cold gas filter under low level excitation, we can
determine the amount of this residual light emission.

We have measured the vibrational temperature of the carbo
ing mode ν_1 ($\sim$ 2000 cm^{-1}) as a function of COF_2 pressure for f
TEA laser excitation. The carbonyl stretch is populated from
pumped C-F symmetric stretch ν_2 via the processes[9]

$$COF_2(0) + h\nu\ (10.6\mu) \rightarrow COF_2(\nu_2) \quad \text{laser pump}$$

$$2COF_2(\nu_2) \rightleftarrows COF_2(0) + COF_2(2\nu_3) \quad \text{V-V up pumping}$$

$$COF_2(2\nu_2) + M \rightleftarrows COF_2(\nu_1) + M \quad \text{intermode V-V}$$

Steps (6) and (7) occur in approximately 30 gas kinetic collisi
intermode V-V step is atypically fast since it is aided by Ferm
of the $2\nu_2$ and ν_1 states. Because the V-V processes (6) and (7
nearly resonant, the vibrational temperatures of the pumped mod
carbonyl stretch ν_1 should be essentially the same ($T_1 = T_2$).

The vibrational temperature of the ν_1 mode is plotted as a
of COF_2 pressure in Figure 1. The observed pressure dependence
qualitatively explained in the following way. As the number of
over the fixed laser pulse width (2-3 μsec) increases, V-V ladd
(6) should become more important in enhancing the level of exci
the coupled ν_1 and ν_2 modes. Further, increasing the pressure

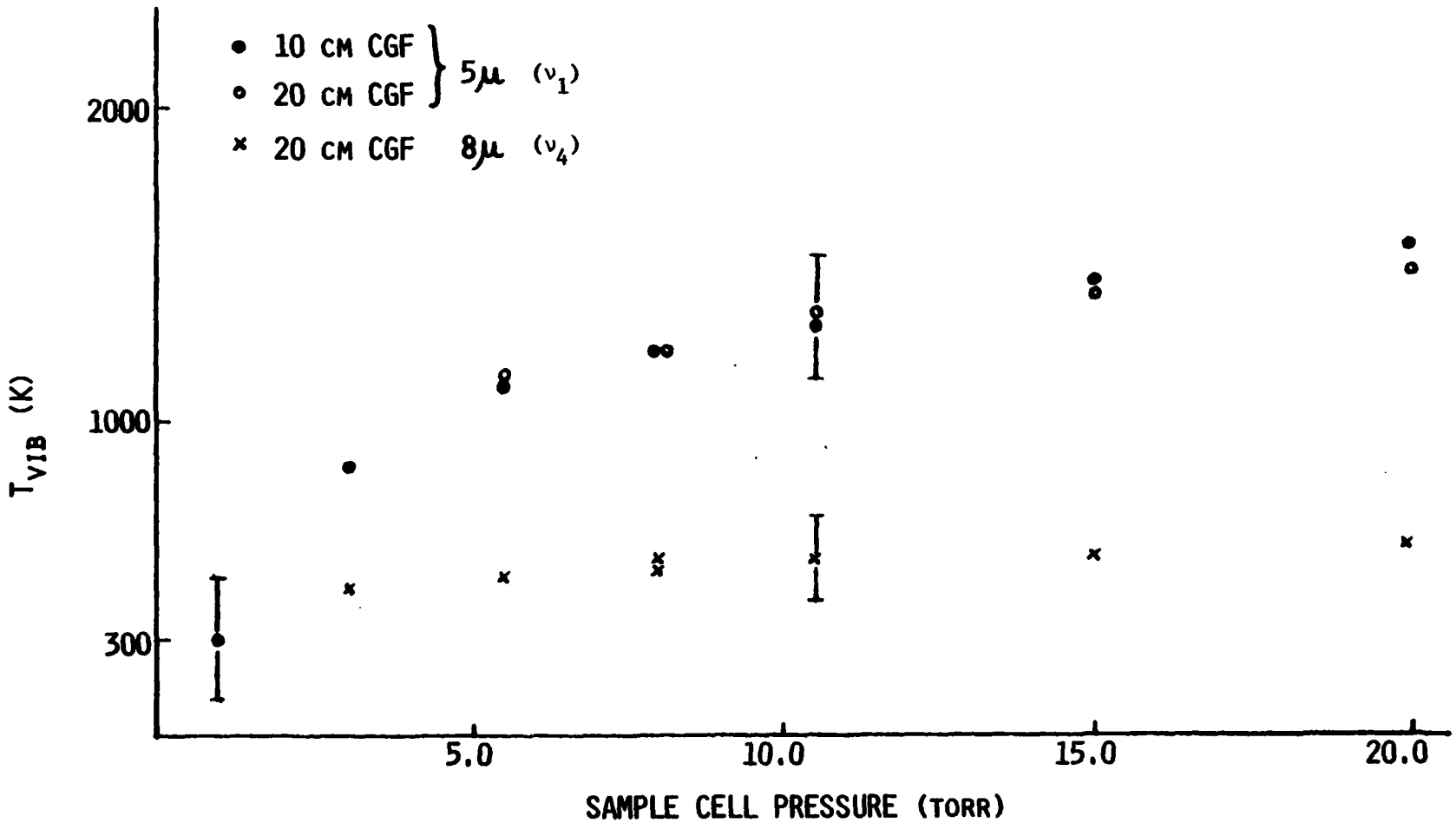
• 10 CM CGF
o 20 CM CGF
5μ (ν1)
× 20 CM CGF 8μ (ν4)
2000
1000
300
T VIB (K)
5.0
10.0
15.0
20.0
SAMPLE CELL PRESSURE (TORR)

Figure 1

pressure broaden the absorption linewidth leading to increased overlap with the laser line profile. The maximum temperature reached to date, even at higher pressures is approximately 1500K. This is surprisingly low considering that COF_2 both photofragments and emits vis-UV luminescence under similar excitation conditions. This suggests that the initial energy distribution produced by the laser and probably <u>not</u> the steady state energy distribution caused by collisions is responsible for these processes. Collisions probably play at most a minor role (e.g. reducing rotational bottlenecks).

We have also measured the vibrational temperature of the antisymmetric C-F stretch mode ν_4 ($\sim$ 1244 cm^{-1}). The COF_2 pressure dependence of these results are also shown in Figure 1. At every pressure studied, the ν_4 mode has a significantly lower temperature than ν_1. Since ν_1 and ν_2 are expected to be at the same temperature, this suggests that the ν_4 mode is endothermically coupled to ν_2 via the intermode process

$$COF_2(\nu_2) + M \rightleftarrows COF_2(\nu_4) + M - 290\ cm^{-1} \qquad (8)$$

IR fluorescence studies have indicated that this step occurs in $\sim$ 500 gas kinetic collisions.[10] The steady state condition for this process, on a time scale short compared to V-T/R relaxation, leads to a relationship between the temperatures T_2 and T_4 of the modes ν_2 and ν_4 given by

$$\frac{\nu_2}{T_2} - \frac{\nu_4}{T_4} = \frac{(\nu_2 - \nu_4)}{T} \qquad (9)$$

where T is the instantaneous translational/rotational temperature. For $T \approx 300K$ and ν_2 (964 cm^{-1}) < ν_4 (1244 cm^{-1}), equation (9) yields the

result $T_4 < T_2$ as observed. For an initial excitation level of $T_2 \sim$ 1200 K, equation (9) predicts a vibrational temperature of $\sim$ 700K for ν_4. This simple 3 mode picture (ν_2, ν_1, ν_4) is in amazingly good agreement with the observed vibrational temperature for ν_4 of $\sim$ 550K. Within the approximation of a 3 mode model for COF_2, the vibrational temperatures observed for ν_1 and ν_4 correspond to a mean excitation level of $\sim$ 0.8 CO_2 quanta absorbed per molecule at 8 torr and $\sim$ 1.3 photons absorbed per molecule at 20 torr. For both cases cited, these excitation levels are well in excess of the conventional 2-level saturation limit.

The results of the vibrational temperature measurements for ν_1 and ν_4 have interesting ramifications with regard to possible laser action in COF_2. Recently, it has been shown that population inversions can be achieved in laser pumped molecules which establish metastable steady state population distributions.[11] The conditions which favor a population inversion are: (1) rapid endothermic coupling of the pumped mode fundamental to the fundamental of another mode; (2) rapid near-resonant coupling of the overtone of the pumped mode to a fundamental of another mode; and (3) low translational temperature. All three of these conditions are met in COF_2 allowing for a population inversion of the ν_1 state (Fermi mixed to the pumped mode overtone $2\nu_2$) with respect to the ν_4 state (endothermically coupled to ν_2). Once again assuming a 3 mode model for COF_2 (ν_2, ν_1, ν_4), a population inversion between these states (ν_4 and ν_1) can be achieved at the modest excitation level of $\sim$ 1 photon absorbed per molecule. Our present results suggest that the conditions necessary for population inversion between the ν_1 and ν_4 states have already been realized at COF_2 pressures above 8 torr.

Future work includes cold gas filter measurements of the vibrational temperatures in the low lying modes of $COF_2(\nu_3, \nu_5$ and $\nu_6)$ to gain additional information on the mechanism for vibrational energy transfer in the molecule. The effects of laser energy, pulse width, and wavelength, as well as rare gas dependence will be investigated to determine the extent to which they influence the steady state population distribution.

*This research was also supported by the Department of Energy under Contract DE-AS02-78ER04940 and by the National Science Foundation under Grant NSF-CHE77-24343.

(1) E. Weitz and G. W. Flynn, "Vibrational Energy Flow in the Ground Electronic States of Polyatomic Molecules," (to be published in Advances in Chemical Physics).

(2) I. Shamah and G. W. Flynn, J. Am. Chem. Soc. 99, 3191 (1977).

(3) I. Shamah and G. W. Flynn, J. Chem. Phys. 69, 2474 (1978).

(4) C. E. Treanor, J. W. Rich, and R. G. Rehm, J. Chem. Phys. 48, 1798 (1968).

(5) R. S. Sheorey and G. W. Flynn, "HF^+ Emission as a Probe of Multiphoton Dissociation of Carbonyl Fluoride," submitted for publication, Chemical Physics.

(6) J. W. Hudgens, J. L. Durant, Jr., D. J. Bogan, and R. A. Coveleskis, J. Chem. Phys. 70, 5906 (1979).

(7) R. E. McNair, S. F. Fulghum, G. W. Flynn, M. S. Feld, and B. J. Feldman, Chem. Phys. Lett. 48, 241 (1977).

(8) R. A. Forber, R. E. McNair, S. F. Fulghum, M. S. Feld, and B. J. Feldman, "Collision-Induced Energy Absorption and Vibrational Excitation by Intense Laser Radiation in CH_3F," J. Chem. Phys., accepted for publication.

(9) K. H. Casleton and G. W. Flynn, J. Chem. Phys. 67, 3133 (1977).

(10) R. Bohn, K. H. Casleton, Y. V. C. Rao, and G. W. Flynn, work in progress.

(11) I. Shamah and G. Flynn, "Vibrational Relaxation Induced Population Inversions in Laser Pumped Molecules," submitted for publication, Chem. Phys.

C. INTERMOLECULE VIBRATIONAL ENERGY TRANSFER DYNAMICS IN IR LASER PUMPED $SO_2/^{18}O_2$ MIXTURES*

(M. I. Lester, G. W. Flynn)

Vibrational energy transfer processes in $SO_2/^{18}O_2$ mixtures have been observed by monitoring fluorescence emission from the SO_2 ν_3 mode following pulsed CO_2 laser excitation of the ν_1 mode.[1][2] The kinetic mechanism determined from these fluorescence studies allows for intermode vibrational energy transfer in SO_2[3][4] due to collisions with both SO_2 and $^{18}O_2$ as well as an intermolecule vibrational energy exchange process between SO_2 and $^{18}O_2$. The energy crossover from SO_2 to $^{18}O_2$ occurs via the step

$$SO_2(\nu_3) + {}^{18}O_2 \underset{}{\overset{k_{30}}{\rightleftharpoons}} SO_2(0) + {}^{18}O_2(1) - 107\ cm^{-1} \qquad (1)$$

The rate constant for this vibrational energy sharing process (k_{30}) was found to be 5.74 ($\pm$ 0.91) $msec^{-1}$ (torr $^{18}O_2)^{-1}$ or approximately 1400 gas kinetic collisions.

Kinetic modeling of the vibrational energy transfer processes in $SO_2/^{16}O_2$ mixtures has clarified an inconsistency in the SO_2/O_2 literature. An ultrasound investigation[5] had reported an energy crossover process from the ν_3 state of SO_2 to the v=1 level of $^{16}O_2$; yet, no energy sharing process has been observed by the infrared fluorescence technique.[4] Kinetic modeling of the population deviation in the fluorescing SO_2 ν_3 state has indicated that the amplitude of a crossover step which occurs on the time scale reported by the ultrasound study would be too small to be observed by present IR fluorescence experimental techniques.

The probability of a vibrational transition during a bimolecular collision as a result of short-range spherically symmetric repulsive forces

can be determined from the SSH breathing sphere model.[6]-[8] Vibrational energy transfer probabilities have been calculated by this method for the intermolecule vibrational energy sharing process in $SO_2/^{18}O_2$ and $SO_2/^{16}O_2$ mixtures. The SSH model predicts probabilities of energy transfer per SO_2-O_2 collision in the range of 3.6×10^{-4} to 1.3×10^{-3} for energy crossover to $^{18}O_2$ and a corresponding range of 5.6×10^{-5} to 3.7×10^{-4} for crossover to $^{16}O_2$ (see Table I). The intermolecular repulsion parameter, α, was varied from 4.5×10^8 cm^{-1} to 6.5×10^8 cm^{-1}.

Another approach for calculating the probability of a vibrational energy transfer during a bimolecular collision is based on the roll of long-range multipolar forces in effecting the transition. The theory of energy transfer caused by dipole-dipole and dipole-quadrupole interactions has been developed by Sharma and Brau.[9][10] The probability of V-V energy transfer due to long-range interactions is strongly dependent on the energy mismatch of the collision pair. As a result of the range of the multipolar potential, the probability of energy transfer falls off rapidly as the energy discrepancy is increased. Only 'near-resonant' processes have been shown to contribute significantly to the energy transfer cross section.

In the present investigation of intermolecule energy transfer in SO_2/O_2 mixtures, long-range interactions might at first glance appear to have little consequence for the overall transition probability. The energy gaps for the crossover processes from SO_2 (ν_3) to $^{18}O_2(1)$ and $^{16}O_2(1)$, - 107 cm^{-1} and - 195 cm^{-1}, respectively, are too large for the transitions to be considered as near-resonant. However, since the lowest order multipole interaction is between the instantaneous dipole moment of SO_2 and the

TABLE I

Experimental and Theoretical
Intermolecule Energy Transfer Probabilities

$$SO_2\ (\nu_3) + O_2(0) \underset{}{\overset{k_{30}}{\rightleftharpoons}} SO_2\ (0) + O_2\ (1) + \Delta E$$

	$^{18}O_2$	$^{16}O_2$
ΔE	$-107\ cm^{-1}$	$-195\ cm^{-1}$
k_{30} [a]	$5.74\ (\pm\ 0.91)$	0.26 [b]
$P_{EXP}=k_{30}/k_{gk}$ [c]	7.0×10^{-4}	3.1×10^{-5}
P_{SSH} [d]		
α [e] $= 4.5 \times 10^8\ cm^{-1}$	3.6×10^{-4}	5.6×10^{-5}
$\alpha = 5.5 \times 10^8\ cm^{-1}$	7.6×10^{-4}	1.7×10^{-4}
$\alpha = 6.5 \times 10^8\ cm^{-1}$	1.3×10^{-3}	3.7×10^{-4}
P_{SB} [f]	6.5×10^{-4}	1.2×10^{-5}

a. Rate constants are in units of $msec^{-1}\ (torr\ O_2)^{-1}$.

b. Reference (5) in text.

c. k_{gk} is the gas kinetic rate.
$k_{gk} = 2.56 \times 10^3[(\sigma_{SO_2} + \sigma_{O_2})/2]^2/\mu^{1/2}\ (msec^{-1}\ torr^{-1})$
at T=300K. μ is the reduced mass of the collision partners in amu. All σ's are taken from Reference (11).

d. Probabilities calculated from SSH breathing sphere model (References (6)-(8)).

e. α is the range parameter of the intermolecular potential.

d. Probabilities calculated from Sharma-Brau theory (Ref. (9)(10)).

quadrupole moment of O_2, rotational degrees of freedom turn out to cancel much of the relatively large vibrational band center mismatch. The Sharma-Brau long range theory predicts a probability of intermolecule energy transfer per SO_2-O_2 collision of 6.5×10^{-4} for $SO_2/^{18}O_2$ mixtures and a corresponding probability of 1.2×10^{-5} for $SO_2/^{18}O_2$ mixtures.

A comparison of experimental and theoretical results can be obtained by examination of Table I. The experimental probability for intermolecule energy sharing ($P_{EXP} = k_{30}/k_{gk}$) in $SO_2/^{18}O_2$ mixtures falls well within the range of probabilities predicted by the SSH breathing sphere model. The probability of energy exchange in $SO_2/^{16}O_2$ mixtures as determined by the ultrasound measurements is somewhat lower than the predictions of the short-range model. The origin of this discrepancy could be in the simple theory used or in the experimental results for $SO_2/^{16}O_2$ mixtures. Accurate determination of the energy sharing rate constant by ultrasound methods is difficult since oxygen contributes only a small amount to the total vibrational heat capacity in these experiments. However, the qualitative agreement between experiment and theory is sufficient in both cases to conclude that short-range repulsive forces may have some role in these energy transfer processes.

The probability of energy crossover from SO_2 to $^{18}O_2$ calculated from the long-range force model is in excellent agreement with the present experimental results. In contrast, the probability of energy sharing predicted by the long-range theory for $SO_2/^{16}O_2$ mixtures is significantly smaller than the probability reported in the ultrasound study. The agreement between theory and experiment in the $SO_2/^{18}O_2$ case suggests that long-range multipolar forces are a viable means for energy transfer in

this system. Long-range interactions appear to be much less important in $SO_2/^{16}O_2$ mixtures simply because the energy mismatch of the vibrational band centers is much greater for this oxygen isotope.

Comparison of calculated and experimentally observed probabilities indicates that both short-range and long-range forces contribute to the intermolecule energy transfer process in $SO_2/^{18}O_2$. A similar comparison for the $SO_2/^{16}O_2$ system suggests that long-range forces have little role in the energy transfer process and that short-range forces probably dominate the interaction.

A technique has been developed for calculating the propagating error in the kinetic rate constants due to the experimental uncertainties of the measured eigenvalues in polyatomic molecule energy transfer experiments. The standard deviation for each rate constant, σ_{K_i} can be expressed in terms of the standard deviations of the eigenvalues, σ_{λ_j}, as

$$\sigma_{K_i} = \left[\sum_{j=1}^{n} \left[\frac{\partial K_i}{\partial \lambda_j} \right]^2_{\lambda_{\ell \neq j}} \sigma^2_{\lambda_j} \right]^{1/2}$$

where n is the number of independent eigenvalues associated with the system. For convenience in evaluation, the partial derivations above can be rewritten in terms of partial derivatives of the form $\left[\frac{\partial \lambda_j}{\partial K_i}\right]_{K_{\ell \neq i}}$ by means of a Jacobian transformation.

A full manuscript describing this work has been accepted for publication and is scheduled to appear in the Journal of Chemical Physics during June 1980.

*This research was also supported by the National Science Foundation under Grant NSF-CHE-77-24343.

(1) CRL Progress Report #29, March 31, 1979, p. 55.

(2) M. I. Lester and G. W. Flynn, J. Chem. Phys. 72, 0000 (1980).

(3) D. Siebert and G. W. Flynn, J. Chem. Phys. 62, 1212 (1975).

(4) G. A. West, R. E. Weston, and G. W. Flynn, J. Chem. Phys. 67, 4873 (1977).

(5) B. Anderson, F. D. Shields, and H. E. Bass, J. Chem. Phys. 56, 1147 (1972).

(6) R. N. Schwartz, Z. I. Slawsky, and K. F. Herzfeld, J. Chem. Phys. 20, 1951 (1952).

(7) F. I. Tanczos, J. Chem. Phys. 25, 439 (1956).

(8) J. L. Stretton, Trans. Faraday Soc. 61, 1053 (1965).

(9) R. D. Sharma and C. A. Brau, Phys. Rev. Lett. 19, 1273 (1967).

(10) R. D. Sharma and C. A. Brau, J. Chem. Phys. 50, 924 (1969).

(11) J. O. Hirschfelder, C. F. Curtis, and R. B. Bird, Molecular Theory of Gases and Liquids (Wiley, New York, 1954).

D. VIBRATIONAL ENERGY TRANSFER MAP FOR OCS*

M. L. Mandich and G. W. Flynn

Although vibrational energy transfer processes have been investigated in a large number of molecules,[1] the impact of most of these studies has been limited by the variety of possible interpretations which fit the experimental results. Kinetic rate constants are by far the most useful quantities for describing vibrational energy transfer, but these constants can only be determined when their associated kinetic events can be identified. Usually, the available experimental rate data consists of time dependent population changes which just yield eigenvalues of a rate matrix corresponding to convolutions of several coupled kinetic events. Bridging the gap between measured eigenvalues and kinetic rate constants requires solving the rate matrix formed by all of the competing energy transfer processes. While this has never been completely achieved for any polyatomic molecule, the most advanced knowledge of this type exists for CH_3F[2][3] and SO_2.[4][5] A partial mapping for OCS, well known as a chemical[6] and infrared laser,[7] has been attempted by several laboratories with conflicting results.[8]-[13] In this work, these differences have been resolved and we report an energy transfer map for OCS which includes all of the major kinetic pathways plus their rates.[14] The pathways and rates can be used to describe the flow of excess vibrational energy among the three OCS vibrational modes as well as overall relaxation into rotations and translations.

The essential ingredients required to construct a kinetic map are the measured eigenvalues and amplitudes describing the time dependent behavior of the perturbed vibrational state populations. In OCS, the

initial excess population is placed in the first overtone of the bending vibration, $2\nu_2$, by way of a CO_2 laser pump pulse. Improved detectors and signal averaging equipment have permitted accurate measurement of time dependent fluorescences emanating from all three fundamental vibrational states and two other combination states. (See Figure 1 and Table I.)

From the fluorescence data and subsequent kinetic analysis, the following sequence of events is deduced for the vibrational energy transfer map in OCS.[14]

1) Initially, the $2\nu_2$ level is pumped with the CO_2 laser,

$$OCS(0) \xrightarrow[CO_2 \text{ laser}]{9.6\mu \; P(22)} OCS(2\nu_2) \quad .$$

2) The bending modes rapidly equilibrate (in about 10-30 gas kinetic collisions) by near resonant up-the-ladder collisional processes such as:

$$OCS(2\nu_2) + OCS(0) \rightleftarrows OCS(\nu_2) + OCS(\nu_2)$$

$$OCS(2\nu_2) + OCS(\nu_2) \rightleftarrows OCS(3\nu_2) + OCS(0)$$

$$OCS(3\nu_2) + OCS(\nu_2) \rightleftarrows OCS(4\nu_2) + OCS(0) \quad .$$

3) The first intermode V-V energy transfer occurs on a much longer timescale as the asymmetric stretch, ν_3, is populated via

$$OCS(4\nu_2) + OCS \rightleftarrows OCS(\nu_3) + OCS + 43 \text{ cm}^{-1}$$

at a rate corresponding to 680 gas kinetic collisions. This unfavorable exchange of what is formally five vibrational quanta is the most rapid intermode V-V energy transfer process.

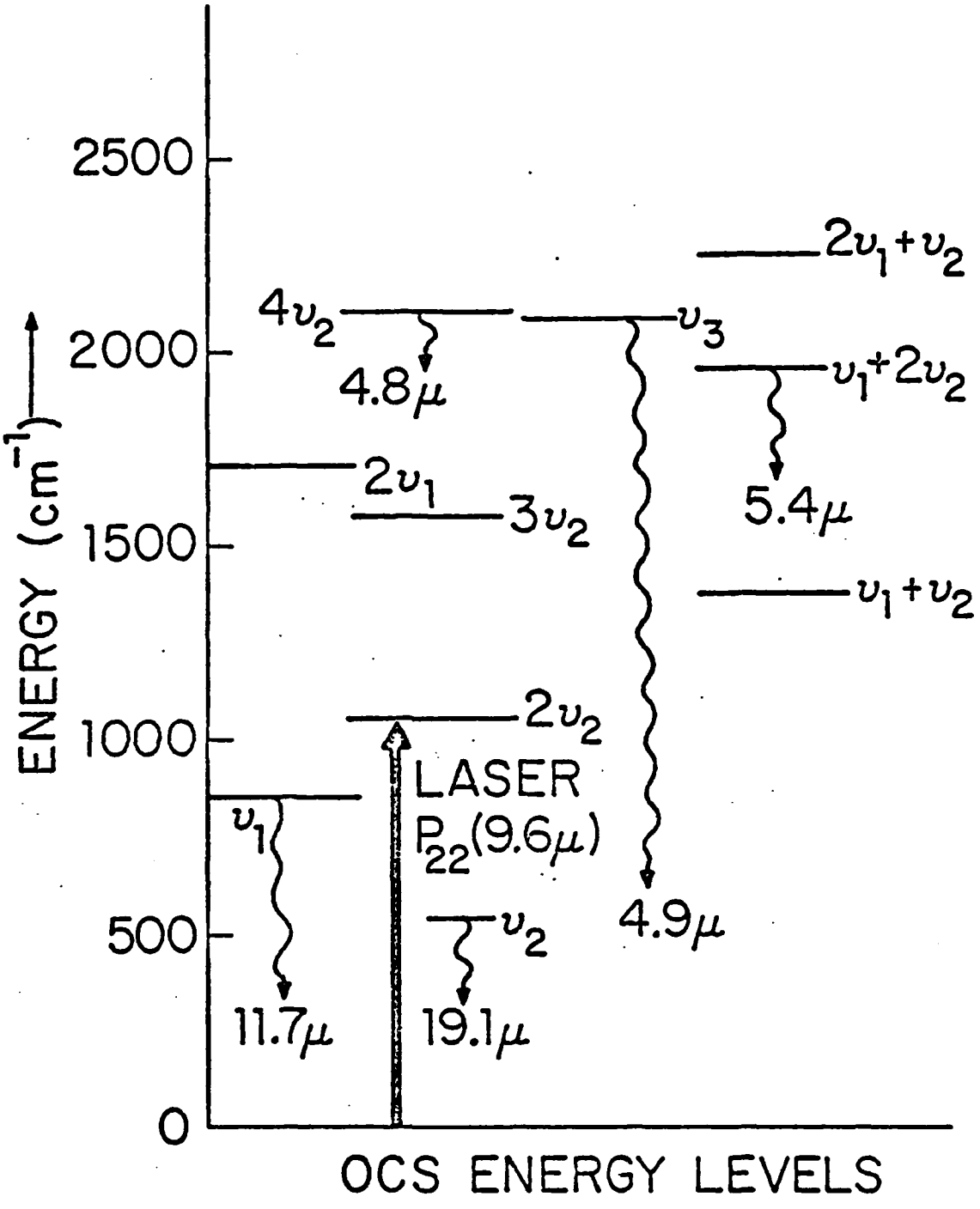

Figure 1: Experimentally observed OCS fluorescences are depicted on this OCS energy level diagram for energies up to 2400 cm^{-1}. All of these fluorescences (marked with wavy lines) terminate on the ground state. The pulsed CO_2 laser excitation is marked with a heavy arrow.

TABLE I

Experimental Fluorescence Eigenvalues ($msec^{-1} torr^{-1}$)[a]

$-\lambda_2$ ("ν_1 filling")	$-\lambda_3$ ("V-T" decay)	$-\lambda_4$ ("ν_3 filling")
5.6 ± .6 (4.94 μ decay)	1.8 ± .15 (4.94 μ decay)	47 ± 4 (4.94 μ rise)
5.5 ± .4 (11.7 μ rise)	1.7 ± .2 (11.7 μ decay)	
	1.8 ± .2 (19.1 μ decay)	
	1.7 ± .2 (5.36 μ decay)	

a. errors reported are ± two standard deviations.

4) The symmetric stretch equilibrates more slowly via

$$OCS(2\nu_2) + OCS \rightleftarrows OCS(\nu_1) + OCS + 188\ cm^{-1}$$

at a rate corresponding to 2400 gas kinetic collisions. This vibrational mode may also be populated by a secondary path of

$$OCS(\nu_2) + OCS \rightleftarrows OCS(\nu_1) + OCS - 339\ cm^{-1}$$

at a much slower rate requiring more than 24,000 gas kinetic collisions.

5) Loss of total excited vibrational population through V-T/R relaxation,

$$OCS(\nu_2) + OCS \rightleftarrows OCS(0) + OCS + 520\ cm^{-1}$$

occurs at a rate corresponding to 3400 gas kinetic collisions.

Combining these kinetic steps with their accompanying rate constants, the population fluctuations of the vibrational levels can be calculated as a function of time which is shown in graphical form in Figure 2 for the pumped mode ($2\nu_2$) and the three fundamental modes (ν_1, ν_2 and ν_3).

The probabilities measured for energy transfer in OCS-OCS collisions can be directly compared to calculated energy transfer probabilities using a model based on either short range repulsive forces[15-17] or long range attractive forces.[18] The relative agreement and disagreement between various predicted and measured values highlight the nature of the interaction potential and the importance of mechanical and electrical anharmonicities in determining the kinetic paths. The short range force model calculation gives theoretical values for all intermode vibration-vibration probabilities which are grossly below the observed probabilities when the states are approximated by simple harmonic oscillators.

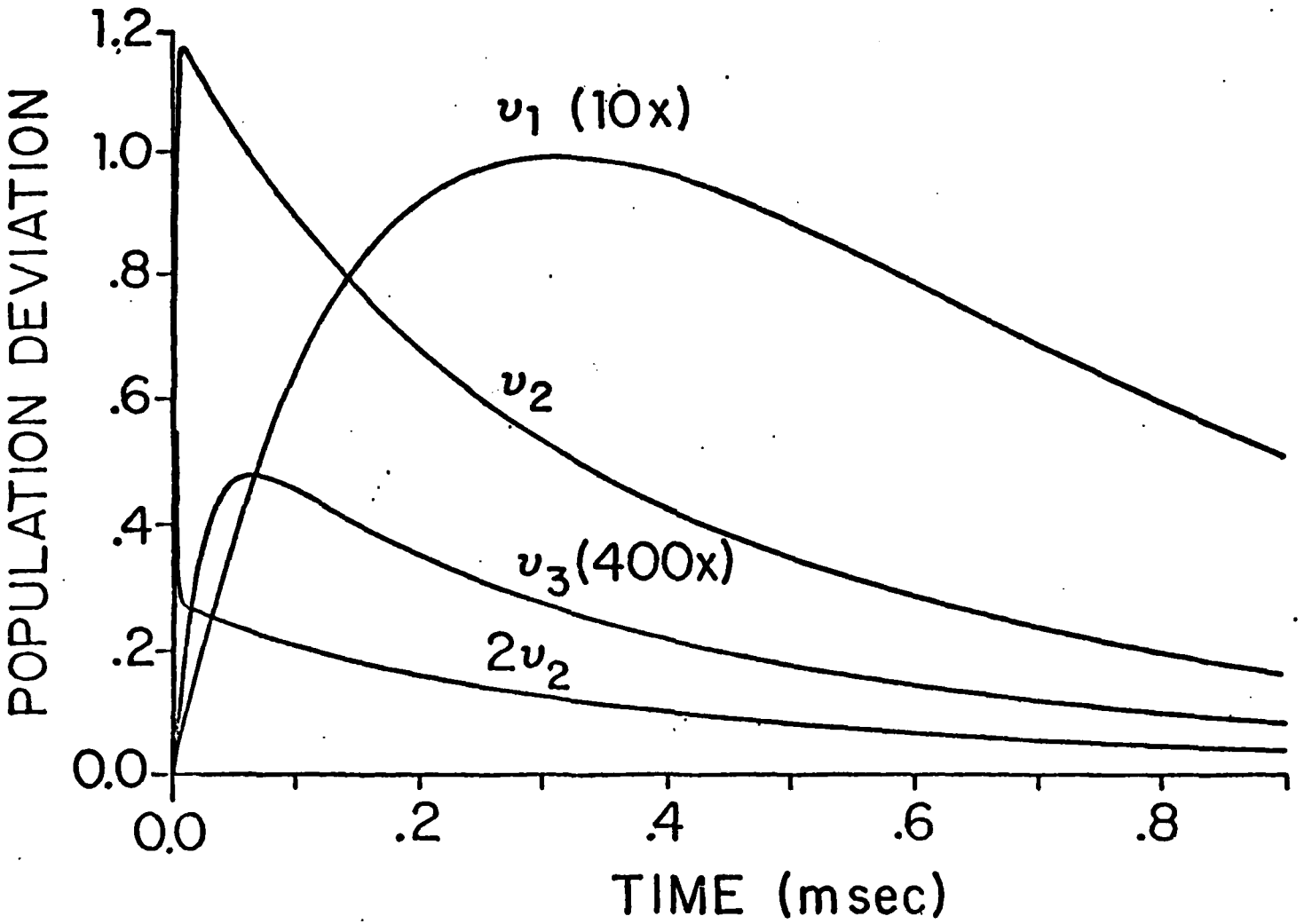

Figure 2: Time evolution of the perturbed populations in the three OCS fundamental levels (ν_1, ν_2 and ν_3) plus the pumped level ($2\nu_2$).

However, when anharmonically mixed states[19]-[21] are used in the calculation, the short range force model calculation adequately describes the qualitative features of V-V and V-T/R energy transfer probabilities in OCS but gives theoretical probabilities which are lower than the experimentally measured quantities. The probability for intermode V-V transfer from $4\nu_2$ to ν_3 calculated using a long range force model is also close to the measured value but is too large by about a factor of three. (See Table II.) Almost certainly, anharmonic mixing of the vibrational states and the large electrical anharmonicity of the ν_2 mode are crucial factors in promoting intermode vibrational energy transfer in OCS.

A complete manuscript describing this work has been accepted for publication in the Journal of Chemical Physics.

*This research was also supported by the National Science Foundation under Grants NSF-MPS-75-04118 and NSF-CHE-77-24343.

(1) (a) E. Weitz and G. W. Flynn, Ann. Rev. Phys. Chem. 25, 275 (1974); (b) E. Weitz and G. Flynn, "Vibrational Energy Flow in the Ground Electronic States of Polyatomic Molecules." (to be published in Advances in Chemical Physics.); (c) G. W. Flynn in "State to State Chemistry," P. R. Brooks and E. F. Hayes, Ed. ACS Symposium Series #56, 1977, p. 145.

(2) R. S. Sheorey, R. C. Slater, and G. W. Flynn, J. Chem. Phys. 68, 1058 (1978).

(3) R. S. Sheorey and G. W. Flynn, J. Chem. Phys. 72, 0000 (1980).

(4) B. L. Earl, A. M. Ronn, and G. W. Flynn, Chem. Phys. 9, 307 (1975).

(5) D. Siebert and G. Flynn, J. Chem. Phys. 62, 1212 (1975).

(6) D. Kligler, H. Pummer, W. Bischel, and C. K. Rhodes, J. Chem. Phys. 69, 4652 (1968).

(7) H. R. Schlossberg and H. R. Fetterman, Appl. Phys. Lett. 26, 316 (1975).

TABLE II

Experimental and Theoretical Energy Transfer Probabilities for OCS

Transition[a]	Experimental[b]	SSH-Harmonic Oscillator States[c]	SSH-Anharmonic Mixed Stated[d]	Sharma-Brau[e]
$OCS(4\nu_2)+OCS \rightleftarrows OCS(\nu_3)+OCS+43cm^{-1}$	$1.5\pm0.3\times10^{-3}$	4.2×10^{-12}	5.1×10^{-4}	4.7×10^{-3}
$OCS(2\nu_2)+OCS \rightleftarrows OCS(\nu_1)+OCS+188cm^{-1}$	$4.2\pm0.6\times10^{-4}$	8.0×10^{-7}	2.9×10^{-5}	-
$OCS(\nu_1)+OCS \rightleftarrows OCS(\nu_2)+OCS-339cm^{-1}$	$<4\times10^{-5}$	3.8×10^{-6}	-	-
$OCS(\nu_2)+OCS \rightleftarrows OCS(0)+OCS+520cm^{-1}$	$2.9\pm0.7\times10^{-4}$	8.7×10^{-5}	-	-

a. A positive ΔE denotes an exothermic process, a negative ΔE denotes an endothermic process.

b. Errors are reported to $\pm$ 3 standard deviations.

c. Energy transfer probability as calculated using the "SSH-Breathing Sphere" model (see Refs. 15-17) with all vibrational states derived from a purely harmonic oscillator model.

d. Same as c. above except anharmonically mixed vibrational states are used.

e. Energy transfer probability as calculated using the dipole-dipole long range attractive force model according to the method of Sharma and Brau.

(8) D. R. Siebert and G. W. Flynn, J. Chem. Phys. 64, 4973 (1976).

(9) K. Hui and T. Cool, J. Chem. Phys. 65, 3536 (1976).

(10) B. M. Hopkins, A. Baronavski, and H. Chen, J. Chem. Phys. 59, 836 (1973).

(11) A. Hariri and C. Wittig, J. Chem. Phys. 67, 4454 (1977).

(12) J. K. Hancock, D. F. Starr, and W. H. Green, J. Chem. Phys. 61, 3017 (1974).

(13) Progress Report, March 31, 1979, pp. 60-64.

(14) M. L. Mandich and G. W. Flynn, "Vibrational Energy Transfer Map for OCS," accepted for publication J. Chem. Phys.

(15) R. N. Schwartz, Z. I. Slawsky and K. F. Herzfeld, J. Chem. Phys. 20, 1591 (1952).

(16) F. I. Tanczos, J. Chem. Phys. 25, 439 (1956).

(17) J. L. Stretton, Trans. Faraday Soc. 61, 1053 (1965).

(18) R. D. Sharma and C. A. Brau, J. Chem. Phys. 50, 924 (1969).

(19) W. Low, Phys. Rev. 97, 1664 (1955).

(20) Y. Morino and T. Nakagawa, J. Mol. Spectrosc. 26, 496 (1968).

(21) Y. Morino and C. Matsumura, Bull. Chem. Soc. Japan. 40, 1095 (1967).

E. COLLISIONAL RELAXATION OF VIBRATIONALLY EXCITED OCS IN RARE GAS MIXTURES*

(M. L. Mandich, G. W. Flynn)

An energy transfer map describing the major vibrational relaxation processes for OCS has been presented in a previous study.[1] The rates of these relaxation events due to collisions of OCS with other non-OCS partners can provide additional information about the nature of the intermolecular interaction potential for collisional vibrational energy transfer. Other investigations of the energy transfer kinetics for OCS have included measurements of vibrational energy relaxation rates in mixtures of OCS with the various rare gases, O_3, Br, CO, HCl, and HBr.[2]-[7] All of these studies predate a detailed understanding of the major kinetic pathways in OCS.

We have measured the rates for the collisional vibration-vibration (V-V) energy transfer between the ν_1 level of OCS and the ν_2 bending mode as well as the overall vibration to translation/rotation (V-T/R) relaxation of OCS in mixtures of OCS with ^{4}He, Ne, Ar, Kr and Xe (see Table I). From these measured rates plus further kinetic analysis based on the vibrational energy transfer map known for pure OCS,[1] the experimental probabilities for the bimolecular kinetic events,

$$OCS(2\nu_2) + M \underset{k_{-A}}{\overset{k_A}{\rightleftharpoons}} OCS(\nu_1) + M + 188\ cm^{-1} \qquad (1)$$

and

$$OCS(\nu_2) + M \underset{k_{-T}}{\overset{k_T}{\rightleftharpoons}} OCS(0) + M + 520\ cm^{-1} \qquad (2)$$

TABLE I

Eigenvalues Measured[a] ($msec^{-1}$ $torr^{-1}$)[b] From ν_1 Fluorescence

	"ν_1 Filling"	"V-T Decay"
OCS : ^{4}He : Xe (3 : 1 : 10)[c]	- 3.2 ± .3	-1.0 ± .1
OCS : Ne (1 : 1)[c]	-3.3 ± .4	- 1.1 ± .1
OCS : Ar (1 : 3)[c]	-2.4 ± .3	-.48 ± .05
OCS : Kr (1 : 6)[c]	-1.5 ± .2	-.25 ± .04
OCS : Xe (1 : 6)[c]	-1.7 ± .2	-.27 ± .06

a) Errors are reported to ± 3 σ.

b) Eigenvalues are reported per torr of total pressure in OCS-M mixtures at constant mole fraction.

c) Relative mole ratio of constituents used in the mixtures which are prepared at constant mole fraction.

for the five possible rare gas collision partners (M = ^{4}He, Ne, Ar, Kr, and Xe) have been determined (see Table II).

The corresponding theoretical probabilities have also been determined using the spherically symmetric, short range repulsive interaction potential model.[8]-[10] The theoretical and measured probabilities are in reasonable qualitative agreement (although absolute numbers vary by as much as a factor of ten, depending on the steepness assumed for the repulsive potential wall) except for the rate of crossover $2\nu_2 \rightarrow \nu_1$ derived from the experimental data for the OCS-^{4}He mixture. Here, the experimental probability is at least five times larger than any reasonable value obtained from the model calculations (see Figures 1 and 2).

A cyclic kinetic path in OCS-^{4}He mixtures may account for the unexpectedly large experimental rate measured for the equilibration of ν_1 with the bending manifold. This cyclic path is as follows,

$$OCS(2\nu_2) + OCS(0) \underset{k_{12}}{\overset{k_{21}}{\rightleftharpoons}} 2OCS(\nu_2) + 7\ cm^{-1}$$

$$OCS(2\nu_2) + He \underset{k^{He}_{-A}}{\overset{k^{He}_{A}}{\rightleftharpoons}} OCS(\nu_1) + He + 188\ cm^{-1}$$

$$OCS(\nu_2) + He \underset{k^{He}_{-B}}{\overset{k^{He}_{B}}{\rightleftharpoons}} OCS(\nu_1) + He - 339\ cm^{-1}$$

$$OCS(\nu_2) + He \underset{k^{He}_{-T}}{\overset{k^{He}_{T}}{\rightleftharpoons}} OCS(0) + He + 520\ cm^{-1}$$

The model calculations suggest that this cyclic relaxation mechanism is

Table II

Experimental Energy Transfer Rate Constants and Probabilities for OCS with Rare Gas Collision Partners [a]

Collision Partner	K_A^M [b] ($msec^{-1}$)	$P_A^M = \frac{K_A^M}{Z}_{OCS-M}$ [c] ($\times 10^4$)	K_T^M [d] ($msec^{-1}$)	$P_T^M = \frac{K_T^M}{Z}_{OCS-M}$ [c] ($\times 10^4$)
OCS [e]	3.3 ± .5	4.2 ± .6	2.3 ± .5	2.9 ± .6
^4He [f]	8 ± 3	5 ± 2	17 ± 2	12 ± 2
Ne	≤ 1.3	≤ 1.7	1.1 ± .6	1.4 ± .8
Ar	.9 ± .3	1.2 ± .4	.2 ± .2	.3 ± .3
Kr	.5 ± .1	.8 ± .2	.1 ± .1	.2 ± .2
Xe	.7 ± .1	1. ± .2	.1 ± .1	.1 ± .1

a) Errors are reported to ± 3σ; all K's are quoted at a pressure of one torr. Note that the value listed for K_M is at one torr of M ($X_M = 1$).

b) K_A^M refers to the energy transfer process in eqn. 1 of the text where $K_A = X^{OCS}K_A^{OCS} + X^M K_A^M$.

c) $Z_{OCS-M} = 2.56 \times 10^3 \, (R_o^{OCS} + R_o^M)/4\mu^{1/2}$ at 1 torr (in a.u.).

d) K_T^M refers to the energy transfer process in eqn. 2 of the text where $K_T = X^{OCS}K_T^{OCS} + X^M K_T^M$.

e) Values for pure OCS are obtained from reference 1.

f) These probabilities are calculated assuming that only $2\nu_2 \rightarrow \nu_1$. There is evidence, as discussed in the text, that the path $\nu_2 \rightarrow \nu_1$ may be comparably favorable in OCS-^{4}He collisions. The net result would be that the probability for $2\nu_2 \rightarrow \nu_1$ (P_A^{He}) can range from 0 to 7 x 10^{-4}, that the probability for $\nu_2 \rightarrow \nu_1$ (P_B^{He}) can range from 0 to 1 x 10^{-4}, and that the probability for V-T/R (P_T^{He}) can range from 7 to 13 x 10^{-4}, depending on the relative contribution of each path to the V-V coupling of ν_1 with the bending manifold.

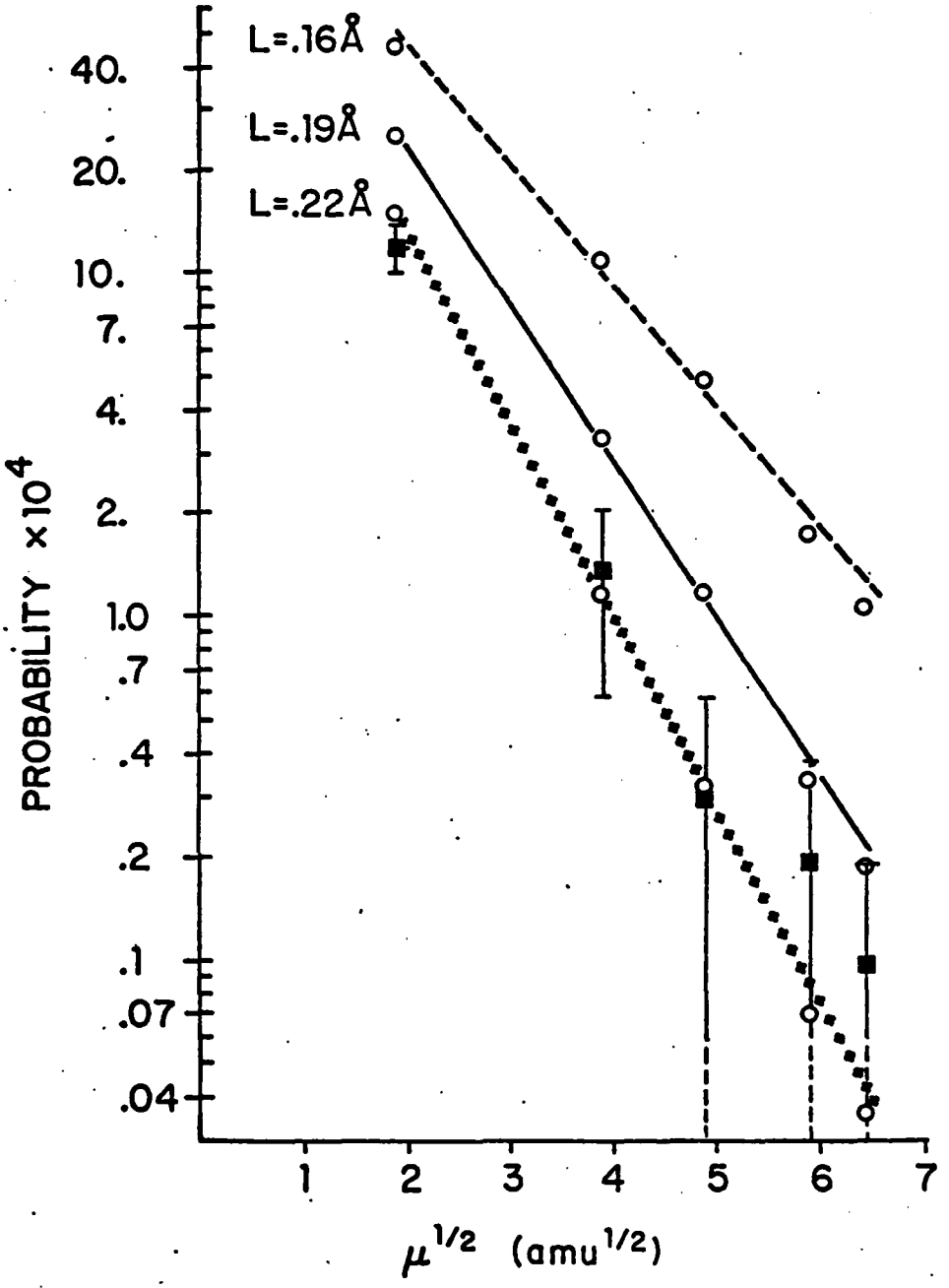

Figure 1: Experimental and calculated (SSH-breathing sphere) probabilities vs. square root of the reduced mass for the vibration-translation/rotation relaxation of OCS by ^{4}He, Ne, Ar, Kr, and Xe. The calculated probabilities are indicated by circles and the experimentally derived probabilities are shown as solid squares with associated error bars. The error bars with a dashed line instead of a lower limit actually have a lower limit of zero which cannot be shown on the ℓn scale. The model calculated values are shown for three reasonable values of L (the steepness of the repulsive potential wall). The dashed line is the approximate relationship between the probability and $\mu^{1/2}$ for L = .16Å; similarly, the solid line corresponds to L = .19Å and the dotted line corresponds to L = .22Å.

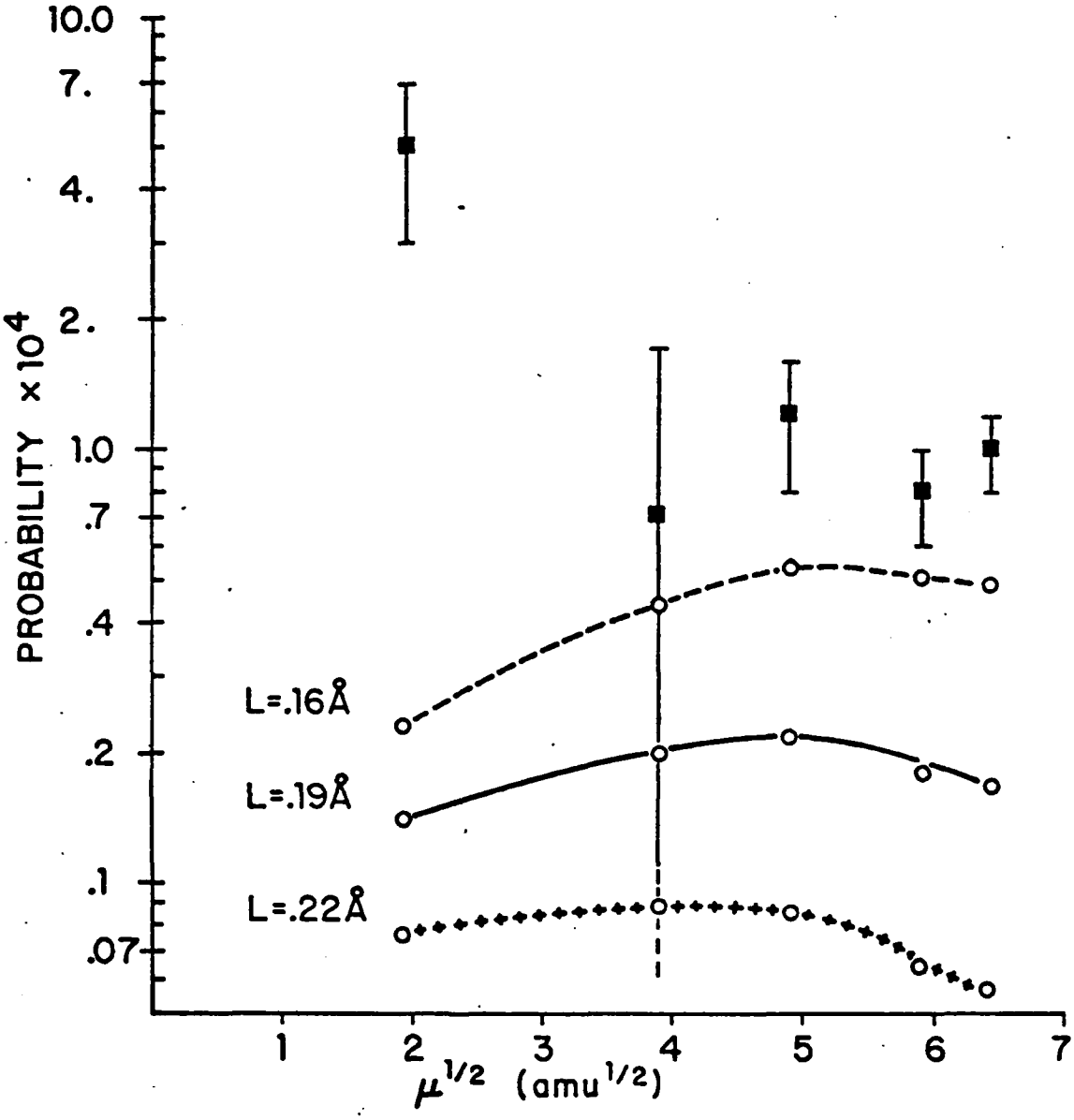

Figure 2: Experimental and calculated (SSH-breathing sphere) probabilities vs. square root of the reduced mass for the vibration-vibration relaxation from $2\nu_2 \rightarrow \nu_1$ of OCS by ^{4}He, Ne, Ar, Kr, and Xe. The calculated probabilities are indicated with circles and the experimentally derived probabilities are shown as solid squares with associated error bars. The error bar with a dashed line instead of a lower limit actually has a lower limit of zero which cannot be shown on the ℓn scale. The model calculated values are shown for three reasonable values of L (the steepness of the repulsive potential wall). The dashed line is the approximate relationship between the probability and $\mu^{1/2}$ for L = .16Å; similarly, the solid line corresponds to L = .19Å and the dotted line corresponds to L = .22Å.

reasonable, but its presence cannot be definitely established from the experimental data obtained in these experiments.

Cyclic relaxation pathways, in general, may occur in the overall vibrational relaxation mechanism of many molecules.[1][11]-[15] A cyclic path can enhance overall V-V relaxation rates if it connects states which all have relatively sizable populations. Moreover, if the cyclic path is also "unstable" it will increase the rate of V-T/R relaxation.[1][11]-[12] Many cyclic paths can be expected to require population flow through a "bottle-neck" state which has a small ambient population; such cycles will not effect either rapid V-V or V-T/R relaxation. However, in complex or highly excited molecules, there may occur cyclic paths which can be termed "catastrophic"; these cycles can greatly speed up both V-V and V-T/R relaxation and thus quickly destroy any mode selective vibrational excitation placed in the molecule.

A complete manuscript describing the results of OCS-rare gas collision studies and model calculations for cyclic paths has been submitted for publication.

*This research was also supported by the National Science Foundation under Grants NSF-MPS-75-04118 and NSF-CHE-77-24343.

(1) M. L. Mandich and G. W. Flynn, "The Vibrational Energy Transfer Map for OCS," accepted for publication to J. Chem. Phys.

(2) D. R. Siebert and G. W. Flynn, J. Chem. Phys. 64, 4973 (1976).

(3) K. Hui and T. Cool, J. Chem. Phys. 65, 3536 (1976).

(4) B. M. Hopkins, A. Baronavski, and H. Chen, J. Chem. Phys. 59, 836 (1973).

(5) J. K. Hancock, D. F. Starr, and W. H. Green, J. Chem. Phys. 61, 3017 (1974).

(6) A. Hariri and C. Wittig, J. Chem. Phys. 67, 4454 (1977).

(7) D. R. Siebert, Ph.D. Thesis (Columbia University, 1973).

(8) R. N. Schwartz, Z. I. Slawsky, and K. F. Herzfeld, J. Chem. Phys. 20, 1591 (1952).

(9) F. I. Tanczos, J. Chem. Phys. 25, 439 (1956).

(10) J. L. Stretton, Trans. Faraday Soc. 61, 1053 (1965).

(11) A. Ben-Shaul and K. L. Kompa, Chem. Phys. Lett. 55, 560 (1978).

(12) I. Shamah and G. Flynn, J. Chem. Phys. 69, 2474 (1978); J. Am. Chem. Soc. 99, 3191 (1977).

(13) F. Lepoutre, Ph.D. Thesis (Université de Paris-Sud, Centre D'Orsay, March 1979).

(14) R. S. Sheorey, R. C. Slater, and G. W. Flynn, J. Chem. Phys. 68, 1058 (1978).

(15) R. S. Sheorey and G. Flynn, J. Chem. Phys. 72, 1175 (1980).

F. IR LASER PUMPING AND ENERGY DIAGNOSTICS OF SUPERSONIC NOZZLE EXPANSIONS*

(D. Coulter, L. Casson, F. Grabiner, R. B. Bernstein, G. W. Flynn)

Molecular beam reactive scattering experiments involving diatomic reagents have shown clearly that vibrational energy can be utilized to overcome activation barriers in simple bimolecular reactions.[1]-[3] It is of interest to extend these studies to include polyatomic molecules, e.g., SF_6, CH_3F, etc. To this end, we have carried out experiments in our laboratory aimed at producing internally excited beams of SF_6 by irradiating with a low power, continuous wave CO_2 laser.[4] During the course of these experiments we have developed a technique which makes possible the determination of the average energy of the beam molecules and the distribution of this energy between the internal and translational degrees of freedom.

Gases expanding in the throat of a supersonic nozzle pass rapidly from a high pressure (collisional) region into an essentially collision free environment. The expanding gas is irradiated in the high pressure region near the nozzle exit where the number density is high, the absorption lines are collisionally broadened, rotational hole filling keeps saturation effects at a minimum and relatively large amounts of energy can be deposited through collisional up-pumping processes.[5] Following excitation, the molecules move rapidly into the collision free region "freezing" a large fraction of the absorbed energy in the internal degrees of freedom. Changes in total beam energy are monitored with a liquid He-cooled bolometer[6] while a standard mass spectrometer-time-of-flight device[7] is used to measure beam intensity and translational energy.

Initially, the SF_6 beam was irradiated immediately down stream of the nozzle exit with a loosely focussed CO_2 laser (5 watts at 10.6 μm [P(16)]).

Under typical conditions, there was a 7-8% laser-induced increase in total energy content of the transmitted beam molecules, corresponding to a net energy deposition of 0.11 IR photons per SF_6 molecule in the beam. Vibration-translation relaxation converted some of the absorbed infrared energy into translational kinetic energy as manifested by an increase in both transverse and axial velocity of the SF_6 molecules. A significant loss of forward beam flux due to the enhanced transverse velocity component was observed. Approximately 70-80% of the absorbed energy was found to be "frozen" in the internal degrees of freedom of the SF_6.

In more recent experiments, a nozzle was fabricated from ZnSe, an infrared transmitting material, to allow irradiation upstream of the nozzle exit. By irradiating at the proper point in the nozzle, it should be possible to maximize the energy deposition while still maintaining high levels of internal excitation. Preliminary studies reveal an order of magnitude increase in the amount of energy deposited per SF_6 molecule with the new nozzle. Work is continuing with the new configuration to find the optimum conditions for laser pumping.

In addition to providing fundamental information about energy transfer processes and chemical reactions of vibrationally excited species, the techniques developed here can be used as diagnostic tools to study the dynamics of supersonic expansions.

*This research was also supported by the National Science Foundation under Grants NSF-CHE-77-24343 and NSF-CHE-77-11384 and by the Department of Energy under Contract DE-AS02-78ER04940.

(1) T. J. Odiorne, P. R. Brooks, and J. V. Kasper, J. Chem. Phys. 55, 1980 (1971).

(2) H. Dispert, M. Geis, and P. R. Brooks, J. Chem. Phys. 70, 5317 (1979).

(3) Z. Karny and R. N. Zare, J. Chem. Phys. 68, 3360 (1978).

(4) D. R. Coulter, F. R. Grabiner, L. M. Casson, G. W. Flynn, and R. B. Bernstein, J. Chem. Phys. 72, (1980).

(5) E. Weitz and G. W. Flynn, Ann. Rev. of Phys. Chem. 25, 275 (1974).

(6) T. E. Gough, R. E. Miller, and G. Scoles, Appl Phys. Letts. 30, 338 (1977).

(7) K. T. Wu, H. F. Pang, and R. B. Bernstein, J. Chem. Phys. 68, 1064 (1978).

G. ENERGY REDISTRIBUTION IN ULTRAVIOLET LASER PHOTOFRAGMENTED SO_2*

(J. Ahl, J. Chu, G. Flynn)

Considerable work has been done on the transfer of vibrational energy between polyatomic molecules, however, practically all these studies deal with stable species in a singlet ground state. We are currently studying the relaxation of the vibrationally excited triplet radical, $SO(^3\Sigma^-)$ produced by the photodissociation of SO_2.

The ultraviolet photolysis of SO_2 at wavelengths below 2190Å is known to yield $SO(^3\Sigma^-)$ as the primary product.[1] Studies of the translational energy distribution of the fragments, when SO_2 is irradiated at 1930Å, show that less than half of the 6250 cm^{-1} of available excess energy is deposited in the translational degrees of freedom.[2] Furthermore, it can be argued that the degree of rotational excitation is small. Thus, it is expected that the SO fragment vibrational distribution will be vibrationally inverted with most of the population in the v = 3 and 4 states. It should be noted that the $SO(^1\Delta)$ state is not accessible for photolysis at 1930Å.

We are studying the relaxation of vibrational energy in UV photolyzed mixtures of SO_2 and Argon by observing the amplitude of the time dependent infrared emission of the ν_3 mode of SO_2 excited by energy transfer from vibrationally excited SO. The ν_3 mode should be sensitive to the population of SO(v) and therefore to the decay processes of the excited SO. We have observed a minimum of three pressure dependent decay eigenvalues in the ν_3 fluorescence. Further studies of the intensity dependence of these rates are in progress and will aid in the assignment of these eigenvalues to the microscopic rate constants in this system. We are also considering looking at the fluorescence in the 9μ region due to the overlap of the ν_1 mode of

SO_2 and the excited SO. The problem here is to deconvolute the two emissions and it is hoped that the ν_3 data will allow this.

We are also exploring another probe technique for the SO/SO_2 system. A narrow linewidth (< .0001 cm^{-1}) diode laser, tunable from 1075 to 1125 cm^{-1}, will be used to probe the populations of the SO(v = 0-5) and $SO_2(\nu_1)$ states. The diode laser will be used to monitor the time resolved absorptions of selected vibrational/rotational states, and will allow the determination of both the initial V/J distribution of the SO fragments and the rates of vibrational relaxation for each of the vibrational states of the SO. We are currently monitoring the behavior of the $SO_2(\nu_1)$ with encouraging results.

*This research was also supported by the National Science Foundation under Grant NSF-CHE-77-24343 and by the Department of Energy under Contract DE-AS02-78ER04940.

(1) H. Okabe, Photochemistry of Small Molecules, Wiley, New York, 1978, p. 247.

(2) A. Freedman, S. Yang, and R. Bersohn, JCP 70, 5313 (1979).

III. PICOSECOND ENERGY TRANSFER AND PHOTOFRAGMENTATION SPECTROSCOPY

A. PICOSECOND LASER STUDIES OF PHOTO-INDUCED DISSOCIATION OF MOLECULES*

(G. Korenowski, C. Dupuy, W. Hetherington, M. McAuliffe, and K. B. Eisenthal)

We are using the methods of picosecond spectroscopy to determine the pathways and dynamics of molecular photodissociation. The molecular system we are investigating is dephenyldiazomethane $\phi_2C = N_2$

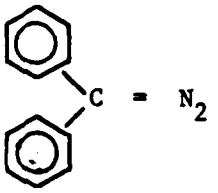

in a 3-methylpentane solvent. This molecule was selected because it generates the diphenyl carbene $\phi_2C:$ on photodissociation.[1] This radical and the entire class of carbenes $R_1R_2C:$ play a key role as intermediates in many chemical reactions.[1][2] The central "divalent" carbon is bonded to two groups, R_1 and R_2, and contains two nonbonding electrons which can be anti-parallel (singlet) or parallel (triplet). Due to their importance in chemistry there has been considerable experimental and theoretical research on the structure, spectroscopy and chemical properties of these molecules.[1]-[6]

The sequence of elementary steps involved in fragmenting the parent compound, diphenyldiazomethane, and generating the carbene have been thought to be the following.[1]-[3][5]

a) Excitation $\phi_2C = N_2 + h\omega \rightarrow \langle \phi_2C = N_2 \rangle^*_{S_1}$

(b) Dissociation 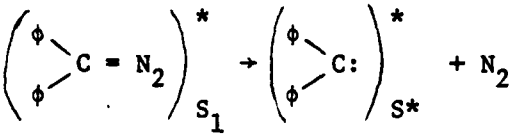

(c) Intersystem Crossing 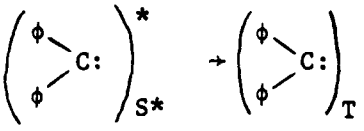

We have used a frequency quadrupled Nd laser at 266 nm to excite the parent compound. We have set up an optical parametric amplifier, OPA, to generate tunable picosecond pulses to monitor the rate of formation of the triplet ground state of the carbene fragment. The idea is to excite the ground state triplet carbene, (its absorption spectrum is known at low temperature[1][3]) with the OPA and to measure the carbene fluorescence ($T^* \rightarrow T_o$). The intensity of the carbene fluorescence as a function of the time separation between the photodissociating pulse (266 nm) and the OPA probe pulse would yield the formation dynamics of the triplet ground state carbene.

In the course of these experiments we discovered something unexpected and important. We found that the excitation pulse at 266 nm was generating some fraction of the diphenylcarbene molecules in an excited triplet state. Thus the sequence of steps must now be extended to include a new channel, unknown prior to this finding, in the decay process, namely the production of excited triplet carbenes. We identified that the triplet carbene was being produced by observing its fluorescence ($T^* \rightarrow T_o$) (Figure 1). One key issue which we have resolved is whether the

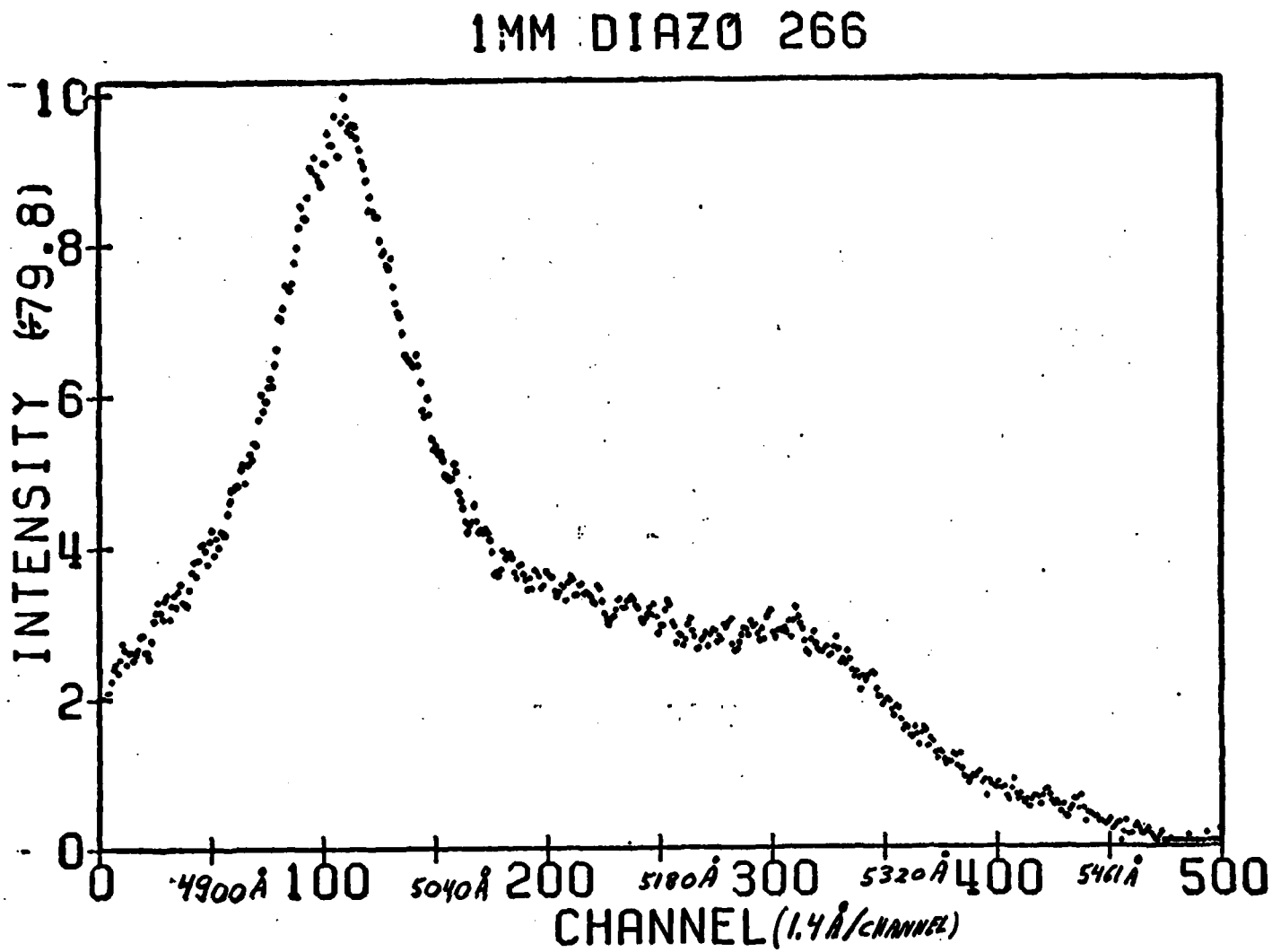

Figure 1: Fluorescence ($T^* \rightarrow T_o$) of diphenyl carbene in 3-methylpentane at room temperature.

excited triplet carbene is produced by a multiphoton process or by a one photon process. In the multiphoton process there are two possible pathways for generating the excited triplet carbene. One channel is a multiphoton absorption of diphenyldiazomethane which fragments from a higher state ($2\nu h$ = 9.3eV) and utilizes the extra energy to produce the excited triplet. Another possibility is one photon absorption by diphenyldiazomethane which fragments to the carbene within the picosecond laser pulse width ($\sim$ 25 psec for the Nd:YAG and 5 psec for the Nd:glass) and a second photon is absorbed by the carbene thereby producing the excited triplet carbene. In the one photon process there would have to be sufficient energy in one photon (266 nm) to fragment the parent molecule and produce the excited triplet carbene. From Figure 2 we see that the carbene fluorescence ($T^* \rightarrow T_o$) is linear with the exciting laser power. The lower curve is the background signal obtained from the 3-methylpentane solvent with no diphenyldiazomethane present. To further confirm that there were no spectral features in the fluorescence which were intensity dependent we measured the fluorescence spectrum at two different laser intensities. On dividing one spectrum by the other we note from Figure 3 that we obtain a horizontal line which indicates that the spectral features are not intensity dependent.

We are presently investigating the rate of formation of the triplet and the pathway by which it is produced.

*This work was also supported by the National Science Foundation under Grant NSF-CHE79-23291 and by the National Institute of Health under Grant HL19488-04.

(1) A. M. Trozzolo, Accts. Chem. Res. 1, 329 (1968).

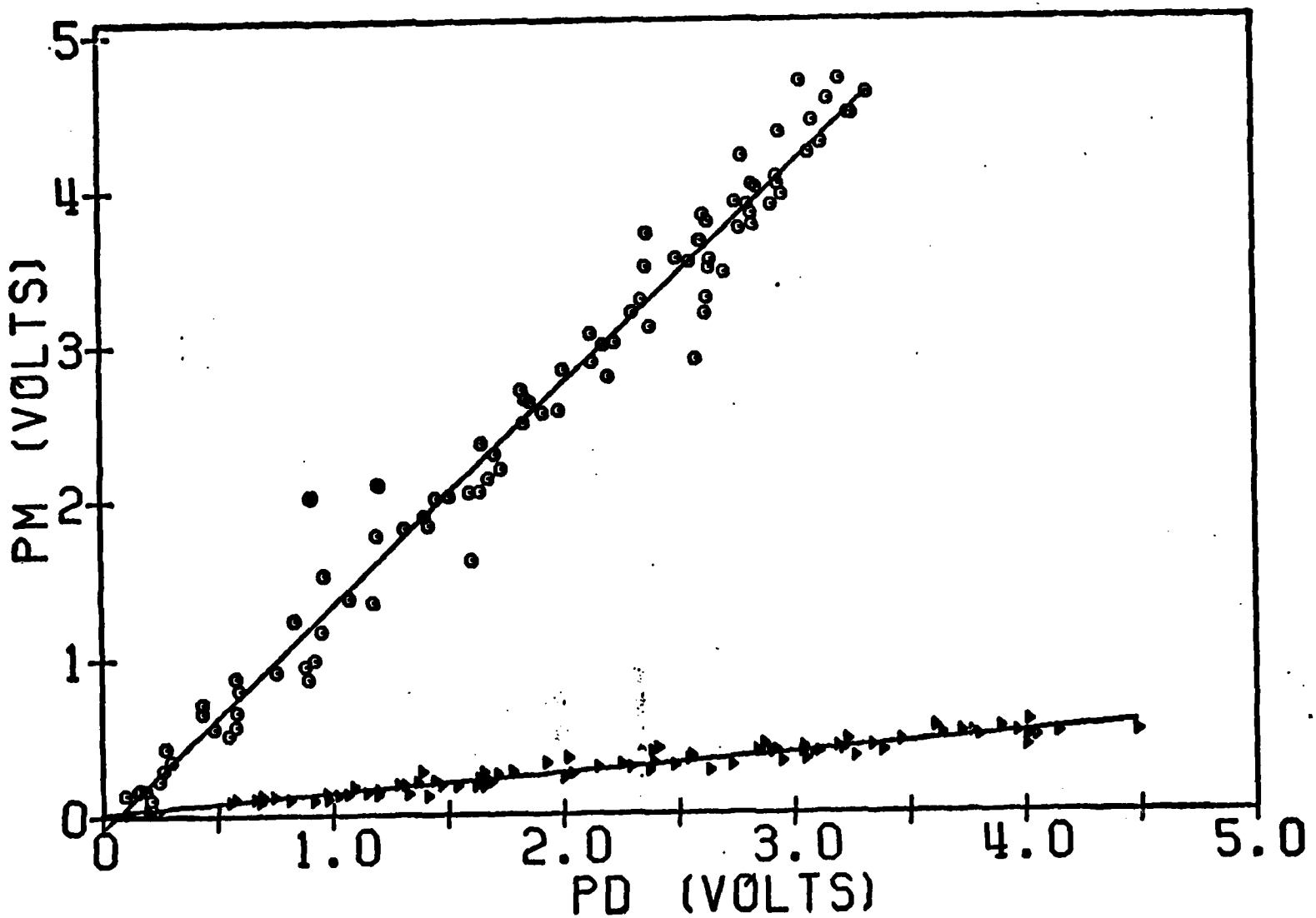

Figure 2: Fluorescence intensity versus exciting laser power. The upper curve (circles) is the carbene fluorescence ($T^* \rightarrow T_0$) versus exciting laser power. The lower curve (triangles) is the 3MP solvent fluorescence background power dependence.

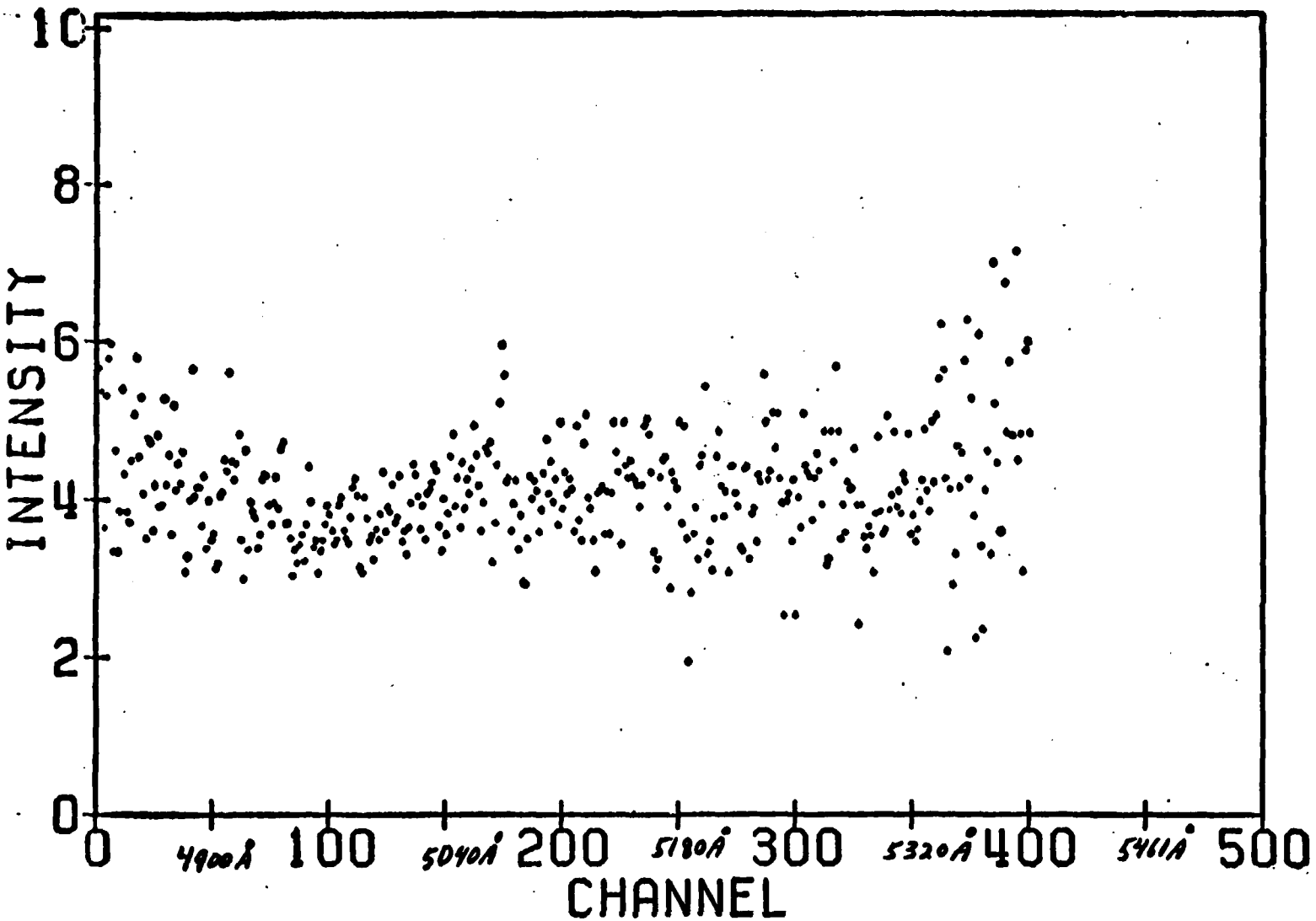

Figure 3: Division of a weak fluorescence spectrum (weak incident laser pulse) by a strong fluorescence spectrum (strong incident laser pulse) shows spectral features are not intensity dependent.

(2) Carbenes, R. A. Moss and M. Jones, Jr. (Eds.), John Wiley & Sons, New York, 1975), Vol. II.

(3) G. L. Closs and B. E. Rabinow, J. Am. Chem. Soc. 98, 8190 (1976).

(4) L. B. Harding and W. A. Goddard III, J. Chem. Phys. 67, 1777 (1977).

(5) K. C. Wu and A. M. Trozzolo, J. Phys. Chem. 82, 1827 (1978).

(6) R. K. Lengel and R. N. Zare, J. Am. Chem. Soc. 100, 7495 (1978).

B. COHERENT ANTI-STOKES EXPERIMENTS ON GAS PHASE BENZENE*

(W. Hetherington, G. Korenowski, K. B. Eisenthal)

In studying ultrafast molecular processes we and other investigators seek to identify the states, structures, and intermediate chemical species through which a system of interest evolves.[1]-[7] A principal tool in these studies is transient electronic absorption and emission. Although it remains as an important method, electronic spectroscopy is often complicated by overlapping broad and featureless electronic transitions. In such cases vibrational or electronic Raman scattering can often provide more unambiguous information than electronic absorption spectroscopy. Two different chemical structures can possess electronic spectra so similar that discrimination between the two is not feasible whereas the Raman spectra of the two species can be resolved. It is therefore advantageous in such cases to use Raman scattering to monitor the evolution of a molecular system through its various chemical species and changing structures.

Besides spontaneous Raman scattering, the coherent anti-Stokes Raman scattering (CARS) is of great utility.[8]-[18] In this technique, beams at frequencies ω_1 and ω_2 are mixed in the system of interest to produce $\omega_3 = 2\omega_1 - \omega_2 = \omega_1 + (\omega_1 - \omega_2) = \omega_1 + \Delta$. A large signal at ω_3 is obtained when the frequency mismatch corresponds to a Raman active transition of the system. We have successfully carried out picosecond CARS experiments on gas phase benzene at room temperature ($P \sim 80$ torr) in a 20 cm. cell. In our initial experiments we used a 532 nm pulse as ω_1 and generated ω_2 by a stimulated Raman scattering method in neat benzene. However, what is generally required to carry out a wide range of experiments is tunability so that $\omega_1-\omega_2$ can be brought into resonance with a Raman active

vibration of interest. To achieve this we have set up an optical parametric amplifier which enables us to tune ω_2 from 400 nm to 700 nm.

Using picosecond light pulses in a collinear geometry at the wavelengths λ_1 = 532 nm and λ_2 = 635.4 nm a resonance was observed which is due to the ground state symmetric C-H stretch at Δ = 3060 cm^{-1} (Figure 1). We then introduced into the benzene gas cell, at the same time as λ_1 and λ_2, a picosecond pulse at the fourth harmonic of Nd:YAG, 266 nm. The 266 nm light excites the benzene although it is about 490 cm^{-1} on the low energy side of the B_{2u} origin. Generating a λ_2 = 638.3 nm with the OPA and mixing it with λ_1 = 532 nm we observed a CARS resonance at Δ = 3130 cm^{-1} which we ascribe to the C-H stretch in the excited singlet B_{2u}. The literature value[19] for the C-H stretch in the B_{2u} state is 3134 cm^{-1}.

In addition to our interest in excited state CARS we were motivated to use CARS to study the fragments generated by photolysis of benzene with 266 nm light pulses. This interest was prompted by the successful work of others[20] in the use of CARS to study the products produced by photolysis of benzene. Our interest was to determine the sequence of fragments generated in the initial steps, namely how does photoexcited benzene break apart on the subnanosecond time scale. On varying ω_2 from 625 nm to 637 nm we could examine resonances, e.g. Figure 2, of Δ = 2800 cm^{-1} to Δ = 3200 cm^{-1} using ω_1 = 532 nm. The strongest fragment signals were observed in the 2900-2935 cm^{-1} region, tailing off on the low energy side. The CARS signal in this region has been attributed[20] to the C_2 fragment. Since the excitation and CARS pulses at ω_1 and ω_2 were not delayed with respect to each other, i.e. coincident in time

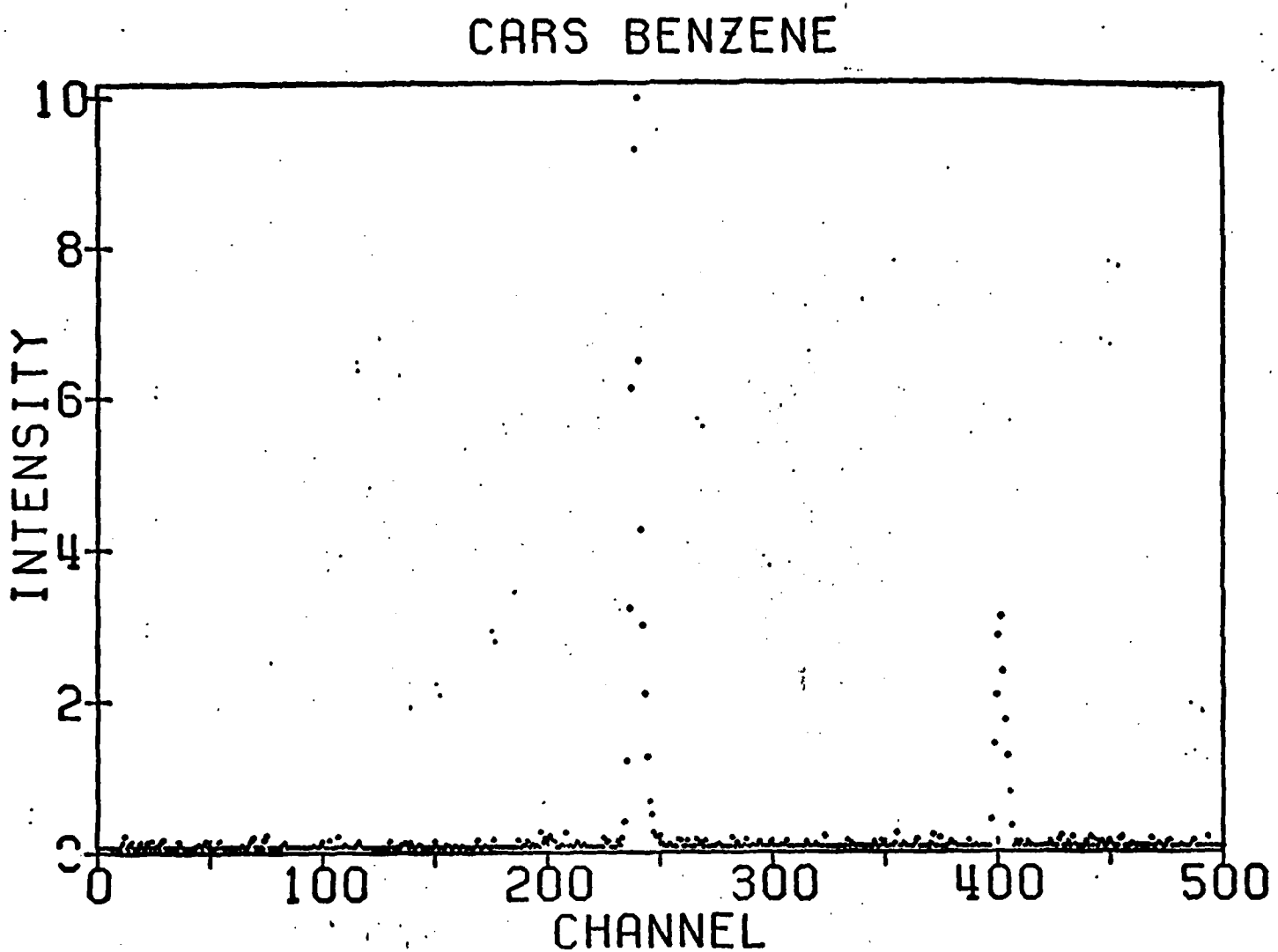

Figure 1: Ground state benzene CARS intensity vs. wavelength. Signal at Channel 239 is 457.5 nm and signal at Channel 400 is a wavelength marker.
λ_1 = 532 nm; λ_2 = 635.4 nm; Δ = 3060 cm^{-1}.

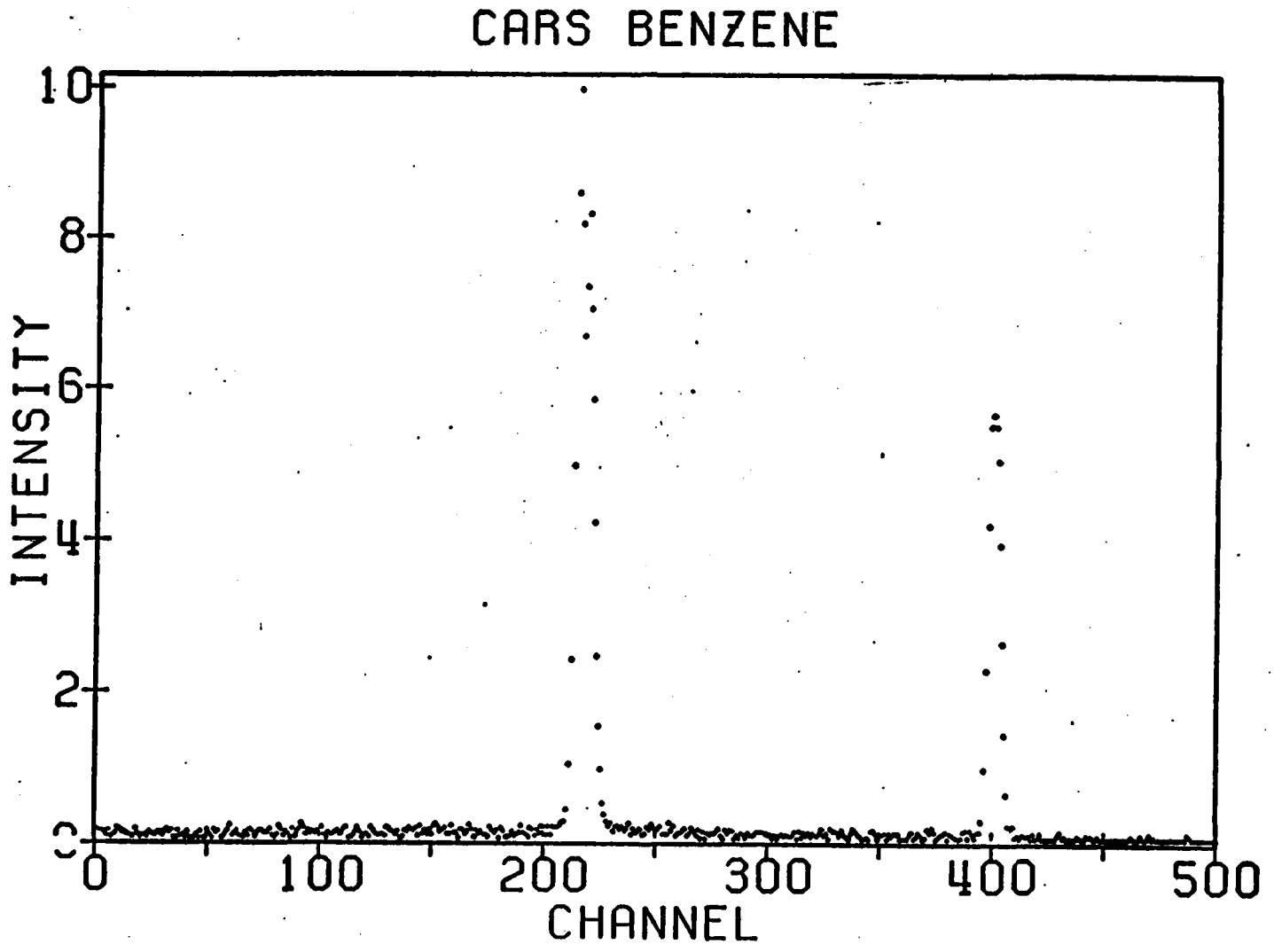

Figure 2: CARS intensity vs. wavelength of the C_2 fragment. Signal at Channel 215 is 460.9 nm and signal at Channel 400 is a wavelength marker. Photolysis at 266 nm. λ_1 = 532 nm; λ_2 = 629.1 nm; Δ = 2901 cm^{-1}

(as well as overlapping spatially), our observation of the CARS signals indicate that (1) benzene undergoes a multiphoton fragmentation to produce, among other products, C_2, and (2) that a fragment as small as C_2 is produced within 25 ps. after photoexcitation of benzene.

We are presently carrying out experiments to identify the different fragments and determine their sequence of formation.

*This work was also supported by the National Science Foundation under Grant NSF-CHE79-23291 and by the National Institute of Health under Grant HL19488-04.

(1) A. Laubereau and W. Kaiser, Ann. Rev. Phys. Chem. 26, 83 (1975).

(2) Ultrashort Light Pulses, S. L. Shapiro (Ed.), (Springer-Verlag, Berlin, 1977).

(3) K. B. Eisenthal, Ann. Rev. Phys. Chem. 28, 207 (1977).

(4) P. M. Rentzepis, Science 202, 174 (1978).

(5) Advances in Laser Chemistry, A. H. Zewail (Ed.), (Springer-Verlag, Berlin, 1978).

(6) Picosecond Phenomena, C. V. Shank, E. P. Ippen, and S. L. Shapiro (Eds.), Springer-Verlag, Berlin (1978).

(7) M. R. Topp, Appl. Spectrosc. Revs. 14, 1 (1978).

(8) A. B. Harvey and J. W. Nibler, Appl. Spectrosc. Rev. 14, 101 (1978).

(9) W. N. Tolles, J. W. Nibler, J. R. McDonald and A. B. Harvey, Appl. Spectrosc. 31, 253 (1977).

(10) R. F. Begley, A. B. Harvey, R. L. Byer and B. S. Hudson, Am. Lab. 6, 11 (1974).

(11) B. Hudson, W. Hetherington III S. Cramer, I. Shabay and G. K. Klauminzer, Proc. Nat. Acad. Sci. USA 73, 3798 (1976).

(12) W. B. Roh, P. W. Schreber and J. P. E. Taran, Appl. Phys. Lett. 29, 174 (1976).

(13) L. A. Carreira, T. C. Maguire, and T. B. Mally, Jr., J. Phys. Chem. 66, (1977).

(14) I. Chabay, G. K. Klauminzer and B. S. Hudson, Appl. Phys. Lett. 28, 27 (1976).

(15) I. Nestor, Th. G. Spiro and G. K. Klauminzer, Proc. Nat. Acad. Sci. USA 73, 3329 (1976).

(16) L. A. Carreira, L. P. Goss and Th. B. Mally, J. Chem. Phys. 6B, 4360 (1977).

(17) J. Hermann and M. Laudmann, Optics Commun. 29, 172 (1979).

(18) B. I. Greene, R. B. Weisman and R. M. Hochstrasser, Chem. Phys. Lett. 59, 5 (1978).

(19) G. Herzberg, Electronic Spectra of Polyatomic Molecules, Van Nostrand-Reinhold Co., New York (1966).

(20) K. B. Gross, D. M. Guthals, and J. W. Nibler, J. Chem. Phys. 70, 4673 (1979).

C. PICOSECOND LASER STUDIES OF ELECTRON SOLVATION IN LIQUIDS*

(Y. Wang, M. Crawford, M. McAuliffe, K. B. Eisenthal)

When low energy excess electrons are injected into a polar fluid they become rapidly thermalized.[1][2] These thermalized electrons are initially localized in shallow potential wells formed by the surrounding solvent molecules. In the absence of a reactive chemical channel, the surrounding solvent dipoles restructure themselves about the electron, deepening the potential well and leading to the formation of the solvated electron.

There has been great activity and progress extending over many years in studies of the effects of ionizing radiation[3]-[6] on materials with electron solvation in liquids as one of the areas of intense interest. In addition to the scientific interest there is marked technological interest due to the importance of lithography, e.g. using electrons, to achieve high density storage of information. In pulse radiolysis experiments the energy transferred to the medium generates local regions of ionization, and molecular electronic, vibrational and rotational excitations. These ionization and excitation events are important in the description of molecular motions, energy relaxation, and the generation of reactive species of materials. To this date the fundamental processes involved in electron solvation in liquids are poorly understood.

We have approached the problem of electron solvation in polar liquids by picosecond laser transient absorption spectroscopy. Although picosecond laser methods have been used in a prior study[7] to measure electron solvation in water it was found that the solvation process was completed within the laser pulse width and thus time resolved dynamics was not obtained. In the experiments reported here we have obtained time resolved

information for the first time using picosecond laser methods. The electrons are generated in the liquids methanol and ethanol by picosecond laser two photon ionization[8] of the pyrene solute molecules present.

$$\text{Pyrene} + 2h\nu \rightarrow \text{Pyrene}^{+} + e^{-} \qquad (1)$$

The electrons are very rapidly trapped[6] ($<10^{-12}$ sec.) and ultimately become solvated electrons. We obtain the kinetics of solvation by measuring the growth of the absorption characteristic of the solvated electron in the alcohols used.[4]-[9]

A laser triggered flash lamp and picosecond streak camera are used to obtain the time dependence of the solvation dynamics (Figure 1). This technique is quite different from the variable delay and transmission echelon techniques[7] which utilize one or more laser probe pulses. These latter techniques require many laser shots in order to yield the time dependent absorption profile, whereas in our method the continuous time absorption is obtained in one laser shot. It is also worthwhile to note the potential use of our system for experiments in which both time and wavelength dependences of the transient absorption signal can be obtained in one laser firing.

Solvation times measured in this work are listed in Table I together with those determined by pulse radiolysis. The values obtained by photoionization are larger than those obtained by pulse radiolysis. We ascribe these differences to the local heating effect resulting from pulse radiolysis. In pulse radiolysis experiments the secondary electrons generated by the incident ionizing radiation dissipate their energy very rapidly through ionizations and excitations (electronic, vibrational and

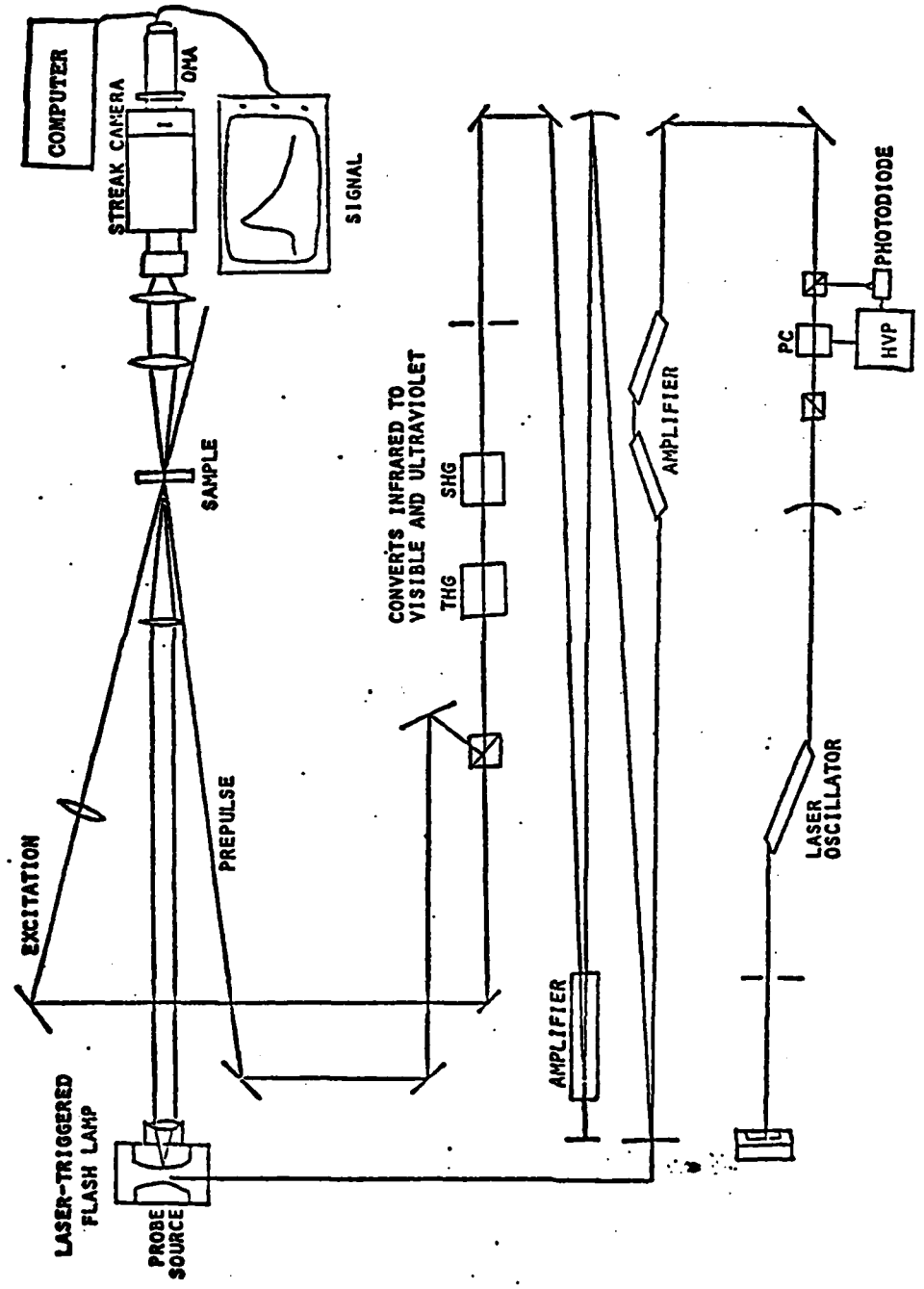

Figure 1: Schematic of experimental set-up. PC: Pockells cell. SHG: second harmonic generating crystal. THG: third harmonic generating crystal.

TABLE I

Picosecond Formation Times of Solvated Electrons in Alcohols at 293°K

	Solvation Times psec			Dielectric relaxation times[d] psec				
	picosecond laser	pulse radiolysis		τ_1	τ_2	τ_3	τ_1'	τ_2'
methanol	17 ± 3[a]	10.7 ± 1[b]	10.7 ± 1[c]	52	13	1.4	9.4	10
ethanol	26 ± 5[a]	23 ± 2[b]	18 ± 2[c]	191	17	1.6	30	13

a. This work.

b. Reference 4.

c. Reference 5.

d. τ_1, τ_2 and τ_3 are the dielectric relaxation times under constant external field. τ_1' and τ_2' are the corrected values of τ_1 and τ_2 according to $\tau' = \tau\ \varepsilon_\infty/\varepsilon_o$.

2. Values of ε_∞ and ε_o are either obtained or extrapolated from reference 17.

rotational). This thermalization process typically occurs within 1 psec after the initial ionization.[6] The sudden transfer of electron kinetic energy to vibrational and rotational energy of the surrounding molecules in a small region (spur) causes a jump in local temperature and accelerates the solvation of the electron.

By comparing the pulse radiolysis data with the picosecond laser data we can make an estimate of the spur temperature. It is found that the pulse radiolysis data at 261°K in methanol and 277°K in ethanol have the same solvation rates as the corresponding rates measured in our study at 293°K. Assuming that these differences arise from the local heating phenomena in pulse radiolysis, this implies an "effective" temperature jump of 32°K for methanol and 16°K for ethanol in the pulse radiolysis experiments. These estimates are consistent with a theoretical model[6] of small spurs ($\sim$ 20Å) and an average energy deposition of 30 eV in a spur. The existence of a significant temperature jump in the spur is thus for the first time directly supported by experiment.

Next we turn our attention to the relationship between the solvation and dielectric relaxation times. In Table I we list the various dielectric relaxation times associated with these liquids. τ_1 is interpreted as the time required for the breaking of intermolecular hydrogen bonds followed by reorientation of the molecule, τ_2 is the time required to reorient a free monomer, and τ_3 is the reorientation time of OH dipoles. All of these τ values[4] were obtained under the experimental condition of a constant weak external electric field applied to the system, which is clearly not the case with electron solvation in fluids. When an electron is injected into a medium, the charge of the electron can speed

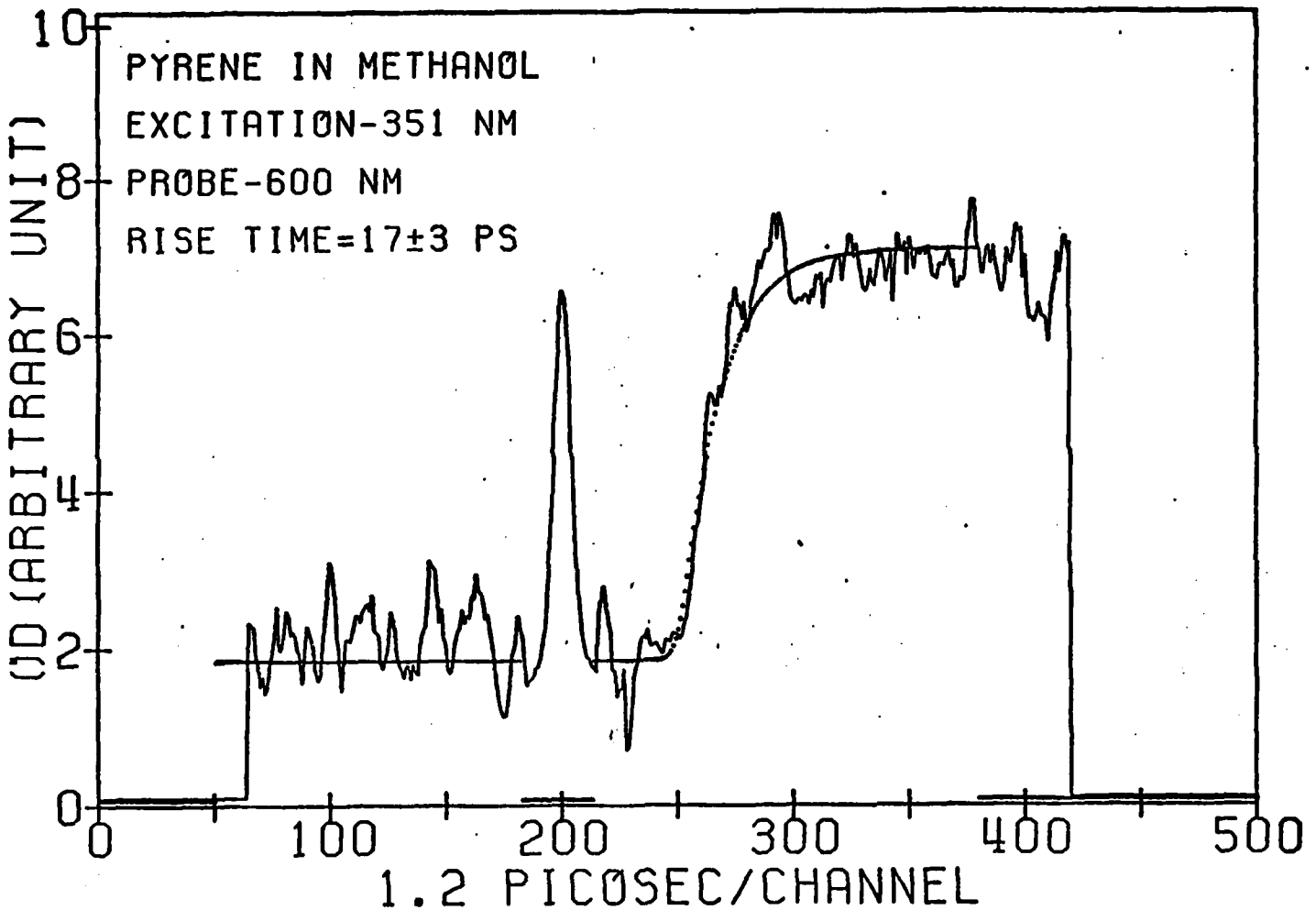

Figure 2: The formation of solvated electron in methanol. Solid curve represents experimental points and broken curve represents theoretical points. The pre-pulse (fwhm is 7 channels) is ahead of the excitation pulse (not shown in the plot) by 52 channels. The data shown here is the average of 10 shots.

up the dielectric relaxation rate.[10] The corrected dielectric relaxation time, τ', under constant charge approximation is given by[10]

$$\tau' = \tau \cdot \varepsilon_\infty / \varepsilon_o \qquad (2)$$

where τ is the normal dielectric relaxation time under constant field, ε_∞ is the limiting high frequency dielectric constant, and ε_o is the limiting low frequency dielectric constant. In Table I, τ_1' and τ_2' are the corrected values of τ_1 and τ_2 respectively according to equation (2).

The fair correlation between the solvation times measured by pulse radiolysis and the reorientation time of a free monomer (τ_2), rather than the τ_1 which is determined by the relaxation of hydrogen bonding structures, has led to the suggestion that in the process of electron solvation the intermolecular hydrogen bonding is not a limiting factor.[4] However, since the relaxation is occurring in the presence of a fixed charge rather than under a constant electric field (as mentioned above), the solvation rate should actually be correlated with the corrected dielectric relaxation rate. It can be seen that our picosecond laser data does not yield good agreement with the calculated values of τ_2' and τ_1' for methanol and ethanol. We must conclude therefore that for these cases at least the solvation dynamics cannot be described solely in terms of any simple molecular motions or dielectric relaxation process. Further measurements of the electron solvation rates as a function of temperature and the extension of measurements to the longer chain alcohols are needed to develop an adequate model of electron solvation in these polar liquids

*This work was also supported by the National Science Foundation under Grant NSF-CHE79-23291 and by the National Institute of Health under Grant HL19488-04.

(1) For a survey of both experiments and theories, see
(a) Conference on "Electrons in Fluids - The Nature of Metal-Ammonia Solutions," J. Phys. Chem. 79, 2789-3081 (1979).
(b) Conference on "Electrons in Fluids," Can. J. Chem. 55, 1797-2277 (1977).

(2) G. A. Kenney-Wallace, Acc. Chem. Res. 11, 433 (1978).

(3) J. H. Baxendale and P. Wardman, J. Chem. Soc., Faraday Trans. I, 69, 584 (1973).

(4) W. J. Chase and J. W. Hunt, J. Phys. Chem. 79, 2835 (1975).

(5) G. A. Kenney-Wallace and C. D. Jonah, Chem. Phys. Lett. 39, 596 (1976).

(6) A. Mozumder in "Advances in Radiation Chemistyr," Vol I, M. Burton and J. L. Magee, Ed., Wiley-Interscience, New York, New York, 1969.

(7) P. M. Rentzepis, R. P. Jones, and J. Jortner, J. Chem. Phys., 59, 766 (1973).

(8) G. Beck and J. K. Thomas, Chem. Phys. Lett. 13, 295 (1972).

(9) G. Dolivo and L. Kevan, J. Chem. Phys. 70, 2599 (1979).

(10) (a) A. Mozumder, J. Chem. Phys. 50, 3153 (1968).
(b) R. Schiller, Chem. Phys. Lett. 5, 176 (1970).

IV. GENERATION AND CONTROL OF RADIATION

A. SPONTANEOUS AND INDUCED COHERENT RADIATION GENERATION AND CONTROL IN ATOMIC VAPORS*

(K. P. Leung, R. Kachru, E. Whittaker, T. W. Mossberg, S. R. Hartmann)

The past year has been quite fruitful with regard to both of our research objectives, which are 1) to advance the basic understanding of the generation of coherent radiation in atomic vapors, and 2) to utilize coherently generated radiation to study atomic processes occurring within such vapors. We first discuss the results of programs which have continued from the previous report.

In the previous interval we reported the discovery that the stimulated photon echo can be generated from the phase information stored in a single atomic state. In light of this fact we pointed out that the collisional degradation of the stimulated echo can be used to determine absolute total elastic scattering cross sections and to study velocity-changing collisions. We have completed experiments on stimulated echoes generated in Na and reported[1][2] the collisional effects associated with Na(3S)-He, Na($3P_{1/2}$)-He and Na(3S)-CO collisions.

In our last report we also presented early results of tri-level echo[3] studies of the collisional broadening of electric-dipole forbidden 3S-nS(nD) transitions in Na. We were able to measure the He-, Ne-, and Ar-induced broadening of transitions for which the upper state was well into the Rydberg regime. These results have been published.[4] In the current interval we have dramatically extended our early work. Broadening rates of the Na 3S-nS(nD) transitions up to n = 40 have been measured for all five noble gases. Our broadening measurements, performed at low perturber-gas pressures, constitute by far the most extensive work to date on

transitions involving Rydberg states. Since the tri-level echo is generated by coupling states of the same parity both Rydberg S and D states can be accessed from the ground 3S state of Na. Interestingly, the broadening of 3S-nS and 3S-nD transitions shows (see Figure 1) interesting differences and, while some work has already been done,[5][6] this result should stimulate theoretical work. The broadening rates of transitions to Rydberg states are important in a practical sense, because of the potential use of these transitions for frequency calibration. Our current results will be published shortly.[7] In the future we plan to extend our measurements to other alkalis and other perturbers. Perturbers such as CO should be particularly interesting since they have a permanent electric dipole moment and can be expected to give rise to a qualitatively different broadening behavior at high n.

We have continued our work on two-photon echoes[8] and have completed an indepth study of noble-gas-induced collisional broadening of the $6^2P_{1/2}$-$6^2P_{3/2}$ electric-dipole forbidden transition of atomic thallium. In contrast to our earlier work in Na,[8] we have been able to produce the two-photon echo (or in this difference-frequency case the "Raman" echo) with the laser fields detuned as much as 600 Ghz from the intermediate $7^2S_{1/2}$ state. This constitutes the first observation of a non-resonantly excited two-photon echo in an atomic vapor. The dependence of Raman echo intensity on Tl number density and on detuning of the laser field from intermediate-state resonance has been studied. Interestingly, it is found that loss of phase-matching resulting from population transfer during the excitation pulses appears to set the maximum echo signal obtainable. Working at temperatures between 750 and 840 degrees K,

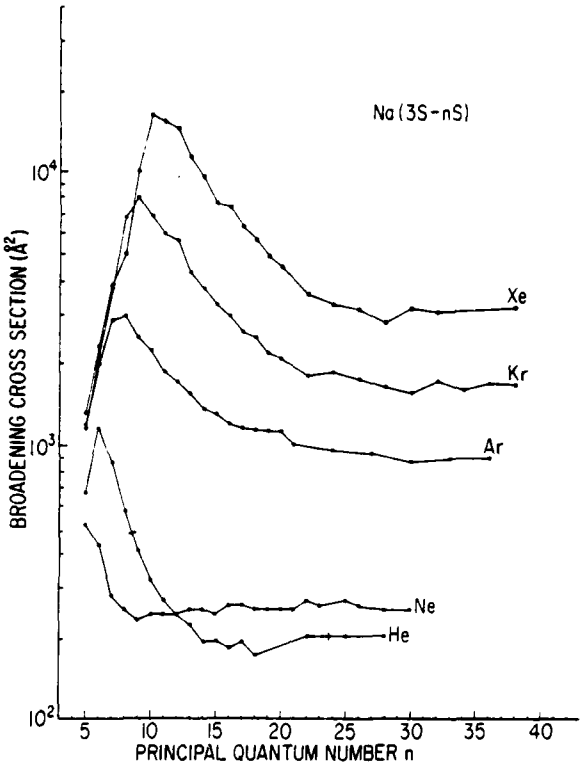
Na(3S-nS)
BROADENING CROSS SECTION (Å²)
10⁴
10³
10²
Xe
Kr
Ar
Ne
He
5
10
15
20
25
30
35
40
PRINCIPAL QUANTUM NUMBER n

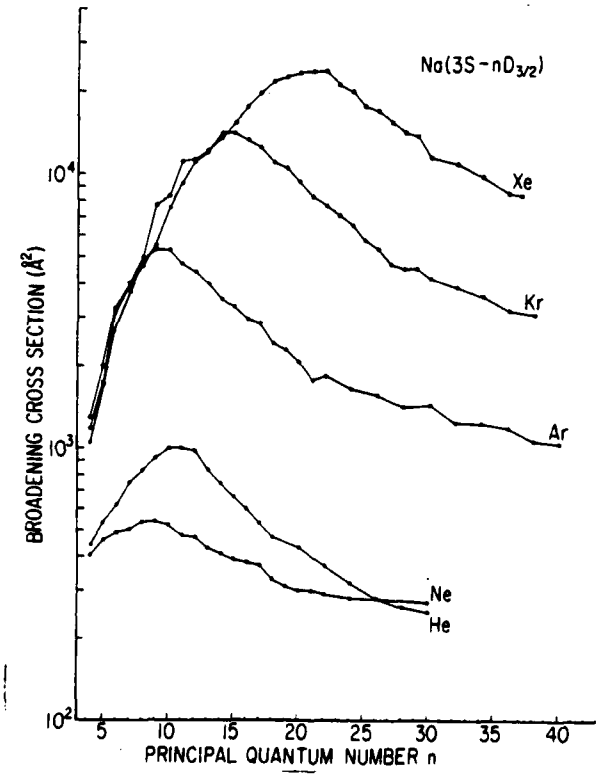
Na(3S-nD3/2)
BROADENING CROSS SECTION (Å²)
10⁴
10³
10²
Xe
Kr
Ar
Ne
He
5
10
15
20
25
30
35
40
PRINCIPAL QUANTUM NUMBER n

Figure 1

we have found the following noble-gas-induced broadening cross sections for the $6^2P_{1/2}$-$6^2P_{3/2}$ transition:

Perturber	Broadening Cross Section ($\AA^2$)
He	59 (6)
Ne	67 (7)
Ar	126 (13)
Kr	166 (17)
Xe	202 (20)

These results are being prepared for publication.

In the current interval we have discovered an entirely new class of reordering phenomena in gases.[9] If an atomic vapor is resonantly excited by a short standing-wave laser pulse, the population in both the ground and excited state exhibits a spatial variation whose spatial periodicity (wavevector) is determined by the wavevector of the excitation field k_e. Specifically, after the standing-wave pulse the ground-state population density ρ_{gg} is given by

$$2\rho_{gg} = 1 + J_o(\theta_1^o) + \sum_{n=1}^{\infty} (-1)^n J_{2n}(\theta_1^o)\cos(2nk_e z), \qquad (1)$$

where J_i is a Bessel function of order i, z is the position coordinate along the direction of the standing-wave field, and θ_1^o is the peak area of the standing-wave field. The spatially modulated population forms a grating and can be detected by scattering a probe beam from it. Note that gratings having as wavevectors all even multiples of k_e are generated. The thermal motion of the atoms rapidly eliminates the spatial modulation.

We have found, however, that a second standing-wave pulse, similar to the first but delayed by a time τ, causes spatial order to appear periodically thereafter. Gratings of spatial periodicity $\lambda/2\beta$, where $\lambda = 2\pi/k_e$ and $\beta = (1, 2, 3, \ldots)$, appear at the times $n\tau/2\beta$ $(n = 1, 2, 3, \ldots)$ after the second pulse. The gratings of periodicity $\lambda/2$, which appear every $\tau/2$ after the second pulse, can be detected by their backscattering of laser radiation which has the same wavelength as the exciting standing-wave pulses. Certain "grating echoes," as we term them, never depend on coherence between the ground and excited state and as such should prove useful in collisional studies.

Recent work[10] has shown that the use of standing-wave excitation pulses in a regular photon echo experiment leads to the emission of multiple echoes. We have performed the first "standing-wave" photon echo experiment in an atomic vapor[11] and have provided experimental checks on theoretical analysis[10] of the effect.

Both "grating" and "standing-wave" echoes are important in terms of their possible applications in spectroscopy. In certain cases both types of echo display oscillations in amplitude as a function of laser frequency when the laser is tuned within the natural width of the transition. The oscillation which under proper conditions is independent of laser spectral width may provide sub-natural width spectroscopic resolution. The origin of the oscillation is found to be similar to that observed in Ramsey fringe experiments.

We have applied the two-pulse photon echo to perform a detailed study of the He-induced collisional broadening of the $3S\text{-}3P_{1/2}$ transition in Na.[12] By monitoring the simple exponential decay $I_e(P) \sim \exp(-\beta P)$ of echo intensity

versus He pressure P we determine β which can be used to determine the collisional broadening rate. We found that β so determined exhibited a non-linear dependence on the excitation pulse separation τ (see Figure 2). The only plausible explanation for this behavior is to assume that collisional velocity changes contribute to echo decay. This is very surprising since it has been predicted[13] the velocity changes should play no role in the broadening of electronic transitions. Our results[12] will undoubtedly provoke a reexamination of certain aspects of the analysis of collisions. It should be noted that broadening measurements performed with echo effects are unhindered by the Doppler-width and the laser spectral width. In certain cases even the natural width is irrelevant. These factors made it possible for us to make our observations of the subtle role of collision velocity changes in the broadening of electronic transitions.

We have completed a theoretical analysis of optical echoes in gaseous media.[14] This treatment provides a general framework for the analysis of the conditions under which traveling-wave excitation pulses will generate echoes in a gas. Our treatment concentrates on echoes which arise from the excitation of more than two distinct energy levels by use of laser excitation pulses of widely different frequencies. We are currently working on a simple intuitive description of generalized echoes which should be very useful in understanding the mechanisms of echo production.

*This research was also supported by the Office of Naval Research under Contract N00014-78-C-0517

(1) T. Mossberg, A. Flusberg, R. Kachru, and S. R. Hartmann, Phys. Rev. Lett. 42, 1665 (1979).

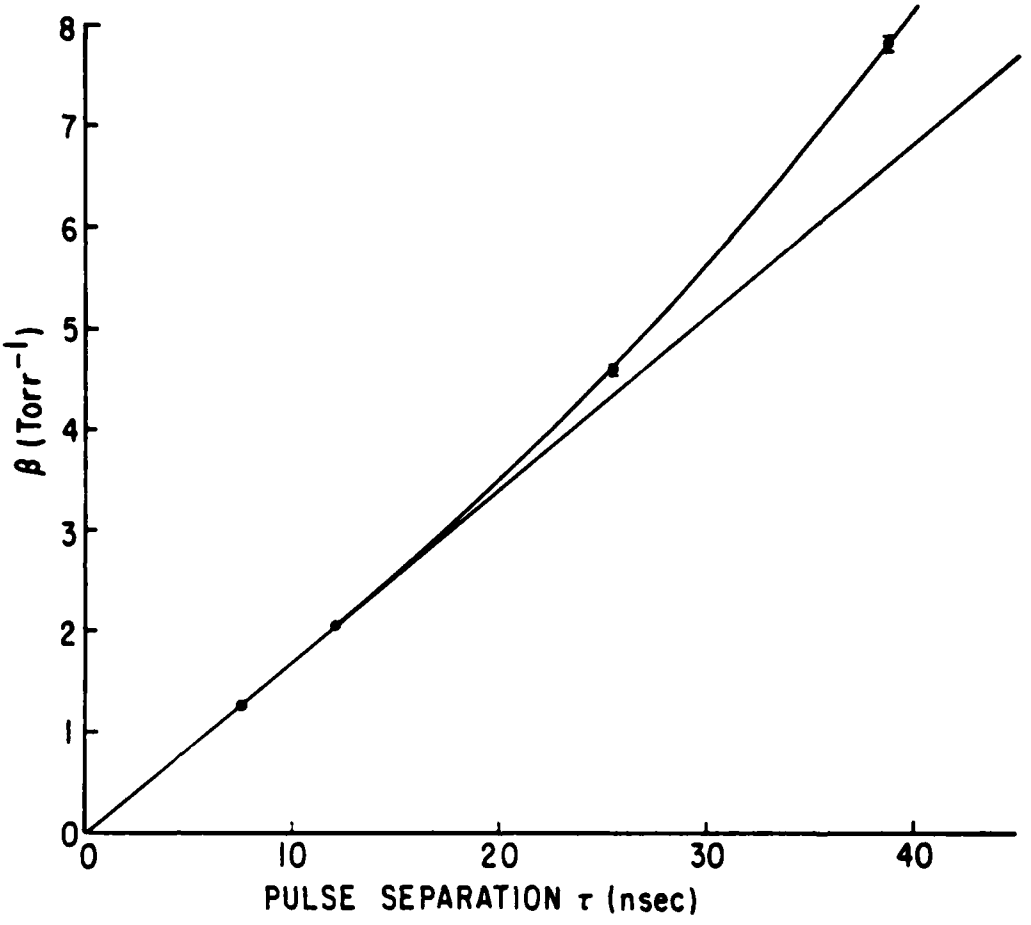

Figure 2

(2) R. Kachru, T. W. Mossberg, and S. R. Hartmann, Opt. Comm. 30, 57 (1979).

(3) T. Mossberg, A. Flusberg, R. Kachru, and S. R. Hartmann, Phys. Rev. Lett. 39, 1523 (1977).

(4) A. Flusberg, R. Kachru, T. Mossberg, and S. R. Hartmann, Phys. Rev. A 19, 1607 (1979).

(5) V. A. Alekseev and I. I. Sobel'man, Zh. Eksp. Teor. Fiz. 49, 1274 (1965) [Sov. Phys. JETP 22, 882 (1966)].

(6) A. Omont, J. Phys. (Paris) 38, 1343 (1977).

(7) R. Kachru, T. W. Mossberg, and S. R. Hartmann, Phys. Rev. A (in press April 1980).

(8) A. Flusberg, T. Mossberg, R. Kachru, and S. R. Hartmann, Phys. Rev. Lett. 41, 305 (1978).

(9) T. W. Mossberg, R. Kachru, E. Whittaker, and S. R. Hartmann, Phys. Rev. Lett. 43, 851 (1979).

(10) V. P. Chebotayev, N. M. Dyuba, M. I. Skvortsov, and L. S. Vasilenko, Appl. Phys. 15, 319 (1978); J.-L. Le Gouët and P. R. Berman, Phys. Rev. A 20, 1105 (1979).

(11) R. Kachru, T. W. Mossberg, E. Whittaker, and S. R. Hartmann, Opt. Comm. 31, 223 (1979).

(12) T. W. Mossberg, R. Kachru, and S. R. Hartmann, Phys. Rev. Lett. 44, 73 (1980).

(13) P. R. Berman, Phys. Rev. A 5, 927 (1972); and 6, 2157 (1972), and references therein.

(14) T. W. Mossberg, R. Kachru, S. R. Hartmann, and A. M. Flusberg, Phys. Rev. A 20, 1976 (1979).

B. RELAXATION AND EXCITATION TRANSFER OF OPTICALLY EXCITED STATES IN SOLIDS*

(K. Chiang, E. Whittaker, S. R. Hartmann)

We recently reported[1] the results of photon echo modulation experiments on the $^3H_4 - {}^3P_o$ transition in Pr^{3+} doped crystals of LaF_3. We demonstrated the feasibility of obtaining information about the hyperfine structure in the terminal levels of the echo transition with a resolution that was not limited by the large inhomogeneous linewidth of the transition or the multi-Ghz linewidth of nitrogen-laser-pumped dye lasers. In addition, by carefully analyzing the detailed form of the echo modulation pattern we were able to determine the relative principal axes orientations of the ground and excited state interaction hamiltonians.

With the aim of investigating the hyperfine structure of the $^1D_2$ state in $LaF_3:Pr^{3+}$, using the techniques that were used in the study of the ^3P_o state, we have performed photon echo experiments on the $^3H_4 - {}^1D_2$ transition in the same crystal. This transition involves the lowest crystal field split components of the $^3H_4$ and $^1D_2$ states; these components are electronic singlets that are each split into three doubly degenerate nuclear levels by the combined influence of the Pr nuclear quadrupolar and second order dipolar interactions. The energy splittings, which are of the order of several Mhz, are small compared to the linewidth of our two lasers; hence, we are able to coherently excite the system into a superposition involving all the sublevels. This leads to photon echo modulation effects that are observable on a time scale of several tens of nanoseconds.

The details of the experimental set up are similar to those used for measurements of the echo signal on the $^3H_4 - {}^3P_o$ transition. We employed

two thyratron triggered nitrogen-laser-pumped dye lasers to provide the two laser pulses necessary for photon echo excitation. The two nitrogen lasers were interfaced, via a multi-pulse generator unit, to a PDP8/e minicomputer, that allowed us to conveniently vary, under program control, the delay in the firing of one laser with respect to the other. The laser pulses were combined and focused to a 200 μ diameter spot in the LaF_3: Pr^{3+} crystal, which was of concentration 1.0 % at. wt. and had a thickness of 4 mm. The c-axis was in the plane of the optically buffed crystal face, and was oriented at right angles to the E-field vectors of the laser pulses.

The oscillator strength of the $^3H_4 - {}^1D_2$ transition is small and accounts for the relatively poor signal-to-noise ratio in our preliminary modulation data. In fact, the experiments of Brewer[2] enable us to place an upper limit of roughly 4.5×10^{-5} debye for the magnitude of the dipole matrix element between the $^3H_4$ and $^1D_2$ states. Assuming a laser power input of 1 kw into the sample, it would be necessary to focus the laser beams to a spot size of roughly 5 μ diameter in order to obtain a 90 degree pulse. For such a small spot size, the distance over which the laser beam cross-section remains roughly constant is only 100 μ, so that we not only have problems with beam overlap in a direction transverse to the direction of the laser beam, but also in a direction along the direction of propagation of the beam. Under the conditions mentioned above, the number of photons in the echo signal for the $^3H_4 - {}^1D_2$ transition for a 1.0 % at. wt. sample, was estimated to be of the order of 10^7. We may contrast this with the number of photons in the echo signal for the $^3H_4 - {}^3P_o$ transition, which for the same laser power of 1 kw, is estimated to be of the order of 10^{11}.

We performed some preliminary experiments to measure the echo signal as a function of laser spot size at the sample, and found that for a 200 μ diameter the echo intensity at a particular fixed pulse separation was a maximum. That the echo signal should experimentally turn out to be larger for the 200 μ spot size is due to the greater ease with which it was possible to obtain spatial overlap of the two laser pulses. In the limit when the "area" of the pulses are small, the echo signal is independent of the spot size at the sample, as long as the distance L, over which the beam diameter remains smaller than twice the narrowest beam waist, does not exceed the thickness of the crystal. Since the thickness of our crystal was 4 mm, the echo signal should have (neglecting spatial overlap factors) gotten smaller for beam spot sizes greater than 50 μ.

In Fig. 1. we present the experimentally observed photon echo intensity versus pulse separation for the $^3H_4 - {}^1D_2$ transition. The fluorescence background from the excitation pulses has not been subtracted. Some care has to be exercised in analyzing the modulation curve because, at the temperatures that we performed these experiments, the measured signal contains contributions from two effects; there is an ordinary two-pulse photon echo component as well as a long-lived stimulated photon echo component. The formation of the latter can be explained as follows. Consider two resonant laser pulses, separated by time τ_{12}, incident upon the sample. The Fourier transform of the two excitation pulses exhibits interference fringes, with a frequency splitting of $1/\tau_{12}$, within the single pulse spectrum profile of 10 Ghz. Therefore, after the passage of the two excitation pulses, the ground state population will also exhibit a frequency dependent sinusoidal variation, the depth of this modulation

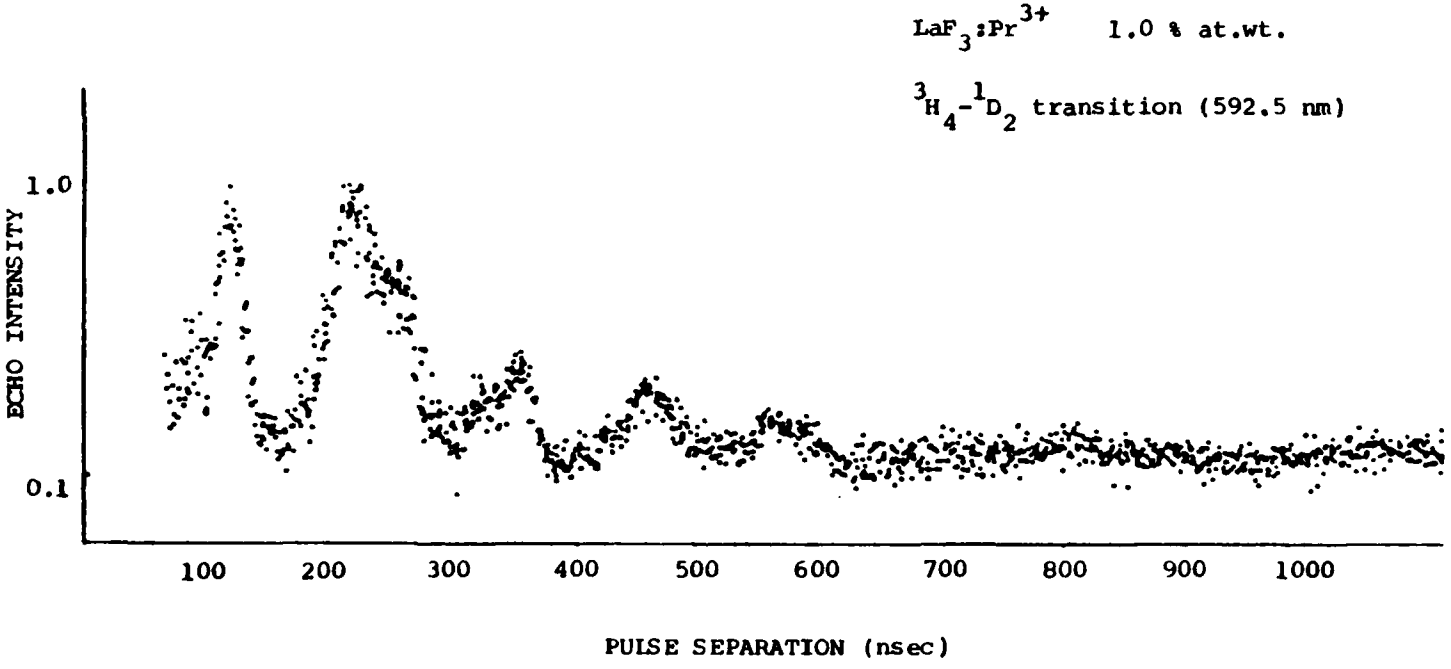

Photon echo modulation of the $^3H_4$-$^1D_2$ transition in $LaF_3:Pr^{3+}$

Figure 1.

pattern depending on the "area" of the excitation pulses. A third laser pulse incident on the sample at a time τ_{23} after the second pulse will then give rise to a stimulated echo, the intensity of which will depend on the depth of the modulation pattern mentioned above. This pattern of modulation in the ground state will persist for very long times if the process of thermalization of populations in the nuclear hyperfine levels of the ground state is slow, and hence stimulated echoes should be observable for pulse separations τ_{23} long compared to the excited state lifetime, which for the $^1D_2$ state is 500 μsec. In our case, the third pulse was, unfortunately, the same as the second pulse in a subsequent two pulse photon echo sequence. Recent photon-echo-nuclear-double-resonance experiments showed that the long-lived stimulated echo component could be effectively eliminated by irradiating the sample with oscillating RF fields of frequency 16.7 Mhz and 8.47 Mha, which correspond to the energy splittings in the ground $^3H_4$ state. Clearly, the RF fields, by inducing transitions between the nuclear hyperfine levels, accelerate the process of thermalization and completely degrade the long-lived stimulated echo.

By means of an optical-RF double resonance experiment, Erickson[3] has shown that the splittings in the state are 3.7 Mhz and 4.7 Mhz resp. From these splittings we can determine the parameters in the interaction hamiltonian for the $^1D_2$ state, and we have calculated the echo modulation pattern for various relative axes orientations of the $^1D_2$ and $^3H_4$ interaction hamiltonians. A cursory comparison shows little agreement between either one of the calculated and experimental curves, which leads us to surmise that the parameters we used in the hamiltonian are wrong, or that the hamiltonian is incompletely known.

Another unexplained observation is the fast decay of the echo modulation envelope. It has been shown that for a 0.05 % $LaF_3:Pr^{3+}$ crystal, the homogeneous linewidth in the absence of any applied magnetic fields is of the order of 50 Khz. Our data seems to indicate that the linewidth is three times larger. As in the case of the $^3H_4 - {}^3P_o$ transition, there appears to be a dependence of the homogeneous linewidth on Pr^{3+} ion concentration.

Although our original aim was to measure nuclear hyperfine splittings in the $^1D_2$ state, so as to obtain the correct parameters in the hamiltonian for our echo modulation calculation, we are currently engaged in performing photon-echo-nuclear-double-resonance (PENDOR) experiments on the $^3H_4 - {}^3P_o$ transition. This would not only provide an independent check of the nuclear hyperfine splittings and linewidths measured using the modulated photon echo technique, but would also enable us to perfect our PENDOR technique on a transition where the photon echo signals are several orders of magnitude larger than those on the $^3H_4 - {}^1D_2$ transition. Preliminary experiments have already shown a degradation of the stimulated echo signal for RF frequencies corresponding to nuclear hyperfine splittings in the $^3H_4$ ground state.

*This work was also supported by the National Science Foundation under Grant NSF-DMR79-06382.

(1) Y. C. Chen, K. Chiang and S. R. Hartmann, Phys. Rev. B, January 1, (1980).

(2) R. G. Devoe, A. Szabo, S. C. Rand and R. G. Brewer, Phys. Rev. Lett. 42, 1560 (1979).

(3) L. E. Erickson, Phys. Rev. B 16, 4731 (1977).

V. QUANTUM DETECTION AND SENSING OF RADIATION

A. COHERENT DETECTION AND SENSING IN THE INFRARED

(R. A. Meyers, P. R. Prucnal, M. C. Teich)

The likelihood-ratio detection of a signal embedded in noise constitutes an important class of classical binary decision problems that has found wide-spread applicability in the synthesis and analysis of many types of systems.[1] These applications range from optical communications[2]-[19] to radar systems.[18]-[22] For complex signal and noise statistics, it is sometimes difficult or impossible to express the likelihood ratio in closed form, however. Even for simple signal and noise statistics, direct implementation of the likelihood ratio as an optimum processor may be rather difficult. It may be possible to reduce the likelihood ratio to a simpler, but equivalent processor by using various ad hoc geometric arguments or lengthy algebraic manipulations.

We have made excellent progress [23] in deriving a simple processor that is optimum for a broad range of classical binary decision problems involving the likelihood-ratio detection of a signal embedded in noise. The class of problems we have considered encompasses the case of N independent (but not necessarily identically distributed) observations of a nonnegative (or nonpositive) signal random variable embedded in an additive, independent, and noninterfering noise random variable, where the range of the signal and noise is continuous. This applies, in particular, to the case of heterodyne detection in the optical, infrared, and submillimeter, where the signal, local oscillator, and noise, can be treated as continuous random variables. We have shown that a comparison of the sum of the N observations with a unique threshold comprises

optimum processing, provided that the logarithm of the noise probability density does not contain a point of inflection. This condition on the noise probability density is not necessary, but is sufficient, to imply our single-threshold processor and does not depend on the signal probability density. The results are applicable to a spatial array of heterodyne detectors exposed to a temporal sequence of observations. We have shown by example that in many cases it is not difficult to test the log of the noise density for a point of inflection analytically. In more difficult cases, a graphical representation of the noise density with a logarithmic ordinate scale may be useful in revealing a point of inflection. We have applied the results to a generalized heterodyning optical communication system and shown that background noise, dark noise, modulation, avalanche multiplication, and channel distortions are easily included in our model.

We had previously[18] derived a limited version of these results for a single observation (N=1) of a nonnegative signal embedded in noise, when the logarithm of the noise density is concave downward. The proof was based on the existence of a nonunique continuous extension of the noise density, so that implementation of the result depended on a proper choice of this continuous extension. We have also previously[22] derived an analogous result for the case of multiple (N>1) independent observations of a nonnegative (or nonpositive) signal random variable embedded in an additive, independent, and non-interfering noise randon variable, where the range of the signal and noise is discrete.

(1) H. L. Van Trees, Detection, Estimation, and Modulation Theory, Part I (Wiley, New York, 1968).

(2) B. Reiffen and H. Sherman, Proc. IEEE 51. 1316 (1963).

(3) C. W. Helstrom, IEEE Trans. Inf. Theory IT-10, 275 (1964).

(4) W. K. Pratt, Laser Communication Systems (Wiley, New York, 1969).

(5) Proc. IEEE (Special Issue on Optical Communications), 58, (1970).

(6) E. Hoversten, "Optical Communication Theory," in Laser Handbook, F. T. Arrechi and E. O. Schulz-DuBois, Eds. (North-Holland, Amsterdam, 1972), Vol. 2.

(7) M. C. Teich and R. Y. Yen, IEEE Trans. Aerosp. Electron. Syst. AES-8, 13 (1972).

(8) R. Y. Yen, P. Diament, and M. C. Teich, IEEE Trans. Inf. Theory IT-18, 302 (1972).

(9) M. C. Teich and S. Rosenberg, Appl. Opt. 12, 2616 (1973).

(10) S. Rosenberg and M. C. Teich, Appl. Opt. 12, 2625 (1973).

(11) E. V. Hoversten, D. L. Snyder, R. O . Harger, and K. Kiromoto, IEEE Trans. Commun. COM-22, 17 (1974).

(12) D. L. Snyder, Random Point Processes (Wiley, New York, 1975).

(13) R. M. Gagliardi and S. Karp, Optical Communications (Wiley, New York, 1976).

(14) C. W. Helstrom, Quantum Detection and Estimation Theory (Academic, New York, 1976).

(15) S. D. Personick, Bell Syst. Tech. J. 50, 3075 (1971).

(16) S. D. Personick, Proc. IEEE 65, 1670 (1977).

(17) S. D. Personick, P. Balaban, J. H. Bobsin, and P. R. Kumar, IEEE Trans. Commun. COM-25, 541 (1977).

(18) M. C. Teich, P. R. Prucnal, and G. Vannucci, Opt. Lett. 1, 208 (1977).

(19) M. C. Teich and B. I. Cantor, IEEE J. Quantum Electron. QE-14, 993 (1978).

(20) G. W. Flint, IEEE Trans. Mil. Electron. MIL-8, 22 (1964).

(21) J. W. Goodman, Proc. IEEE 53, 1688 (1965).

(22) P. R. Prucnal and M. C. Teich, Appl. Opt. 17, 3576 (1978).

(23) P. R. Prucnal and M. C. Teich, IEEE Trans. Info. Theory 25, 213 (1979).

B. THE EFFECTS OF WAVE NOISE ON THE ABSORPTION AND DETECTION OF INFRARED AND OPTICAL RADIATION*

(P. R. Prucnal, M. C. Teich, G. Vannucci)

The great variety of photocounting distributions that can be generated with intensity-modulated radiation is by now well known.[1]-[15] It is evident that modulation broadens these distributions; this can be interpreted as an accentuation of photon bunching since both low- and high-count probabilities are increased at the expense of counts near the mean. Indeed the extent of the broadening appears to depend strongly on the intensity distribution of the underlying radiation.[6] However, the counting distributions for intensity-modulated radiation can be characterized by a number of widely recognized and accepted statistical parameters, which have thus far received little attention.

Such modulation is sometimes deliberate, but more often is unavoidable. It may be imparted to the underlying radiation by mechanisms as diverse as transmission through a stochastic channel (e.g., the turbulent atmosphere[7][9]) and power-supply ripple.[6] It is also important when the source is pulsed (e.g., exponentially decaying[14]) rather than continuous. The analysis presented here applies also to nuclear counting[5] and neural counting.[16] It will generally not be applicable in the presence of dead time.[17]

We have obtained detailed statistical properties such as the cumulants, and the central, factorial, and ordinary moments for counting distributions when the incident radiation is intensity modulated with arbitrary statistics.[18] Our calculations are valid for the case where the integrated intensity is separable into a product of modulation-dependent and modulation-independent components. The results are applied

to the case of triangular, sinusoidal, and square-wave modulation of superposed coherent and chaotic radiation. The coefficient of variation, skewness, and kurtosis have been obtained as a function of modulation depth. Comparison has been made with experimental data in the cases of triangular and sinusoidal modulation of a laser source.

We also recognize that the photon statistics generated by thermal and chaotic light sources have evoked substantial interest ever since the well-known experiment by Hanbury-Brown and Twiss[19][20] demonstrated the occurrence of photon correlation in light generated by natural sources. With most natural sources, however, the time scale over which photon correlation is observable is typically very short and is often virtually negligible; indeed very sensitive and carefully designed experiments are usually required in order to observe such correlation. Correspondingly, the coherence time of the associated electromagnetic field is very short for such sources, as the coherence time provides a measure of the time scale over which variations occur in the intensity of the field.[21]

To circumvent this difficulty, a number of researchers have devised a variety of techniques to generate simulated chaotic light with an increased coherence time in the laboratory. Most of these techniques require a laser as the primary source of light, since they make use of the narrow bandwidth and high degree of coherence of laser radiation. They generate chaotic light by simulating, to different degrees, the physical characteristics of natural sources of chaotic light. One such method[22][23] consists of scattering laser light from particles suspended in a fluid, each particle acting as an independent radiator whose frequency is the laser frequency, Doppler-shifted by the Brownian

motion of the particle. In this configuration, the spectral bandwidth and shape can be adjusted to some extent by manipulating the statistical distribution of the size of the particles. Another method consists of scattering laser light from a moving rough surface, such as a rotating ground-glass screen[24][25] or a rotating roughened wheel;[26] here the different surface elements act as independent radiators, and the bandwidth of the light can be adjusted by varying the speed of motion of the surface. Reference (27) provides a survey of the properties of scattered light in general.

If only the intensity variations of chaotic light are of interest (as is the case for the statistics of photon arrivals), it is possible to use the method suggested by Ruggieri et al.[28] to simulate a superposition of coherent and chaotic radiation. This method uses two independent generators of Gaussian random noise to simulate the in-phase and quadrature components of the radiation field. The sum of the squares of these components yields the simulated light intensity, which is then used to modulate the output of a laser source. It should be noted that this method is less physical than the others cited above, since only the intensity (amplitude) variations of a chaotic radiation field are reproduced (the phase of the field depends solely on the characteristics of the primary laser source). Indeed, the narrow bandwidth and high degree of coherence of laser radiation are not necessary in this type of simulation, since the laser is used only to generate photons with the statistics of a Poisson point process whose rate can be controlled by modulating the intensity of the radiation. An arbitrary source yielding photons with the statistics of a Poisson point process with constant

rate can be used in place of the laser to obtain the same simulated photon statistics (doubly stochastic Poisson process[21]). Furthermore, it should be noted that with independent generators, only a limited class of power spectra can be reproduced.

We have shown how a small laboratory computer can be used to generate the two random processes needed for this particular type of simulation.[29] The computer can drive the modulator directly through a digital-to-analog converter. The advantages of using the computer include increased flexibility since an arbitrary spectral shape can be easily simulated. Increased accuracy and simplicity in the experimental setup are other benefits since critical adjustments, noise filtering, and matching of the two independent noise generators are not necessary.

The most useful application of this technique will likely be in conjunction with another program that simulates a Poisson point process with a given rate, to generate computer-simulated photocounting statistics under arbitrary conditions. This will be very useful for the study of systems that are not amenable to analytic solutions, such as photocounting with different types of dead time in conjunction with chaotic light of a given spectrum.

*Portions of the research were also supported by the National Science Foundation under Grant NSF- ENG78-26498.

(1) G. J. Troup, IEEE J. Quantum Electron. QE-1, 398 (1965).

(2) S. Fray, F. A. Johnson, R. Jones, T. P. McLean, and E. R. Pike, Phys. Rev. 153, 357 (1967).

(3) P. Pearl and G. J. Troup, Phys. Lett. 27A, 560 (1968). Equation (3) in this paper is incorrect and should be replaced by Eq. (38) of Ref. 6.

(4) M. C. Teich and P. Diament, Phys. Lett. 30A, 93 (1969).

(5) M. C. Teich and P. Diament, J. Appl. Phys. 41, 415 (1970).

(6) P. Diament and M. C. Teich, J. Opt. Soc. Am. 60, 682 (1970).

(7) P. Diament and M. C. Teich, J. Opt. Soc. Am. 60, 1489 (1970).

(8) C. Bendjaballah and F. Perrot, C. R. Acad. Sci. (Paris) 271, 1085 (1970).

(9) M. C. Teich and S. Rosenberg, J. Opto-electron. 3, 63 (1971).

(10) W. G. Clark and E. L. O'Neill, J. Opt. Soc. Am. 61, 934 (1971).

(11) L. Mišta, Czech. J. Phys. B23, 715 (1973).

(12) I. Kitazima, Opt. Commun. 10, 137 (1974).

(13) M. C. Teich and G. Vannucci, J. Opt. Soc. Am. 68, 1338 (1978).

(14) M. C. Teich and H. C. Card, Opt. Lett. 4, 146 (1979).

(15) B. Saleh, Photoelectron Statistics (Springer-Verlag, New York, 1978).

(16) M. C. Teich and W. J. McGill, Phys. Rev. Lett. 36, 754, 1473 (1976).

(17) G. Vannucci and M. C. Teich, Opt. Commun. 25, 267 (1978).

(18) P. R. Prucnal and M. C. Teich, J. Opt. Soc. Am. 69, 539 (1979).

(19) R. Hanbury Brown and R. Q. Twiss, Nature 177, 27 (1956).

(20) R. Hanbury Brown and R. Q. Twiss, Nature 178, 1046 (1956).

(21) B. Saleh, Photoelectron Statistics (Springer, Heidelberg, 1978), pp. 160 ff.

(22) H. Z. Cummins, N. Knable, and Y.Yeh, Phys. Rev. Lett. 12, 150 (1964).

(23) H. Z. Cummins, in Photon Counting and Light Beating Spectroscopy, H. Z. Cummins and E. R. Pike, Eds., (Plenum, New York, 1974).

(24) W. Martienssen and E. Spiller, Am. J. Phys. 32, 919 (1964).

(25) F. T. Arecchi, Phys. Rev. Lett. 15, 912 (1965).

(26) M. C. Teich, R. J. Keyes, and R. H. Kingston, Appl. Phys. Lett. 9, 357 (1966).

(27) B. Crosignani, P. Di Porto, and M. Bertolotti, Statistical Properties of Scattered Light (Academic, New York, 1975), pp. 159-212.

(28) N. F. Ruggieri, D. O. Cummings, and G. Lachs, J. Appl. Phys. 43, 1118 (1972).

(29) G. Vannucci and M. C. Teich, Appl. Opt. 19, 548 (1980).

C. PHOTON COUNT ANTIBUNCHING FOR OPTICAL COMMUNICATIONS, RADAR, IMAGING, AND SPECTROSCOPIC APPLICATIONS

(M. C. Teich, G. Vannucci)

In the absence of dead time, the probability $p_o(n|W_s)$ of recording exactly n counts in a time interval T from a detector illuminated by a source of radiation with constant intensity is

$$p_o(n|W_s) = \frac{W_s^n}{n!} \exp(-W_s) \quad . \tag{1}$$

Here $W_s = (\lambda + \lambda_n)T$, where λ is the average number of counts per unit time due to the signal and λ_n is the average number of counts per unit time due to noise (with the assumption that noise presents itself as an independent Poisson point process with constant rate λ_n). This is the well-known Poisson distribution with mean W_s. In the absence of radiation the probability of recording n noise counts is again given by Eq. (1) with W_s replaced by $W_n = \lambda_n T$. If such a counter is used as a threshold detector, we seek the probability that the number of counts registered exceeds a certain threshold value n_t both in the presence and in the absence of radiation, and we denote that quantity by $P_o(n_t, W)$ where W represents either W_s or W_n. Since the events corresponding to $p_o(n_1|W)$ and $p_o(n_2|W)$ are mutually exclusive whenever $n_1 \neq n_2$, $P_o(n_t, W)$ will be given by the expression

$$P_o(n_t, W) = \sum_{n=n_t+1}^{\infty} p_o(n|W) = \sum_{n=n_t+1}^{\infty} \frac{W^n}{n!} \exp(-W) = 1 - \sum_{n=0}^{n_t} \frac{W^n}{n!} \exp(-W) \tag{2}$$

In the presence of a fixed nonparalyzable dead time τ, we can make use of the results obtained by Ricciardi and Esposito[1] and other

workers,[2]-[7] who have provided an expression for the probability of registering exactly n counts in a time interval T, under the assumption that the counts occur as a Poisson point process with constant rate

$$p(n|W,\tau/T) = \begin{cases} \sum_{k=0}^{n} p_0(k|W[1-n\tau/T]) - \sum_{k=0}^{n-1} p_0(k|W[1-(n-1)\tau/T]), & n < T/\tau \\ 1 - \sum_{k=0}^{n-1} p_0(k|W[1-(n-1)\tau/T]), & T/\tau \le n < T/\tau + 1 \\ 0, & n \ge T/\tau + 1. \end{cases} \quad (3)$$

Again, the probability that the number of counts exceeds the threshold value n_t is

$$P(n_t,W,\tau/T) = \sum_{n=n_t+1}^{\infty} p(n|W,\tau/T) = 1 - \sum_{n=0}^{n_t} p(n|W,\tau/T) \quad . \quad (4)$$

Substituting Eq. (3) into Eq. (4) and exchanging the order of summation, we obtain

$$P(n_t,W,\tau/T) = 1 - \sum_{k=0}^{n_t} \frac{[\lambda T(1-n_t\tau/T)]^k}{k!} \exp\{-\lambda T(1 - n_t\tau/T)\} \quad , \quad (5)$$

for $n_t < T/\tau$.

We observe that this expression for $P(n_t,W,\tau/T)$ is identical to the expression for $P_o(n_t,W(1 - n_t\tau/T))$ provided in Eq. (2). Thus, for a counter with nonparalyzable dead time τ and a sampling time interval T,

the probability of exceeding a certain threshold number of counts n_t is the same as for a counter with no dead time that registers counts at the same rate, but during a sampling time $(T - n_t\tau)$.

This fact can be established directly, without making use of Eq. (3), through the following intuitive argument. Imagine that a Poisson point process generator is connected to the inputs of two counters in parallel, designated A and B. Counter A exhibits a nonparalyzable dead time τ after the detection of each and every pulse (i.e., it is unable to detect additional incoming pulses during a time interval of duration τ after the registration of a pulse). Counter B is constructed in such a way that it behaves precisely like counter A for the first n_t pulses, and thereafter behaves like a counter with no dead time.

It is clear that with such a system the probability of exceeding n_t counts is identical for both counters, since both reach n_t counts precisely at the same time. However, for $k > n_t$ the probability that counter B records exactly k counts can be calculated by observing that it has been dead (unable to detect pulses) for an over-all length of time n_tT, while during the remaining time interval $T - n_t\tau$ it has detected k pulses. Since the pulses are Poisson distributed, each pulse is independent of the others, and it is irrelevant in what manner the time interval $T - n_t\tau$ is chopped (as long as there is no correlation between where each dead-time interval τ is placed and the pulses that are possibly killed by it). Therefore, if we denote the rate of the Poisson process as λ, the probability of recording exactly k pulses in that length of time is given by Eq. (1) with W_s replaced by $\lambda(T - n_t\tau)$; i.e.,

$$P_B(k|\lambda T,\tau/T) = p_o(k|\lambda(T - n_t\tau))$$

$$= \frac{[\lambda T(1 - n_t\tau/T)]}{k!} \exp\{-\lambda T(1-n_t\tau/T)\} \quad \text{for } k > n_t \cdot \tag{6}$$

Note that this argument is valid only for $k > n_t$ and not for $k = n_t$; in fact, only in the former case are we certain that the counter is dead during a length of time precisely equal to $n_t\tau$. When k is equal to n_t, the dead-time interval following the last pulse might go beyond the end of the sampling time T. In conclusion, the probability that counter B registers more than n_t counts is

$$P_B(n_t,\lambda T,\tau/T) = \sum_{k=n_t+1}^{\infty} p_B(k|\lambda T,\tau/T)$$

$$= \sum_{k=n_t+1}^{\infty} \frac{[\lambda T(1-n_t\tau/T)]^k}{k!} \exp\{-\lambda T(1-n_t\tau/T)\}$$

$$= 1 - \sum_{k=0}^{n_t} \frac{[\lambda t(1-n_t\tau/T)]^k}{k!} \exp\{-\lambda T(1-n_t\tau/T)\} \tag{7}$$

which is identical to Eq. (5). As we remarked previously, this is the same as the probability that counter A exceeds n_t counts. Equation (7) can now be used to obtain Eq. (3) by observing that

$$p(n|W,\tau/T) = P(n-1, W, \tau/T) - P(n, W, \tau/T). \tag{8}$$

This argument therefore provides an alternate route to Eq. (3), for $n < T/\tau$.

Thus we have demonstrated the equivalence of detectors with and without nonparalyzable dead time in the presence of constant-intensity radiation and additive Poisson noise.

(1) L. M. Ricciardi and F. Espositio, Kybernetik 3, 148 (1966).

(2) J. W. Müller, Nucl. Instrum. Methods 117, 401 (1974).

(3) G. Bédard, Proc. Phys. Soc. 90, 131 (1967).

(4) B. I. Cantor and M. C. Teich, J. Opt. Soc. Am. 65, 786 (1975).

(5) G. Vannucci and M. C. Teich, Opt. Commun. 25, 267 (1978).

(6) M. C. Teich and G. Vannucci, J. Opt. Soc. Am. 68, 1338 (1978).

(7) M. C. Teich and B. I. Cantor, IEEE J. Quantum Electron. QE-14, 993 (1978).

VI. PHYSICAL PROPERTIES AND EFFECTS IN ELECTRONIC MATERIALS

A. CARRIER TRANSPORT ACROSS SEMICONDUCTOR INTERFACES*

(H. C. Card, E. S. Yang, W. Hwang)

Since last year's report we have made substantial progress in the understanding of the interband optical transitions in metal-germanium (Schottky barrier) contacts. We have been able to interpret the wavelength dependence of the quantum efficiencies observed in terms of the fundamental optical parameters of the 50-500 Å thin metal films, and their dependence on metal thickness. We have further extended these experimental studies to the longer wavelength region in which the photoresponse is dominated by internal photoemission of electrons from the metal over the Schottky barrier, and into the conduction band(s) of the germanium.

A theoretical description of this mechanism has been developed in which we take into account the front and back optical absorptance, hot electron scattering, and multiple reflections of excited electrons from the surfaces of the thin electrode film. We have found it necessary to impose a modification of the Fowler theory of photoemission when applied to internal photoemission from thin metal films over a Schottky barrier. This modification relates to an enhanced photoexcitation within the metal films which is attributed in the present theory to a density of states which exhibits a peaked distribution in energy rather than the simple parabolic bands assumed by Fowler.

The results of this work are described in detail in publications 1-3 below.

With regard to our studies of the Si-SiO_2 interface, and of ultrathin SiO_2 layers, the potential barriers of the ultrathin SiO_2 layers in the

thickness range 20-40 Å (range limited by the experimental method) to electrons and holes tunneling between the semiconductor and the metal have been measured independently on the same MOS samples by a new experimental technique. The method combines dark measurements of current and capacitance vs. voltage with measurements of photocurrent suppression under optical illumination. The potential barriers to majority carriers are determined by the preexponential current factor after the barrier heights are obtained.

The potential barriers to minority carriers are determined from suppression of photocurrent due to the tunneling process. Analysis of the data shows that the tunneling barriers for holes are consistently much larger than those for electrons. Interpretation of these tunneling probabilities indicates that a Franz dispersion relation is not obeyed even assuming different carrier masses in the conduction band and valence band of the SiO_2. This work is described in publications 4 and 5.

We have recently developed an experimental method for the measurement of electron and hole capture cross sections of Si-SiO_2 interface states, and for their dependence on electric field. This is accomplished by frequency dependent admittance measurements of MOS structures, in a background of optical illumination, and is described in publications 6 and 7.

Our studies of electronic processes at semiconductor heterojunction interfaces is continuing, and the major studies during this year were concerned with experimental measurements of the carrier transport in AlGaAs-GaAs structures, and with the determination of the energy band discontinuity. This work is described in publications 8 and 9.

We have also discovered recently that minority carrier injection can contribute strongly to or in some cases dominate the transport current in

metal-semiconductor contacts. This work is being prepared for publication in the journal of Applied Physics (publication 10).

*This research was also supported by the Department of Energy under Contract DOE-ET-78R-031876.

(1) E. Y. Chan and H. C. Card, "Infrared Optoelectronic Properties of Metal-Germanium Schottky Barriers," IEEE Trans. on Electron Dev., Special issue on Infrared Materials and Devices, ED-27, 78-83 (1980).

(2) E. Y. Chan and H. C. Card, "Near Infrared Interband Transitions and Optical Parameters of Metal-Germanium Contacts," Applied Optics, scheduled for April 1980.

(3) E. Y. Chan, H. C. Card, and M. C. Teich, "Internal Photoemission Mechanisms at Interfaces Between Germanium and Thin Metal Films," IEEE J. Quantum Elec., in press.

(4) H. C. Card and K. K. Ng, "Tunneling in Ultrathin SiO_2 Layers on Silicon: Comments on Dispersion Relations for Electrons and Holes," Solid St. Commun., 31, 877-879 (1979).

(5) K. K. Ng and H. C. Card, "Asymmetry in the SiO_2 Tunneling Barriers to Electrons and Holes," J. Appl. Phys., in press.

(6) H. C. Card, "Spectroscopy of Si-SiO_2 Interface States using MOS Tunneling Structures," Solid St. Electron, 22, 809-817 (1979)

(7) T. C. Poon and H. C. Card, "Admittance Measurements of Si-SiO_2 Interface States under Optical Illumination," submitted to J. Appl. Phys.

(8) E. S. Yang, C. M. Wu, and R. Y. Hung, "Variation of the Ideality Factor in the Current-Voltage Characteristics of Double Heterostructure Diodes," J. Appl. Phys. 51, 1262-1264 (1980).

(9) C. M. Wu and E. S. Yang, "Current Suppression Induced by Conduction-Band Discontinuity in $Al_{0.35}Ga_{0.65}As$ - GaAs N-p Heterojunction Diodes," J. Appl. Phys., in press.

(10) W. Hwang and H. C. Card, "Comments on Conduction Mechanisms of Metal-Nondegenerate Semiconductor Contacts," in preparation.

PERSONNEL

Faculty

N. D. Bhaskar, Assistant Professor of Physics

H. C. Card, Associate Professor of Electrical Engineering

K. Eisenthal, Professor of Chemistry

G. W. Flynn, Professor of Chemistry, Director

W. Happer, Professor of Physics

S. R. Hartmann, Professor of Physics

W. Hwang, Assistant Professor of Electrical Engineering

J. M. Luttinger, Professor of Physics

P. Prucnal, Assistant Professor of Electrical Engineering

I. I. Rabi, University Professor Emeritus

M. C. Teich, Professor of Engineering Science

P. Thaddeus, Adjunct Professor of Physics

E. Yang, Professor of Electrical Engineering

Research Associates and Physicists

Dr. R. Bohn

Dr. Y. Chen

Dr. R. Cohen

Dr. A. Kerr

Dr. A. Kponou

Dr. T. Mossberg

Dr. M. Wu

Graduate Research Assistants

J. Ahl	J. Chu	M. Mandich	R. Sheorey
T. Allik	M. Hou	T. McClelland	P. Siegel
P. Beeken	M. Islam	R. Novak	B. Suleman
T. Brown	R. Kachru	J. Pietras	N. Tran
J. Camparo	M. Lester	T. Poon	A. Vasilakis
K. Chiang	K. Leung	A. Sharama	E. Whittaker

Technical Research Assistants

Mr. I. Beller

Mr. E. Deery

Physics Department Electronics Engineering and Construction Shop*

Mr. J. Packer

Physics Department Machine Shop*

Mr. E. Jauch

Administration

Ms. I. Moon

Ms. P. Pohlman

Ms. V. Ricketts

*The Machine Shop and Electronics Shop facilities are available for the Columbia Radiation Laboratory.

JSEP REPORTS DISTRIBUTION LIST

DEPARTMENT OF DEFENSE

Director
National Security Agency
ATTN: Dr. T. J. Beahn, R-5
Fort George G. Meade, MD 20755

Defense Documentation Center
(12 copies)
ATTN: DDC-DDA
Cameron Station
Alexandria, VA 22314

Dr. George Gamota
Assistant for Research
Deputy Under Secretary of Defense
for Research and Engineering
(Research & Advanced Technology)
Room 3D1067, The Pentagon
Washington, DC 20301

Defense Advanced Research
Projects Agency
ATTN: (Dr. R. Reynolds)
1400 Wilson Boulevard
Arlington, VA 22209

DEPARTMENT OF THE ARMY

Commander
US Army Armament R&D Command
ATTN: DRDAR-RD
Dover, NJ 07801

Commander
US Army Ballistics Research Lab.
ATTN: DRXRD-BAD
Aberdeen Proving Ground
Aberdeen, MD 21005

Commander
US Army Communication Command
ATTN: CC-OPS-PT
Fort Huachuca, AZ 85613

Commander
US Army Materials and Machanics
Research Center
ATTN: Chief, Applied Sciences Div.
Watertown, MA 02172

Commander
US Army Material Development
and Readiness Command
ATTN: Technical Library, Rm. 7S 35
5001 Eisenhower Avenue
Alexandria, VA 22333

Commander
US Army Missile R&D Command
ATTN: Chief, Document Section
Redstone Arsenal, AL 35809

Commander
US Army Satellite Communications
Agency
Fort Monmouth, NJ 07703

Commander
US Army Atmospheric Sciences Lab.
ATTN: DELAS-DM-A (Tech Writing Sec.)
White Sands Missile Range, NM 88002

Commander
US Army Communications R&D Command
ATTN: DRDCO-COM-D-4 (Mr. John Walker)
Fort Monmouth, NJ 07703

Director
TRI-TAC
ATTN: TT-AD (Mrs. Briller)
Fort Monmouth, NJ 07703

Commander
US Army Electronics R&D Command
Night Vision & Electro-Optics Labs
ATTN: DELNV (Dr. Rudolf G. Buser)
Fort Monmouth, NJ 07703

Director
US Army Electronics R&D Command
ATTN: DELEW-D (Electronic
Warfare Laboratory)
White Sands Missile Range, NM 88002

Executive Secretary, TCC/JSEP
US Army Research Office
P.O. Box 12211
Research Triangle Park, NC 27709

Commander
Harry Diamond Laboratories
ATTN: Mr. John E. Rosenberg
2800 Powder Mill Road
Adelphi, MD 20783

HQDA (DAMA-ARZ-A)
Washington, DC 20310

Director
US Army Electronics Technology
& Devices Lab
ATTN: DELET-E (Dr. Jack A. Kohn)
Fort Monmouth, NJ 07703

Director
US Army Electronics Technology
& Devices Lab
ATTN: DELET-ER (Dr. S. Kronenberg)
Fort Monmouth, NJ 07703

Director
US Army Electronics R&D Command
Night Vision & Electro-Optics Labs
ATTN: Dr. Ray Balcerak
Fort Belvoir, VA 22060

Commander
US Army Research Office
ATTN: DRXRO-MA (Dr. Paul Boggs)
P.O. Box 12211
Research Triangle Park, NC 27709

Commander
US Army Missile R&D Command
Research Directorate
ATTN: DRDMI-TRD
(Dr. Charles Bowden)
Redstone Arsenal, AL 35809

Commander
US Army Missile R&D Command
Advanced Sensors Directorate
ATTN: DRDMI-TER (Dr. Don Burlage)
Redstone Arsenal, AL 35809

Director
US Army Electronics R&D Command
Night Vision & Electro-Optics Labs
ATTN: Mr. John Dehne
Fort Belvoir, VA 22060

Director
US Army Electronics R&D Command
Night Vision & Electro-Optics Labs
ATTN: Dr. William Ealy
Fort Belvoir, VA 22060

Commander
US Army Missile R&D Command
Physical Sciences Directorate
ATTN: DRDMI-TER
(Dr. Michael D. Fahey)
Redstone Arsenal, AL 35809

Commander
US Army Missile R&D Command
Physical Sciences Directorate
ATTN: DRDMI-TRO
(Dr. William L. Gamble)
Redstone Arsenal, AL 35809

Commander
White Sands Missile Range
ATTN: STEWS-ID-SR
(Dr. Al L. Gilbert)
White Sands Missile Range, NM 88002

Commander
US Army Communications R&D Command
ATTN: DRDCO-TCS-BP (Mr. David Haratz)
Fort Monmouth, NJ 07703

Commander
US Army Communications R&D Command
ATTN: DRDCO-COM-RF (Mr. R. A. Kulinyi)
Fort Monmouth, NJ 07703

Commander
US Army Communications R&D Command
ATTN: DRDCO-TCS-BG (Dr. E. Lieblein)
Fort Monmouth, NJ 07703

Director
US Army Electronics Technology
and Devices Lab
ATTN: DELET-M (Mr. V. Gelnovatch)
Fort Monmouth, NJ 07703

Commander
US Army Electronics R&D Command
ATTN: DRDEL-CT (Dr. W. S. McAfee)
2800 Powder Mill Road
Adelphi, MD 20783

Director
US Army Electronics R&D Command
Night Vision and
Electro-Optics Lab.
ATTN: DELNV
Fort Belvoir, VA 22060

Senior Standardization Repres.
US Army Standardization Group,
Canada
National Defense Headquarters
Ottawa, Ontario, Canada K1A 0K2

Commander
US Army Communications R&D Command
ATTN: DRDCO-COM-RM-4
(Dr. Felix Schwering)
Fort Monmouth, NJ 07703

Director
US Army Electronics Technology
and Devices Lab.
ATTN: DELET-I (Dr. K. H. Zaininger)
Fort Monmouth, NJ 07703

Director
US Army Electronics R&D Command
Night Vision & Electro-Optics Lab.
ATTN: Dr. Randy Longshore
Fort Belvoir, VA 22060

Commander
US Army Research Office
ATTN: DRXRO-EL (Dr. James Mink)
P.O. Box 12211
Research Triangle Park, NC 27709

Commander
Harry Diamond Laboratories
ATTN: DELHD-R (Mr. H. Sommer)
2800 Powder Mill Road
Adelphi, MD 20783

Director
US Army Electronics R&D Command
Night Vision & Electro-Optics Labs
ATTN: DELNV-EO (Dr. John Pollard)
Fort Belvoir, VA 22060

Commander
US Army Research Office
ATTN: DRXRO-EL (Dr. William A. Sander)
P.O. Box 12211
Research Triangle Park, NC 27709

Director
Division of Neuropsychiatry
Walter Reed Army Institute of Research
Washington, DC 20012

Commander
USA ARRADCOM
ATTN: DRDAR-SCF-CC (Dr. N. Coleman)
Dover, NJ 07801

Director
US Army Signals Warfare Lab
ATTN: DELSW-OS
Vint Hill Farms Station
Warrenton, VA 22186

Director
US Army Electronics Technology
and Devices Lab
ATTN: DELET-ED (Dr. E. H. Poindexter)
Fort Monmouth, NJ 07703

Director
US Army Electronics Technology
and Devices Lab
ATTN: DELET-ES (Dr. F. Rothwarf)
Fort Monmouth, NJ 07703

U. S. Army Research Office
(3 copies)
ATTN: Library
P.O. Box 12211
Research Triangle Park, NC 27709

Commander
US Army Communications R&D Command
ATTN: DRDCO-COM-RM (Mr. I. Kullback)
Fort Monmouth, NJ 07703

Dr. Sidney Ross
RCA GSD Engineering
Cherry Hill, NJ 08358

DEPARTMENT OF THE AIR FORCE

Mr. Robert Barrett
RADC/ES
Hanscom AFB, MA 01731

Dr. Carl E. Baum
AFWL (ELT)
Kirtland AFB, NM 87117

Dr. E. Champagne
AFAL/DH
Wright-Patterson AFB, OH 45433

Dr. R. P. Dolan
RADC/ESR
Hanscom AFB, MA 01731

Mr. W. Edwards
AFAL/DH
Wright-Patterson AFB, OH 45433

Professor R. E. Fontana
Head Dept. of Electrical Eng.
AFIT/ENG
Wright-Patterson AFB, OH 45433

Dr. Alan Garscadden
AFAPL/POD
Wright-Patterson AFB, OH 45433

USAF European Office of Aerospace
Research and Development
ATTN: Captain A. E. Mardiguian
Box 14, FPO, New York 09510

Mr. Murray Kesselman (ISCA)
Rome Air Development Center
Griffiss AFB, NY 13441

COL R. V. Gomez
Air Force Member, TCC
Air Force Office of Scientific Research
(AFSC) AFOSR/NE
Bolling Air Force Base, DC 20332

Chief, Electronic Research Branch
AFAL/DHR
Wright-Patterson AFB, OH 45433

Dr. Edward Altshuler
RADC/EEP
Hanscom AFB, MA 01731

Mr. John Mott-Smith (TOIT)
HQ ESD (AFSC), Stop 36
Hanscom AFB, MA 01731

Dr. Richard Picard
RADC/ETSL
Hanscom AFB, MA 01731

Dr. J. Ryles
Chief Scientist
AFAL/CA
Wright-Patterson AFB, OH 45433

Dr. Allan Schell
RADC/EE
Hanscom AFB, MA 01731

Mr. H. E. Webb, Jr. (ISCP)
Rome Air Development Center
Griffiss AFB, NY 13441

Dr. Howard Schlossberg
Air Force Office of Scientific Research
(AFSC) AFOSR/NP
Bolling Air Force Base, DC 20332

LTC G. McKemie
Air Force Office of Scientific Research
(AFSC) AFOSR/NM
Bolling Air Force Base, DC 20332

Major Clarence Gardner
Air Force Office of Scientific Research
(AFSC) AFOSR/NE
Bolling Air Force Base, DC 20332

DEPARTMENT OF THE NAVY

Office of Naval Research
800 North Quincy Street
Arlington, VA 22217
ATTN: Codes 220/221
427
432

Commanding Officer
Naval Research Laboratory
Washington, DC 20375
ATTN: Codes 1405 - Dr. S. Teitler
2627 - Mrs. D. Folen
5200 - A. Brodzinsky
5210 - J. E. Davey
5270 - B. D. McCombe
7503 - J. E. Shore
7550 - J. R. Davis
5510 - W. L. Faust
8005 - J. D. Brown

Director
Office of Naval Research
Branch Office
666 Summer Street
Boston, MA 02210

Director
Office of Naval Research
New York Area Office
715 Broadway, 5th Floor
New York, NY 10003

Director
Office of Naval Research
Branch Office
536 South Clark Street
Chicago, IL 60605

Director
Office of Naval Research
Branch Office
1030 East Green Street
Pasadena, CA 91106

Naval Surface Weapons Center
ATTN: Technical Library
Code DX-21
Dahlgren, VA 22448

Dr. J. H. Mills, Jr.
Naval Surface Weapons Center
Code DF
Dahlgren, VA 22448

Naval Air Development Center
Warminster, PA 18974
ATTN: Codes 301 G. Eck
Technical Library

Dr. Gernot M. R. Winkler
Director, Time Service
U. S. Naval Observatory
Mass. Avenue at 34th St., NW
Washington, DC 20390

G. Gould
Technical Director
Naval Coastal Systems Center
Panama City, FL 32407

Technical Director
Naval Underwater Systems Center
New London, CT 06320

Naval Research Laboratory
Underwater Sound Reference Detachment
Technical Library
P.O. Box 8337
Orlando, FL 32856

Naval Ocean Systems Center
San Diego, CA 92152
ATTN: Codes 015 - P. C. Fletcher
9102 - W. J. Dejka
922 - H. R. Wieder
532 - J. H. Richter

Naval Weapons Center
China Lake, CA 93555
Attn: Codes 601 - F. C. Essig
5515 - M. H. Ritchie

Donald E. Kirk
Professor & Chairman,
Electronic Engineering
Sp-304
Naval Postgraduate School
Monterey, CA 93940

Mr. J. C. French
National Bureau of Standards
Electronics Technology Division
Washington, DC 20234

Harris B. Stone
Office of Research, Development,
Test and Evaluation
NOP-987
The Pentagon, Room 50760
Washington, DC 20350

Dr. A. L. Slafkosky
Code RD-1
Headquarters, U.S. Marine Corps.
Washington, DC 20380

Dr. H. J. Mueller
Naval Air Systems Command
AIR-310
Washington, DC 20361

Mr. Reeve D. Peterson
Naval Electronics Systems Command
Code 03R
NC #1
2511 Jefferson Davis Hwy.
Arlington, VA 20360

Naval Sea Systems Command
NC #3
2531 Jefferson Davis Hwy.
Washington, DC 20362
Attn: Code 03C-J. H. Huth

David Taylor Naval Ship Research
and Development Center
Bethesda, MD 20084
ATTN: Code 522.1 - Tech. Library
Code 18 - G. H. Gleissner

Naval Surface Weapons Center
White Oak
Silver Spring, MD 20910
ATTN: Codes WX-40 - Tech. Library
R-45 - R. S. Allgaier

Dr. Edward S. Eby
Code 101E
Naval Underwater Systems Center
New London Laboratory
New London, CT 06320

Dr. Martin Mandelberg
Code 34
Naval Underwater Systems Center
New London Laboratory
New London, CT 06320

Dr. D. F. Dence
Code 34
Naval Underwater Systems Center
New London Laboratory
New London, CT 06320

OTHER GOVERNMENT AGENCIES

Dr. Herbert S. Bennett
Director
Division of Materials Research
National Science Foundation
1800 G Street
Washington, DC 20550

Dr. Jay Harris
Program Director
Devices and Waves Program
National Science Foundation
1800 G Street
Washington, DC 20550

Los Alamos Scientific Laboratory
ATTN: Main Library
P.O. Box 1663
Los Alamos, NM 87545

Dr. Dean Mitchell
Program Director, Solid-State Physics
Division of Materials Research
National Science Foundation
1800 G Street
Washington, DC 20550

M. Zane Thornton
Deputy Director Institute for
Computer Sciences and Technology
National Bureau of Standards
Washington, DC 20234

Head, Electrical Sciences &
Analysis Section
National Science Foundation
1800 G Street, NW
Washington, DC 20550

Deputy Director for Research
Research & Technology Division
Office of Aeronautics & Space Tech.
NASA
Washington, DC 20546

Judson C. French, Director
Center for Electronics &
Electrical Engineering
A361 Technology Bldg.
National Bureau of Standards
Washington, DC 20234

Dr. Ben Rubin
Chief, Sensing & Detection
Electronics Division, Code RE
NASA HQ
600 Independence Ave., SW
Washington, DC 20546

Mr. Herbert Ernst
Manager, Data Management Program,
Code ESI-5
NASA HQ
600 Independence Ave., SW
Washington, DC 20546

Mr. John Sos
Assistant Chief,
Information Processing Division
Code 560
Goddard Space Flight Center
Greenbelt, MD 20771

Mr. Charles Husson
Aerospace Technologist
Langley Research Center
Hampton, VA 23665

Mr. John Gould
Chief, Design Techniques Branch
George C. Marshall Space
Flight Center
Marshall Space Flight Center,
AL 35812

NON-GOVERNMENT AGENCIES

Director
Columbia Radiation Laboratory
Columbia University
538 West 120th Street
New York, NY 10027

Director
Coordinated Science Laboratory
University of Illinois
Urbana, IL 61801

Director
Division of Applied Sciences
Harvard University
Pierce Hall
Cambridge, MA 02138

Director
Electronics Research Center
The University of Texas
P.O. Box 7728
Austin, TX 78712

Director
Electronics Research Laboratory
University of California
Berkeley, CA 94720

Director
Electronics Sciences Laboratory
University of Southern California
Los Angeles, CA 90007

Director
Microwave Research Institute
Polytechnic Institute of New York
333 Jay Street
Brooklyn, NY 11201

Director
Research Laboratory of Electronics
Massachusetts Institute of Tech.
Cambridge, MA 02139

Director
Stanford Electronics Laboratory
Stanford University
Stanford, CA 94305

Director
Edward L. Ginzton Laboratory
Standord University
Stanford, CA 94305

Dr. Lester Eastman
School of Electrical Engineering
Cornell University
316 Phillips Hall
Ithaca, NY 14850

Dr. Carlton Walter
ElectroScience Laboratory
The Ohio State University
Columbus, OH 43212

Dr. Richard Saeks
Department of Electrical Engineering
Texas Tech University
Lubbock, TX 79409

Dr. Roy Gould
Executive Officer for Applied Physics
California Institute of Technology
Pasadena, CA 91125

Director
School of Electrical Engineering
Georgia Institute of Technology
Atlanta, GA 30332

Prof. J. F. Walkup
Department of Electrical Engineering
Texas Tech University
Lubbock, TX 79409


DAT
FILM